FLORIDA INTERNATIONAL UNIVERSITY

Miami, Florida

SYNTHESIS, STRUCTURE-ACTIVITY RELATIONSHIP, AND MECHANISM STUDIES OF POLY (GUANYLUREA)S AGAINST MYCOBACTERIA

A dissertation submitted in partial fulfillment of

the requirements for the degree of

DOCTOR OF PHILOSOPHY

in

CHEMISTRY

by

Michelle Miranda-Vélez

2022

To: Dean Michael R. Heithaus
College of Arts, Sciences and Education

This dissertation, written by Michelle Miranda-Vélez, and entitled Synthesis, Structure-Activity Relationship, and Mechanism Studies of Poly (guanylurea)s against Mycobacteria, having been approved in respect to style and intellectual content, is referred to you for judgment.
We have read this dissertation and recommend that it be approved.

_____
Kevin O'Shea

_____
Yuk-Ching Tse-Dinh

_____
Kalai Mathee

_____
Christopher Dares

_____
Joong Ho Moon, Major Professor

Date of Defense: June 21, 2022

The dissertation of Michelle Miranda-Vélez is approved.

_____
Dean Michael R. Heithaus
College Arts, Sciences and Education

_____
Andrés G. Gil
Vice President for Research and Economic Development
and Dean of the University Graduate School

Florida International University, 2022

DEDICATION

I dedicate this achievement to my family, friends, mentors and especially my parents for their love, and endless support.

ACKNOWLEDGMENTS

First, my utmost gratitude to my mentor, Dr. Joong Ho Moon, without his guidance, patience, support, knowledge, and trust, this would have not been possible. Thank you for your perseverance on always achieving high standards in everything; it shaped me, and I will take such values with me.

I would like to thank the members of my dissertation committee for all your help and feedback throughout these years. Dr. Kevin O'Shea, taking Spectroscopic Techniques and Physical Organic Chemistry was delightful, as his dedication to teaching energized the room and had everyone eager to learn; his organic chemistry knowledge and help was an integral part of my progress. My sincerest appreciation to Dr. Kalai Mathee, and Dr.Yuk-Ching Tse-Dinh, along with Dr. Thirunavukkarasu Annamalai for their help, guidance and availability when I needed help with the biochemistry and microbiological aspect of my work and allowing me to work and train in their labs. I extend my gratitude to Dr. Christopher Dares for his input from an outside perspective, specifically in physical chemistry. The overall constructive feedback of everyone was extremely valuable. Additionally, Dr. Kathleen Rein, thanks for letting me acquire data in the lab and helping me as GPD.

I would like to thank Dr. Kyle Rohde in University of Central Florida and his team, especially Sandra, Priscila, and Breven for supporting my research and making me feel part of your group for the two months I was there. They made the transition seamless by training me, helping me acquire crucial data, encouraging me, and providing feedback.

I want to give special recognition to my colleagues that helped me through this entire process. Past members in Dr. Moon's research group, Dr. Prakash Manandhar and Dr. Md Salauddin Ahmed, thank you for passing down your training, and scientific knowledge without it, the learning curve would have been much steeper. To the current members in the lab, you made the lab environment professional, but friendly and cozy; it made a big positive impact on how the dynamic, productivity and organization of the lab flowed. Alfonso was always open to listening, and helping, both professionally and personally. I could not have asked for a better lab partner throughout these years. Sabbir's positive attitude, hard work and willingness to help every time never went unnoticed. Although Mario joined later, he fit right in, immediately; always putting a smile in everyone's face with his jokes, and enthusiasm to learn. To my undergraduate students throughout the years - Jake, Kelsie, Priya, and Laura- it was a pleasure working with you.

Finally, I must thank the people behind the scenes - my friends and family. Ana Paula always made sure I had someone to rely on when things got hard, no matter how many miles apart we were. Donny, thank you for always listening, helping, and proofreading my work. Jeff, Will and Kim, I cannot thank you enough for a great living environment – keeping me sane, supporting me, and feeding me. To my family that has always there for me, your love and support means the world to me. And lastly, to my parents, Milagros and Michael, your sacrifices, endless love, and encouragement never went unnoticed. Without your help, advice, and support, none of this would have been possible.

ABSTRACT OF THE DISSERTATION

SYNTHESIS, STRUCTURE-ACTIVITY RELATIONSHIP, AND MECHANISM STUDIES OF POLY(GUANYLUREA)S AGAINST MYCOBACTERIA

by

Michelle Miranda-Vélez

Florida International University, 2022

Miami, Florida

Professor Joong Ho Moon, Major Professor

Tuberculosis (TB) continues to be a serious threat worldwide, especially in developing countries. Current first-line treatment for TB infections is a multidrug regimen for 4-9 months; if not taken as prescribed, drug-resistant TB can emerge. In addition, the treatment of nontuberculous mycobacterial (NTM) diseases is rigorous and lengthy, where some have not been proven effective, or might lead to adverse side effects. Novel drugs with unconventional targets are warranted to lessen the lengthy, multidrug treatment of mycobacteria. Antimicrobial polymers mimicking naturally occurring antimicrobial peptides (AMPs) have gained much attention due to their enzymatic stability, tunability, cost-effectiveness, and unique mode of action -directly or indirectly- on bacterial membrane. However, selectivity and toxicity have limited their biological applications. Previously, our group synthesized a novel class of antimicrobial polymers, poly(guanylurea)s (PGUs). Unlike conventional AMP-mimics, poly(guanylurea piperazine)s have a linear architecture (i.e., no pendants) with all key functional groups along the backbone, resulting in low cytotoxicity and selectivity against mycobacteria.

Here, this work explores the inherent antimycobacterial selectivity and bactericidal activity of PGU-P-8K on *M. smegmatis*, as a model organism for mycobacteria. PGU-P-8K showed fast-acting bactericidal activity (i.e., less than a day) at its minimum bactericidal concentration (MBC). This effect was further explored and attributed it to PGU-P-8K interfering with the Proton Motive Force (PMF) via membrane potential disruption in mycobacteria. PGU-P-8K displayed targeting the mycobacterial cell envelope by disrupting intracellular processes while retaining cell membrane integrity, confirmed by imagining of post-treatment cells and overexpression of genes related to cell envelope stress. Targeting membrane energetics is a promising approach to combat drug-resistant or latent mycobacterial infections as both replicating and dormant mycobacteria rely on a polarized membrane for their survival. Additionally, this project investigates how the key functionalities (e.g., aromatic substituents, amphiphilicity, rigidity) along the backbone of PGU-P-8K play a role in its antimycobacterial activity, as little is known of the physicochemical properties required to target the mycobacterial membrane. Preliminary data showed changes along the backbone can broaden antimicrobial and antimycobacterial activity of PGUs. Additionally, increasing PEGylation increased toxicity of PGUs. The in-depth studies on the mode of action and how the key functional groups in the architecture of PGU-P-8K on mycobacteria affect selectivity and bactericidal activity on mycobacteria contributes to the development of a novel class of membrane-targeting drugs or drug adjuvants for improving TB treatment. Furthermore, modifications along the backbone of can widen the biological applications of PGUs.

TABLE OF CONTENTS

LIST OF TABLES

TABLE PAGE

LIST OF FIGURES

FIGURE PAGE

LIST OF SCHEMES

SCHEMES PAGE

ABBREVIATIONS AND ACRONYMS

AMP	antimicrobial peptide
AMR	antimicrobial resistance
ATP	adenosine triphosphate
Bce	*B.cepacia*
BCG	*M. bovis BCG*
BED	bedaquiline
boc	di-tert-Butyloxycarbonyl
Cal	*C.albicans*
CCCP	cyanide m-chlorophenyl hydrazone
$CDCl_3$	deuterated chloroform
CFU	colony forming unit
CIP	ciprofloxacin
CLZ	clofazimine
DCM	dichloromethane
$DiSC_3(5)$	3,3'-dipropylthiadicarbocyanine iodide
DMF	dimethylformamide
DMSO	dimethylsulfoxide
Eco	*E.coli*
EtBr	ethidium bromide
FICI	fractional inhibitory concentration
GPLs	glycopetidolipids

HEPES	4-(2-hydroxyethyl)-1-piperazineethanesulfonic acid
Mab	*M. abscessus*
MBC	minimum bactericidal concentration
MDR	multi-drug resistant
MeOH	methanol
MIC	minimum inhibitory concentration
M_n	number average molecular weight
Msm	*M. smegmatis*
Mtb	*Mycobacterium tuberculosis*
MTT	(3-(4,5-dimethylthiazol-2-yl)-2,5-diphenyltetrazolium bromide
M_w	weight average molecular weight
NMR	nuclear magnetic resonance
NPN	N-phenyl-2-naphthylamine
OD	optical density
PBS	phosphate buffered saline
PCR	polymerase chain reaction
PDI	polydispersity index
PGUs	poly(guanylurea)s
PMF	proton motive force
qRT-PCR	real-time quantitative reverse transcription-polymerase chain
R-PE	R-phycoerythrin
RIF	rifampicin

SAR	structure-activity relationship
Sau	*S.aureus*
STP	streptomycin
TB	tuberculosis
TEA	triethylamine
TEM	transmission electron microscope
TLC	thin-layer chromatography
TFA	trifluoroacetic acid
THF	tetrahydrofuran
VER	verapamil

CHAPTER 1: INTRODUCTION TO ANTIMYCOBACTERIAL POLY(GUANYLUREA)S

1.1 Antimicrobial Resistance

The World Health Organization (WHO) has been warning the public about the detrimental consequences of pathogens evolving resistance to medications.[1] Antimicrobial resistance (AMR) occurs when a microorganism develop mechanisms that make antibiotic treatment ineffective.[1–3] They can naturally develop resistant gene(s) after exposure to antibiotic. Then the microbes can replicate or pass down the resistant gene, resulting in a mostly antibiotic-resistant environment. AMR can be easily spread through humans, animals, food, or environment; misuse and overuse of antibiotics has worsened the situation. This can lead to harder-to-treat infections; where second-line or third-line treatments can cause adverse side effects, or in severe cases (i.e., no treatment options are available) it can be deadly.[4]

1.1.1 Threats of Antimicrobial Resistance

The Centers for Disease and Control and Prevention (CDC) declares antibiotic resistance as one of the biggest public health challenges with at least 2.8 million infections and an estimated 35,000 deaths annually in the United States.[4] One of the major public health threats of untreatable infections (i.e., "superbugs") is the risk that it would pose for routine surgeries, life-saving medical procedures, or treatment of patients with compromised immune system. Additionally, the pipeline of novel antibiotics has been slow while the rise of drug-resistance rises (Figure 1.1).[1,4,5]

Figure 1.1 Rate at resistant germ strain has been identified in comparison to the pipeline of antibiotics. [5]

1.1.2 AMR in Bacteria

A rise of resistant strains has been observed world-wide for conventional antibiotics used to treat common bacterial infections while the pipeline for new antibiotics have been slowing down.[5] For example, the rate of resistance for Ciprofloxacin (CIP) varied from 8.4% to 92.9% for *Escherichia coli* (*E.coli*) and from 4.1% to 79.4% for *Klebsiella pneumoniae* reported in the Global Antimicrobial Resistance and Use Surveillance System (GLASS), a system aiming to standardized global data collection of AMR by countries and monitor AMR trends in fast-growing bacteria causing common infections.[6] Although slow-growing bacteria is not part of GLASS monitoring system, it is the second cause of death from a single infectious agent (after COVID-19).[6]

1.1.3 AMR in Tuberculosis

Tuberculosis (TB) is a slow-growing bacteria caused by *Mycobacterium tuberculosis* (*Mtb*). Globally, about 10 million people get infected with TB every year. Although treatable, an approximate 1.5 million people die every year from TB;[6–8] TB is one of the top leading causes of death, where most of the burden is on developing countries (Figure

1.2). It is estimated that about one-quarter of people in the world have been infected with latent TB, but about 5-10% untreated cases might eventually develop TB disease, where immunocompromised individuals are at most risk.[9]

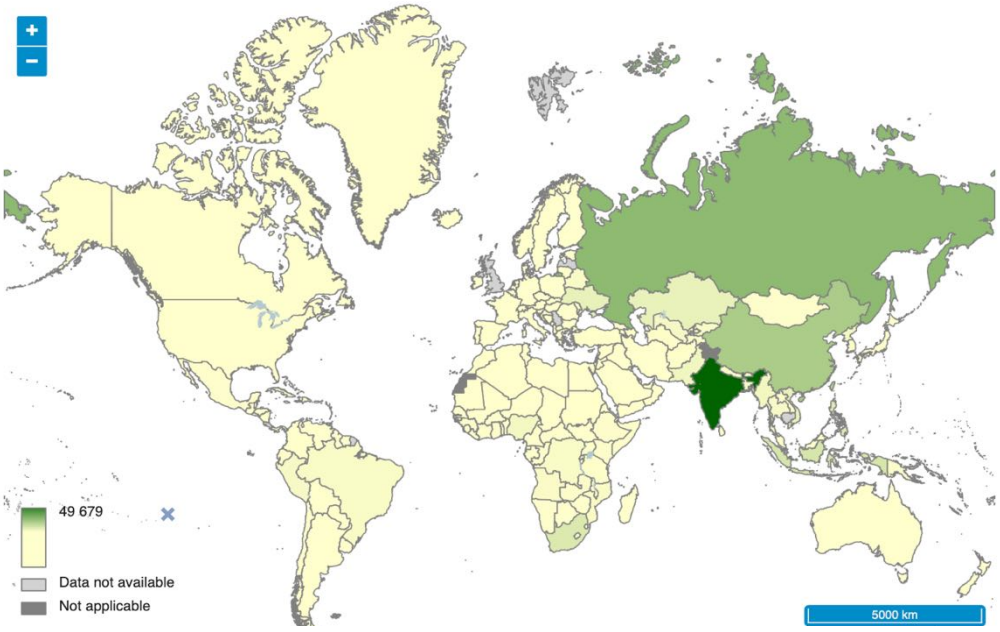

Figure 1.2 Countries around the world with the highest incident cases of MDR TB in 2020, reported as absolute numbers, where the most cases were reported in developing countries.[10]

1.2 Challenges in TB treatment

TB can be a curable infection if the rigorous regimen, consisting of a combination of four drugs for a period of 4 to 9 months, is followed as prescribed.[2] Patient must be instructed, supervised and provided with pure medicaments to successfully treat TB.[8] If not followed and two or more drugs from the first-line treatment become ineffective, then multi-drug resistance TB (MDR TB) can emerge (Figure 1.3).[11] A major challenge of eradicating TB is the emergence of MDR TB, and extensively drug-resistant TB (XDR

RB) which leads to expensive and prolonged treatment with adverse side effects, burdening low-income countries the most. .

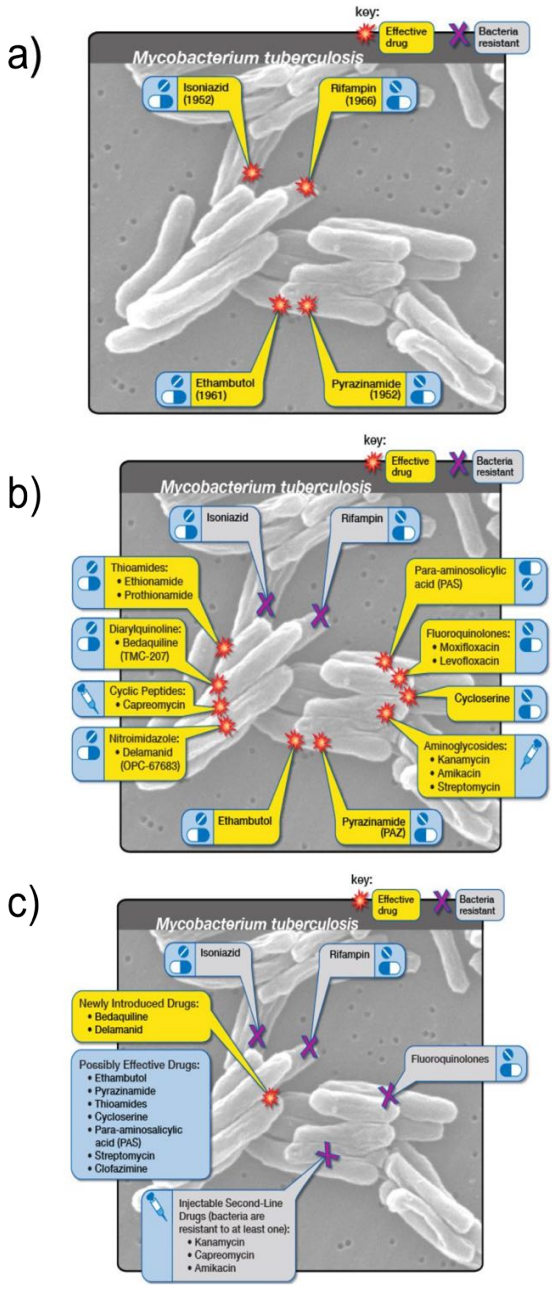

Figure 1.3. Treatments: a) First-line for Drug-Sensitive, b) Second-line for Multidrug-Resistant (MDR TB) and c) Extensively Drug- Resistant (XDR TB) tuberculosis. [11]

1.2.1 Mechanism of Action of Anti-TB drugs

TB drug development warrants shortening and improving the treatment of both drug-sensitive and drug-resistant TB. Most current anti-TB drugs are small molecules that have a specific target site and disrupt intracellular function(s) (Figure 1.4). [2] As shown in Table 1.1, most anti-tb drugs from first-, second- and third-line of treatment have functions and target sites intracellularly with identified resistance for these therapeutics, including the most recently introduced anti-TB drugs.

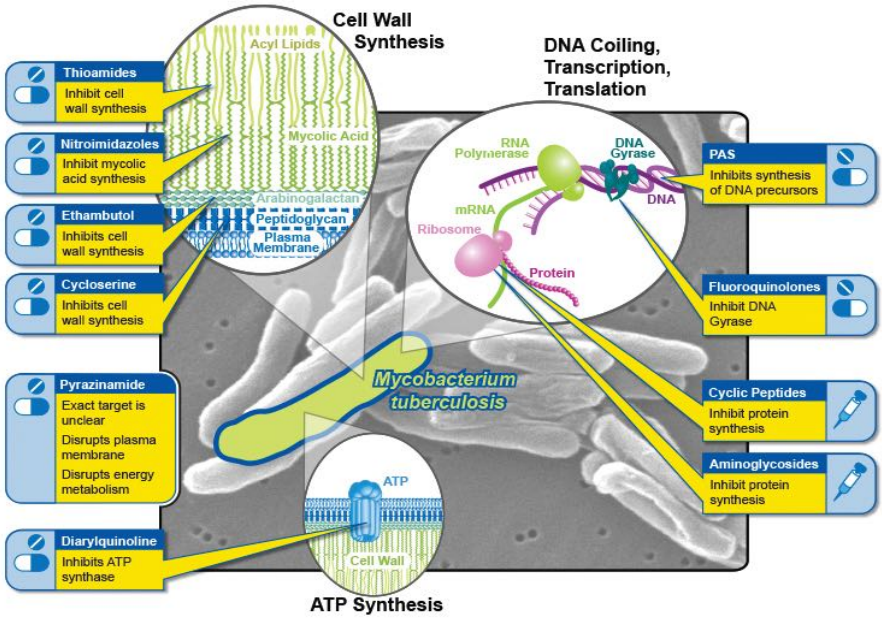

Figure 1.4 Target sites of current anti-TB drugs.[11]

Bacteria can develop resistance via mechanisms that result in the ineffectiveness of one or more antibiotics, including: the overexpression efflux pumps, alteration or loss of porins, modification of the binding site, or enzymatic degradation (Figure 1.5). The development of novel antibiotics using unconventional modes of action is urgently needed.

Table 1.1. Current anti-tb drugs, mechanisms of action and common genes identified in resistance in *Mtb*. Adapted from [2].

Drug	Abbreviation	Common genes involved in resistance in *Mycobacterium tuberculosis*	Mechanism of Action
Isoniazid	INH	katG inhA kasA	Inhibition of cell wall mycolic acid synthesis
Rifampicin	RIF	rpoB	Inhibition of RNA synthesis
Ethambutol	EMB	embB ubiA	Inhibition of cell wall arabinogalactan biosynthesis
Pyrazinamide	PZA	pncA rpsA panD	Reduction of membrane energy; Inhibition of trans-translation Inhibition of pantothenate and coenzyme A synthesis
Streptomycin	STP	rpsL rrs gidB	Inhibition of protein synthesis
Ciprofloxacin	CIP	gyrA gyrB	Inhibition of DNA synthesis
Capreomycin, amikacin, and kanamycin	CAP AMK KAN	rrs eis tlyA	Inhibition of protein synthesis
Ethionamide	ETH	ethA mshA ndh inhA inhA promoter	Inhibition of cell wall mycolic acid synthesis
Para-amisosalicylic acid	PAS	thyA folC ribD	Inhibition of folic acid and thymine nucleotide metabolism
Bedaquiline	BED	rv0678 atpE pepQ	Inhibition of mycobacterial ATP synthase
Clofazimine	CLZ	rv0678 rv1979c rv253c ndh pepQ	Inhibits mycobacterial growth Binds preferentially to mycobacterial DNA May also bind to bacterial potassium transporters
Delamanid, pretonamid	DEL PRE	fgd1 fbiC fbiA fbiB ddn	Specific and selective inhibition of mycolic acid biosynthesis
Linezolid	LIN	rplC rrl	Inhibition of protein synthesis

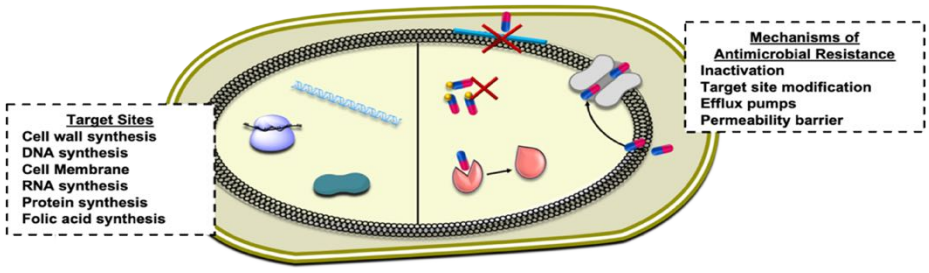

Figure 1.5 Left side: Common antibiotics intracellular target sites. Right side: Bacterial mechanisms that lead to antimicrobial resistance. Adapted from [12,13].

A major challenge to TB drug development is the mycobacteria's cell wall. The rigidity of the cell wall in mycobacteria hinders drug interactions and permeability resulting in the lengthy and multi-drug regimen.[14,15] Although challenging, the mycobacteria membrane itself is a putative drug target; since the membrane is the site of many critical processes including transport of nutrients and wastes, and metabolic energy transduction.[15–18] Moreover, unlike other microorganisms, the destabilization of the mycobacterial membrane potential is detrimental for the survival of both active (replicating) and dormant (nonreplicating) TB, since TB is dependent on an intact membrane for cellular processes.[17–19]

1.3 Bacterial Cell Wall

Living organisms have a symbiotic relationship with bacteria, but propagation of pathogenic bacteria can cause bacterial infections; therefore, selectivity when treating pathogens is essential. The foundation of all bacterial cell walls is composed of peptidoglycan, but structural differences in the cell walls define the type of bacteria.[20] Generally, Gram-negative bacteria have a thin peptidoglycan layer between an inner cell membrane and an outer bacteria membrane (Figure 1.6a).[21–23] In contrast to Gram-positive bacteria that have a thick peptidoglycan layer, but no outer membrane (Figure 1.6b). The outer membrane in Gram-negative bacteria makes them less susceptible to antibiotics. The surrounding environment of both Gram-negative and -positive bacteria is highly anionic majorly due to the phosphate groups in the phospholipid bilayer. This anionic environment allow initial electrostatic interactions and the successive diffusion of cationic amphiphiles with Gram- positive and -negative bacteria.[24]

On the other hand, the membrane of mycobacteria is more hydrophobic and rigid due to the mycolyl-arabinogalactan-peptidoglycan (mAGP) complex (Figure 1.6c).[16] The robust membrane serves as a barrier limiting the compounds with antimycobacterial effect. Although some cationic amphiphiles have been identified to be effective against mycobacteria, the physicochemical properties to target the mycobacterial membrane are not well-understood.[18] In addition, mycobacteria can be found inside of macrophages[25]; therefore, balancing amphiphilicity must be considered for an effective and non-toxic antimycobacterial agent .

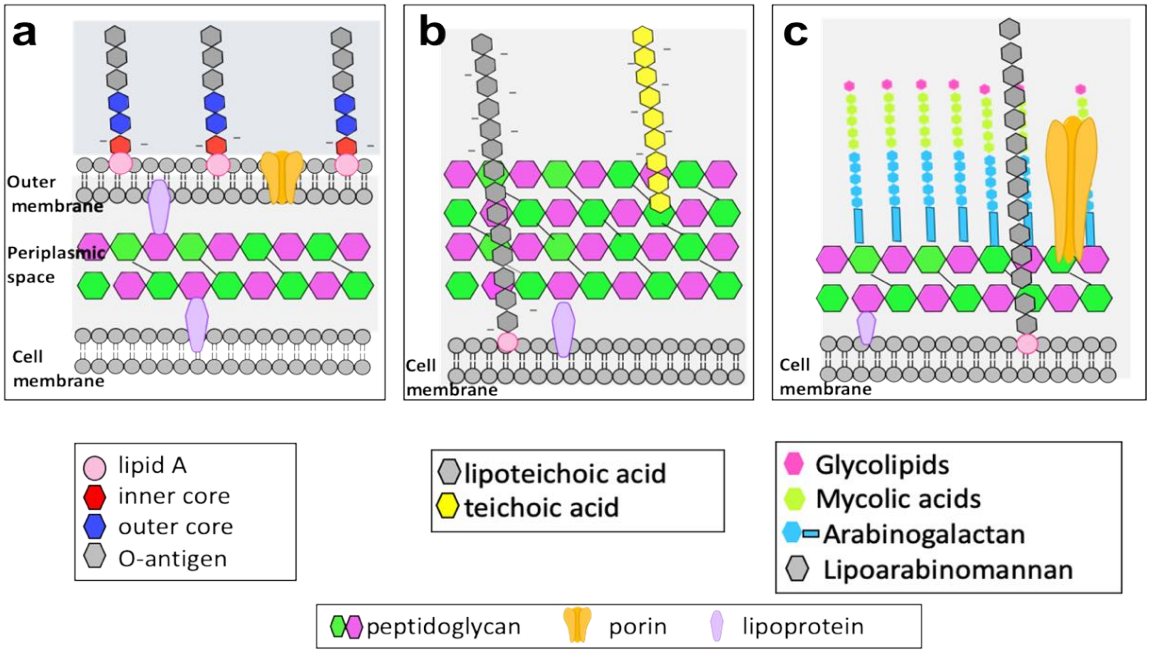

Figure 1.6. Composition of the cell wall structure of a) Gram-negative b) Gram-positive, and c) Mycobacteria (adapted from [26]).

1.3.1 Eukaryotic Cell Membrane

Unlike prokaryotes, eukaryotic cells possess internal membranes that encase their organelles. The plasma membrane of eukaryotic cells are more complex with increased hydrophobicity than bacterial cell walls, where the outer leaflet is mostly

composed of phosphatidylcholine, sphingomyelin, and glycolipids while the inner leaflet is more anionic due to the presence of phosphatidylserine, and phosphatidylinositol (Figure 1.7).[27,28] These substantial differences make the chemical environment surrounding eukaryotic cells dissimilar to that of Gram- negative and -positive bacterial cells, but rather challenging when designing selectivity towards mycobacteria, due its waxy and hydrophobic cell wall.

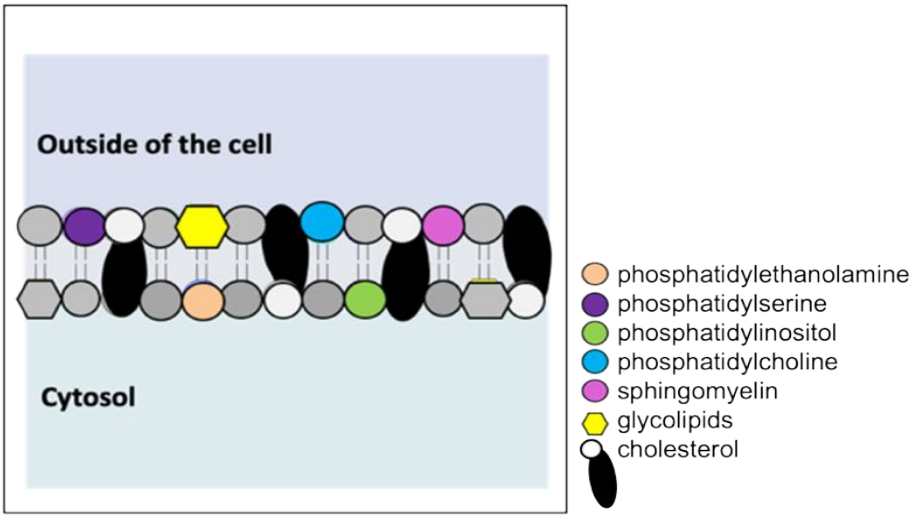

Figure 1.7. The lipid components of the plasma membrane. (adapted from [27]).

1.3.2 Membrane Targeting Anti-TB Drugs

There are two main categories of mycobacterial membrane targeting agents. The first class of agents are characterized by being cationic amphiphiles where balanced hydrophobicity and positive charge density is crucial for direct disruption of the membrane integrity.[17,32] The second class are known for disrupting the function of proteins in the membrane. It is not well-defined what are the physicochemical requirements for the latter agents to effectively target the mycobacteria membrane without disrupting it.[18]

1.4 Antimicrobial Peptides and Synthetic Mimics

Cationic amphiphiles tend to be modeled after naturally occurring antimicrobial peptides (AMPs). AMPs are ubiquitous short peptides in multicellular organisms.[33] The two main functions of AMPs are to modulate the host immune system, and to kill bacteria without harming the host cells. AMPs are secondary structures containing mostly cationic and hydrophobic amino acid residues responsible for its potent activity against microbes.[34] Due to the highly anionic environment of most bacteria, initial electrostatic interactions occur; then the interaction of the hydrophobic moieties and the lipids can cause membrane disruption (Figure 1.8). Alternatively, the initial adsorption causes an indirect effect in the membrane by disruption intracellular functions via various mechanisms (Figure 1.8).[33,35,36]

The innate selectivity of AMPs against bacterial over mammalian cells is attributed to the careful balancing of amphiphilicity and cationic density, as increasing lipophilicity can result in toxicity to mammalian cells. AMPs are an appealing candidate for antimicrobial treatment due to their innate selectivity of over mammalian cells, unconventional mode of action, and broad-spectrum activity.[33,34] Nonetheless, potential toxicity, enzymatic stability and selectivity to specific microbes have limited AMPs to topical use in clinical applications.[35]

To overcome these pitfalls, synthetic mimics of AMPs are being studied as a tunable alternative to increase selectivity against specific microbes, stability against hydrolysis by proteases and offer a more cost-effective synthetic pathway. Generally, AMP-mimics design includes biocidal backbones, biocide-releasing or biocidal pendants with cationic and hydrophobic moieties that lead to its broad-spectrum potent activity against microbes.

The biocidal agents can kill bacteria upon contact and can be either cationic biocides, antimicrobial peptides, or antibiotics, where the mode of action is dependent on the biocidal agent.[37,38]

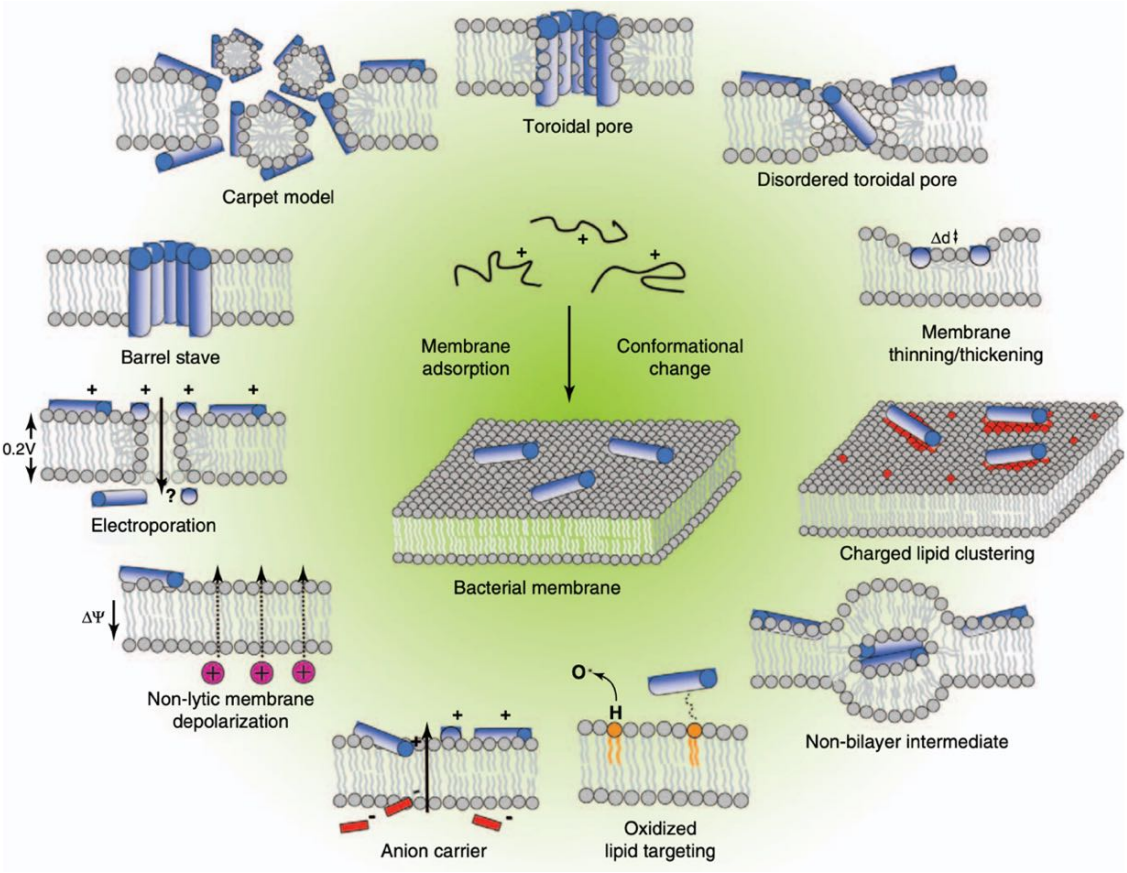

Figure 1.8. Proposed mechanisms of AMPs acting on bacterial membrane.[35]

Some common modifications of cationic biocidal mimics include positively charged quaternary ammonium or guanidium as the cationic moiety, due to the ubiquitous presence of lysine and arginine. Aida et al. reported stronger interaction of guanidinium ions with the membrane over the ammonium ions. The effect was attributed to the deprotonation of adjacent ammonium ions to minimize charge repulsion. Due to the H-

bonding capabilities of guanidium, guanidinium ions are able to minimized charge repulsion effectively via divalent salt-bridge with phosphate ions on the membrane (Figure 1.9).[39]

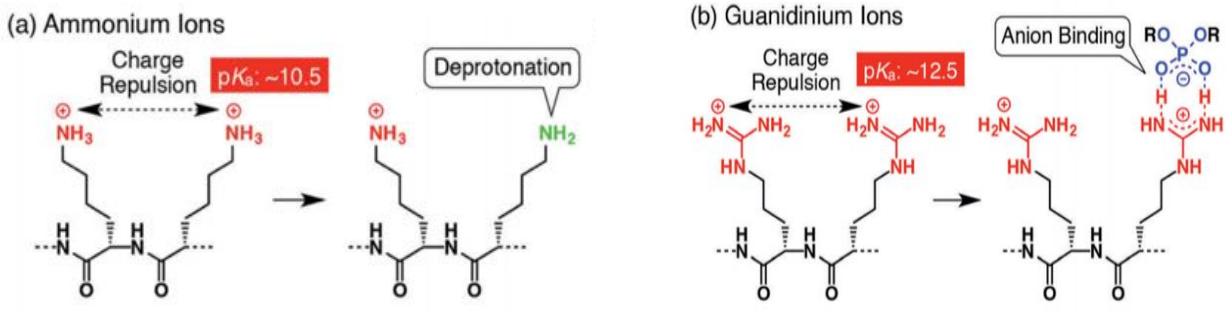

Figure 1.9. Minimization of intramolecular charge repulsion between (a) proximal ammonium ions by deprotonation and (b) proximal guanidinium ions by anion binding to phosphate groups.[39]

Furthermore, Tew et al. showed amphiphilic cationic polymers can be tuned to be highly active toward bacteria while retaining low cytotoxicity (Figure 1.10). The high density of positive charged guanidium on a cationic polymer showed to increase adsorption onto negatively charged bacterial membranes in comparison to the ammonium analogue, and Magainin, a naturally occurring AMP.[40]

Although AMPs and AMP-mimics effectiveness against mycobacteria is scarce in comparison to Gram- positive and -negative bacteria, a few have been reported in literature. For example, Purdy et al. concluded that Ub2, cationic amphiphile ubiquitin-peptide synthetic agent disrupted the bacterial membrane.[14] Phillips et al. reported poly(dimethylaminoethyl methacrylate), a cationic synthetic AMP-mimic that showed selective antimycobacterial properties over Gram-positive bacteria, via an alternative mechanism than the predicted outer memabrane damage. [41] Furthermore, Li et al.

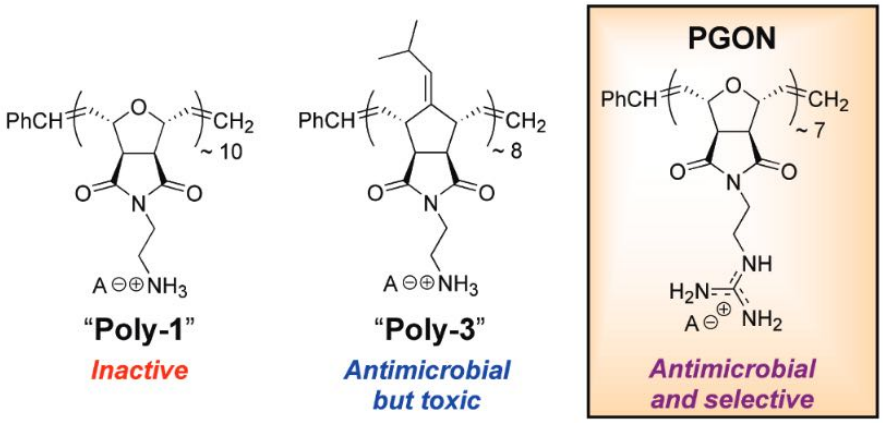

Figure 1.10. Tew et al showed guanidium pendant polymers showed broader spectrum activity as well as selectivity in comparison to ammonium analog and known AMP, Magainin. [40]

investigated triphenylphosphonium (TPP) indole, a cationic amphiphile, and concluded its antimycobacterial properties were due to caused depolarization of the mycobacterial membrane.[42] Similarly, Chen and coworkers observed that the known efflux pump inhibitor, verapamil caused dissipation of the membrane energetics in mycobacteria which triggered an indirect inhibition of efflux pumps, not direct as previously speculated.[43] These examples demonstrated that cationic amphiphiles mimicking AMPs can be designed to target the mycobacteria membrane, directly or indirectly**.**

1.5 Guanylurea Functional Group

Guanidine-derivatives containing guanylurea (i.e., amidinourea) functional group are a class of underexplored compounds composed of guanidine and urea, the extending H-bonding combabilities (Figure 1.11). Castagnolo et al discovered that both macrocyclic and linear amidinourea derivatives contained antifungal and antiviral activity.[44,45] Guanylurea

derivatives have also shown antiproliferative properties; it was speculated to be due to their ability to mimic the natural nucleobases and interact with DNA.[46]

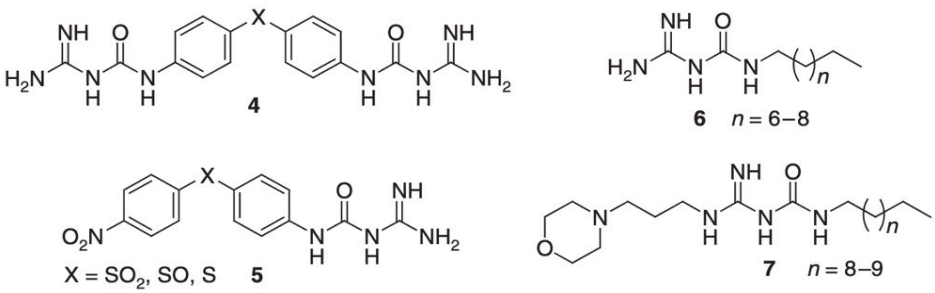

Figure 1.11. Examples of guanylurea derivatives.[47]

Furthermore, our research group reported the rigidity around guanylurea and the extended hydrogen bonding capabilities from guanylurea in poly(guanylurea)s-piperazine (PGU-P) had significant selective antimicrobial property towards mycobacteria, *M. smegmatis*, in comparison to Gram-positive and Gram-negative bacteria (Figure 1.12).[48] Previous work gave the motivation to further investigate the mechanism of action against mycobacteria and explore the structure-activity relationship (SAR) of these novel compounds.

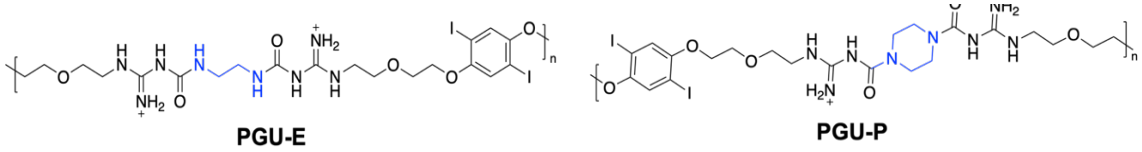

Figure 1.12. Structures of PGU-E and PGU-P previously tested for antimicrobial properties, where PGU-P was found to have better antimicrobial activity against mycobacteria.[48]

1.5.1 Synthesis of Poly(guanylurea)s

A simple polymerization technique was used to make affordable and non-toxic oligomers. Step-growth polycondensation allowed to have one-pot synthesis of a controlled addition of bifunctional monomers without the need of a catalyst while yielding oligomers due to small number of repeating units (Scheme 1.1).[49]

Scheme 1.1. Schematic of polycondensation of bifunctional monomers with guanylurea backbone.

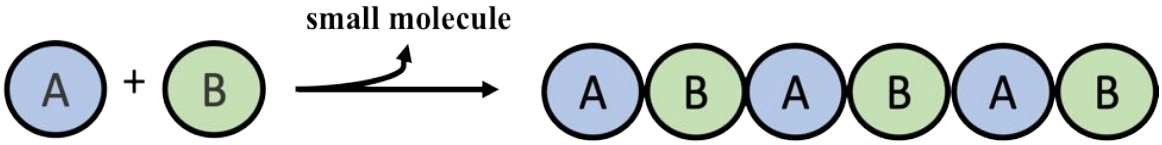

1.5.2 Mechanism of Poly(guanylurea)s

Following the basic principles of step-growth polymerization, guanylurea oligomers were synthesize by using bi-functional monomers *a* and *b*. For simplicity, monomer a shows one sided *N,N'*-di-tert-butyloxycarbonyl (boc) protected guanidine in Scheme 1.2. The addition of a base or the diamine initiates the reaction by extracting the most acidic proton adjacent to the boc-group leading to the formation of the isocyanate intermediate. The diamine performs a nucleophilic attack on the isocyanate producing the guanylurea.[50] The successive repetition of this process links monomer *a* and monomer *b* forming guanylurea in the backbone and producing the desired alternating copolymer (Scheme 1.1). Similarly, some polymers were made using a diisocyanate bifunctional monomer and a guanidinium monomer where the initial acid-base reaction is omitted for a synthetic pathway.

Scheme 1.2. Schematic of the mechanism for the formation of guanylurea in the backbone.[50]

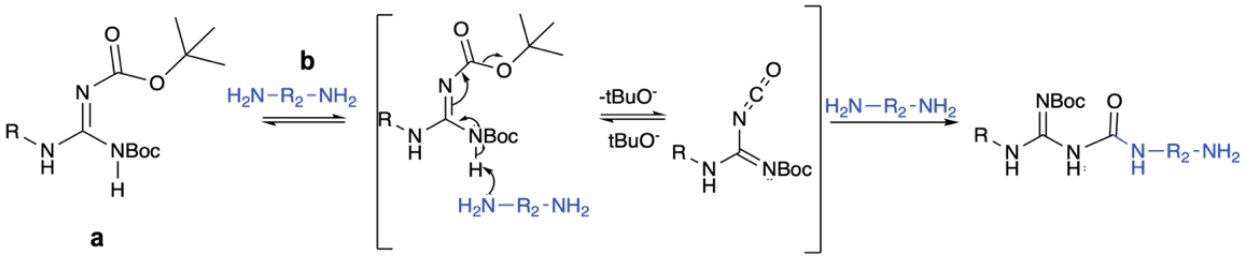

1.6 Previous Work on Poly(guanylurea)s

Our group previously reported that the rigidity in the poly(guanylurea) backbone influences the minimum inhibitory concentration (MIC) and hemolytic activity of PGUs (Figure 1.12).[48] The results of the ethidium bromide assay after treating *M. smegmatis, S. aureus* and *S. flexneri* with PGU-P-8K and PGU-E-11K suggested that the increased fluorescence intensity was due to possible membrane disruption (Figure 1.13C). Additionally, few transmission electron microscopy (TEM) images appeared to show a severely damaged membrane integrity by PGU-P-8K 24 h treatment (Figure 1.13B). Preliminary results showed that the primary mechanism of action was due to disruption of the membrane, as many AMPs and AMP-mimics do.[48] SAR studies showed that rigidity in the backbone structure played an important role in antimicrobial properties (Figure 1.13), but further analysis was required for a thorough understanding of the mode of action and selectively from PGU-P-8K on the mycobacterial membrane.

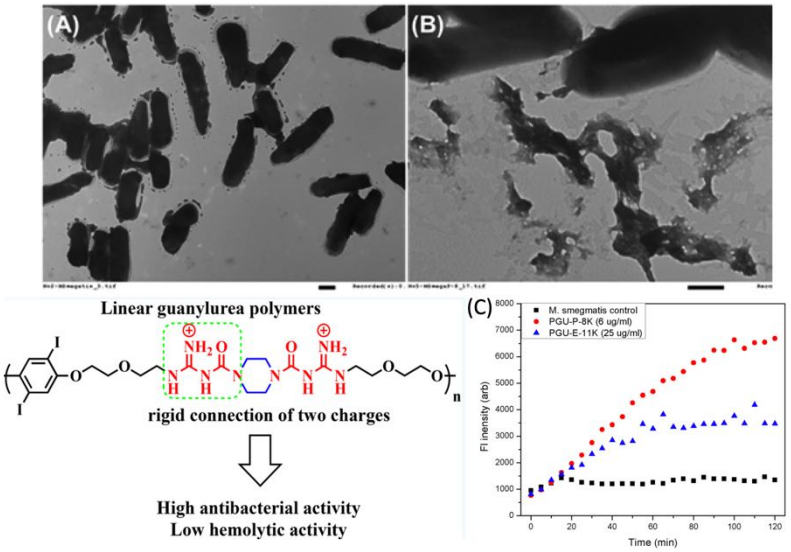

Figure 1.13. PGU-P previously that rigidity in the backbone structure played an important role in antimicrobial properties. TEM image of *M. smegmatis.* (A) intact cells and (B) cells treated with PGU-P-8K. Scale bars: 500 nm (C) Kinetics of EB membrane permeation and nucleic acids intercalation.[48]

1.7 Summary

The continuation of previously reported work PGUs was focused on the mechanism of action of these novel compounds. It additionally explored various degrees of amphiphilicity, rigidity and aromaticity to understand the innate selective antimycobacterial properties of PGUs. The overall aim of this dissertation was to thoroughly study PGU-P-8K to identify the necessary key factors for innate selectively on the mycobacterial membrane. Therefore, contributing to the development of unconventional membrane targeting anti-TB drugs or drug adjuvants to improve TB treatment.

Chapter 2 emphasized on elucidating the mechanism of action of PGU-P-8K against the mycobacteria model organism, *M. smegmatis* for future improvements TB therapy; the unique selectivity of PGU-P-8K was due membrane targeting effect. PGU-

P-8K was found to disrupt bioenergetics in mycobacterial membrane, resulting in a selective and fast-acting bactericidal agent.

Chapter 3 explored how the key functionalities (i.e., aromatic substituents, amphiphilicity, rigidity) along the backbone of PGUs affect interaction to the mycobacterial membrane and inherit antimycobacterial properties. Pathogenic mycobacteria showed the most sensitivity to minor structural changes, where retaining hydrophobicity in PGUs showed to be crucial for membrane interaction.

Lastly, the summation of the work investigated the translational outlook of PGUs due to activity on hydrophobic cell membrane, non-toxicity, and possible cellular entry. Preliminary R-PE delivery was performed using PGUs as a vehicle of intracellular delivery of proteins.

1.8 References

(1) Antimicrobial Resistance https://www.who.int/news-room/fact-sheets/detail/antimicrobial-resistance#:~:text=What is antimicrobial resistance%3F,spread%2C severe illness and death.

(2) Dookie, N.; Rambaran, S.; Padayatchi, N.; Mahomed, S.; Naidoo, K. Evolution of Drug Resistance in Mycobacterium Tuberculosis: A Review on the Molecular Determinants of Resistance and Implications for Personalized Care. *J. Antimicrob. Chemother.* **2018**, *73* (5), 1138–1151. https://doi.org/10.1093/jac/dkx506.

(3) Tommasi, R.; Brown, D. G.; Walkup, G. K.; Manchester, J. I.; Miller, A. A. ESKAPEing the Labyrinth of Antibacterial Discovery. *Nature reviews. Drug discovery*. England August 2015, pp 529–542. https://doi.org/10.1038/nrd4572.

(4) Centers for Disease Control and Prevention. About Antibiotic Resistance. *Antibiot. / Antimicrob. Resist. (AR / AMR)*.

(5) Antibiotic/ Antimicrobial Resistance (AR/AMR) https://www.cdc.gov/drugresistance/about.html.

(6) Global Antimicrobial Resistance and Use Surveillance System (GLASS) /GLASS-AMR Module https://www.who.int/initiatives/glass/glass-routine-data-surveillance.

(7) WHO. Tuberculosis https://www.who.int/health-topics/tuberculosis#tab=tab_2.

(8) WHO. https://www.who.int/health-topics/tuberculosis#tab=tab_1.

(9) CDC. Treatment of Tb Disease https://www.cdc.gov/tb/topic/treatment/tbdisease.htm.

(10) Global Tuberculosis Data https://www.who.int/teams/global-tuberculosis-programme/data.

(11) Tuberculosis Drugs and Mechanisms of Action. *Natl. Inst. Allergy Infect. Dis.* **2016**.

(12) Xu, X.; Xu, L.; Yuan, G.; Wang, Y.; Qu, Y.; Zhou, M. Synergistic Combination of Two Antimicrobial Agents Closing Each Other's Mutant Selection Windows to Prevent Antimicrobial Resistance. *Sci. Rep.* **2018**, *8* (1), 1–7. https://doi.org/10.1038/s41598-018-25714-z.

(13) Andersen, J. L.; He, G. X.; Kakarla, P.; Ranjana, K. C.; Kumar, S.; Lakra, W. S.; Mukherjee, M. M.; Ranaweera, I.; Shrestha, U.; Tran, T.; Varela, M. F. Multidrug Efflux Pumps from Enterobacteriaceae, Vibrio Cholerae and Staphylococcus Aureus Bacterial Food Pathogens. *Int. J. Environ. Res. Public Health* **2015**, *12* (2), 1487–1547. https://doi.org/10.3390/ijerph120201487.

(14) Purdy, G. E.; Niederweis, M.; Russell, D. G. Decreased Outer Membrane Permeability Protects Mycobacteria from Killing by Ubiquitin-Derived Peptides. *Mol. Microbiol.* **2009**, *73* (5), 844–857. https://doi.org/10.1111/j.1365-2958.2009.06801.x.

(15) Lederer, E. The Mycobacterial Cell Wall. *Pure Appl. Chem.* **1971**, *25* (1), 135–166. https://doi.org/10.1351/pac197125010135.

(16) Brennan, P. J. Structure, Function, and Biogenesis of the Cell Wall of Mycobacterium Tuberculosis. *Tuberculosis* **2003**, *83* (1–3), 91–97. https://doi.org/10.1016/S1472-9792(02)00089-6.

(17) Chen, H.; Nyantakyi, S. A.; Li, M.; Gopal, P.; Aziz, D. B.; Yang, T.; Moreira, W.; Gengenbacher, M.; Dick, T.; Go, M. L. The Mycobacterial Membrane: A Novel Target Space for Anti-Tubercular Drugs. *Front. Microbiol.* **2018**, *9* (JUL), 1–11. https://doi.org/10.3389/fmicb.2018.01627.

(18) Hurdle, J. G.; O'Neill, A. J.; Chopra, I.; Lee, R. E. Targeting Bacterial Membrane Function: An Underexploited Mechanism for Treating Persistent Infections. *Nat. Rev. Microbiol.* **2011**, *9* (1), 62–75. https://doi.org/10.1038/nrmicro2474.

(19) Rao, S. P. S.; Alonso, S.; Rand, L.; Dick, T.; Pethe, K. The Protonmotive Force Is Required for Maintaining ATP Homeostasis and Viability of Hypoxic, Nonreplicating Mycobacterium Tuberculosis. *Proc. Natl. Acad. Sci. U. S. A.* **2008**, *105* (33), 11945–11950. https://doi.org/10.1073/pnas.0711697105.

(20) GM, C. Cell Membranes https://www.ncbi.nlm.nih.gov/books/NBK9928/.

(21) Beveridge, T. J. Structures of Gram-Negative Cell Walls and Their Derived Membrane Vesicles. *J. Bacteriol.* **199AD**, *181*, 4725–4733.

(22) Kulp, A.; Kuehn, M. J. Biological Functions and Biogenesis of Secreted Bacterial Outer Membrane Vesicles. *Annu. Rev. Microbiol* **2010**, *64*, 163–184.

(23) Costerton, J. W., Ingram, J. M. & Cheng, K. J. Structure and Function of the Cell Envelope of Gramnegative Bacteria. *Bacteriol. Rev.* **1974**, *38*, 87–110.

(24) Shockman, G. D. & Barrett, J. F. Structure, Function, and Assembly of Cell Walls of Gram-Positive Bacteria. *Annu. Rev. Microbiol.* **1983**, *37*, 501–527.

(25) Roux, A. L.; Viljoen, A.; Bah, A.; Simeone, R.; Bernut, A.; Laencina, L.; Deramaudt, T.; Rottman, M.; Gaillard, J. L.; Majlessi, L.; Brosch, R.; Girard-Misguich, F.; Vergne, I.; de Chastellier, C.; Kremer, L.; Herrmann, J. L. The Distinct Fate of Smooth and Rough Mycobacterium Abscessus Variants inside Macrophages. *Open Biol.* **2016**, *6* (11). https://doi.org/10.1098/rsob.160185.

(26) Brown, L.; Wolf, J. M.; Prados-Rosales, R.; Casadevall, A. Through the Wall: Extracellular Vesicles in Gram-Positive Bacteria, Mycobacteria and Fungi. *Nat. Rev. Microbiol.* **2015**, *13* (10), 620–630. https://doi.org/10.1038/nrmicro3480.

(27) GM, C. The Cell: A Molecular Approach; Sinauer Associates: Suderland, 2000.

(28) Lombard, J. Once upon a Time the Cell Membranes: 175 Years of Cell Boundary Research. *Biol. Direct* **2014**, *9*, 32. https://doi.org/10.1186/s13062-014-0032-7.

(29) Schorey, J. S.; Sweet, L. The Mycobacterial Glycopeptidolipids: Structure, Function, and Their Role in Pathogenesis. *Glycobiology* **2008**, *18* (11), 832–841. https://doi.org/10.1093/glycob/cwn076.

(30) Jankute, M.; Nataraj, V.; Lee, O. Y. C.; Wu, H. H. T.; Ridell, M.; Garton, N. J.; Barer, M. R.; Minnikin, D. E.; Bhatt, A.; Besra, G. S. The Role of Hydrophobicity in Tuberculosis Evolution and Pathogenicity. *Sci. Rep.* **2017**, *7* (1), 1–10. https://doi.org/10.1038/s41598-017-01501-0.

(31) Brennan, P. J.; Goren, M. B. Structural Studies on the Type-Specific Antigen and Lipids of the Mycobacterium Avium. Mycobacterium Intracellulare. Mycobacterium Scrofulaceum Serocomplex. Mycobacterium Intracellulare Serotype 9. *J. Biol. Chem.* **1979**, *254* (10), 4205–4211. https://doi.org/10.1016/s0021-9258(18)50716-x.

(32) Cholo, M. C.; Mothiba, M. T.; Fourie, B.; Anderson, R. Mechanisms of Action and Therapeutic Efficacies of the Lipophilic Antimycobacterial Agents Clofazimine and Bedaquiline. *J. Antimicrob. Chemother.* **2017**, *72* (2), 338–353. https://doi.org/10.1093/jac/dkw426.

(33) Hancock, R. E. W.; Sahl, H. G. Antimicrobial and Host-Defense Peptides as New Anti-Infective Therapeutic Strategies. *Nat. Biotechnol.* **2006**, *24* (12), 1551–1557. https://doi.org/10.1038/nbt1267.

(34) van der Does, A. M.; Hiemstra, P. S.; Mookherjee, N. *Antimicrobial Host Defence Peptides: Immunomodulatory Functions and Translational Prospects*; 2019; Vol. 1117. https://doi.org/10.1007/978-981-13-3588-4_10.

(35) Nguyen, L. T.; Haney, E. F.; Vogel, H. J. The Expanding Scope of Antimicrobial Peptide Structures and Their Modes of Action. *Trends Biotechnol.* **2011**, *29* (9), 464–472. https://doi.org/10.1016/j.tibtech.2011.05.001.

(36) Wimley, W. C. Describing the Mechanism of Antimicrobial Peptide Action with the Interfacial Activity Model. *ACS Chem. Biol.* **2010**, *5* (10), 905–917. https://doi.org/10.1021/cb1001558.

(37) Hutnick, M. A.; Pokorski, J. K. Polymeric Interventions for Microbial Infections: A Review. *Mol. Pharm.* **2018**, *15* (8), 2910–2921. https://doi.org/10.1021/acs.molpharmaceut.8b00342.

(38) Santos, M. R. E.; Fonseca, A. C.; Mendonça, P. V.; Branco, R.; Serra, A. C.; Morais, P. V.; Coelho, J. F. J. Recent Developments in Antimicrobial Polymers: A Review. *Materials*. MDPI AG 2016. https://doi.org/10.3390/MA9070599.

(39) Mogaki, R.; Hashim, P. K.; Okuro, K.; Aida, T. Guanidinium-Based "Molecular Glues" for Modulation of Biomolecular Functions. *Chem. Soc. Rev.* **2017**, *46* (21), 6480–6491. https://doi.org/10.1039/c7cs00647k.

(40) Gabriel, G. J.; Madkour, A. E.; Dabkowski, J. M.; Nelson, C. F.; Nüsslein, K.; Tew, G. N. Synthetic Mimic of Antimicrobial Peptide with Nonmembrane-Disrupting Antibacterial Properties. *Biomacromolecules* **2008**, *9* (11), 2980–2983. https://doi.org/10.1021/bm800855t.

(41) Phillips, D. J.; Harrison, J.; Richards, S. J.; Mitchell, D. E.; Tichauer, E.; Hubbard, A. T. M.; Guy, C.; Hands-Portman, I.; Fullam, E.; Gibson, M. I. Evaluation of the Antimicrobial Activity of Cationic Polymers against Mycobacteria: Toward Antitubercular Macromolecules. *Biomacromolecules* **2017**, *18* (5), 1592–1599. https://doi.org/10.1021/acs.biomac.7b00210.

(42) Li, M.; Nyantakyi, S. A.; Gopal, P.; Aziz, D. B.; Dick, T.; Go, M. L. Indolylalkyltriphenylphosphonium Analogues Are Membrane-Depolarizing Mycobactericidal Agents. *ACS Med. Chem. Lett.* **2017**, *8* (11), 1165–1170. https://doi.org/10.1021/acsmedchemlett.7b00287.

(43) Chen, C.; Gardete, S.; Jansen, R. S.; Shetty, A.; Dick, T.; Rhee, K. Y.; Dartois, V. *Verapamil Targets Membrane Energetics in Mycobacterium Tuberculosis*; 2018.

(44) Manetti, F.; Castagnolo, D.; Raffi, F.; Zizzari, A. T.; Rajamaki, S.; D'Arezzo, S.; Visca, P.; Cona, A.; Fracasso, M. E.; Doria, D.; Posteraro, B.; Sanguinetti, M.; Fadda, G.; Botta, M. Synthesis of New Linear Guanidines and Macrocyclic Amidinourea Derivatives Endowed with High Antifungal Activity against Candida Spp. and Aspergillus Spp. *J. Med. Chem.* **2009**, *52* (23), 7376–7379. https://doi.org/10.1021/jm900760k.

(45) Toscani, A.; Denaro, R.; Pacheco, S. F. C.; Biolatti, M.; Anselmi, S.; Dell'oste, V.; Castagnolo, D. Synthesis and Biological Evaluation of Amidinourea Derivatives against Herpes Simplex Viruses. *Molecules* **2021**, *26* (16), 1–8. https://doi.org/10.3390/molecules26164927.

(46) Bass, R.; Jenkinson, S.; Wright, J.; Smulders-Srinivasan, T.; Marshall, J. C.; Castagnolo, D. Synthesis and Biological Evaluation of Amidinourea and Triazine Congeners as Inhibitors of MDA-MB-231 Human Breast Cancer Cell Proliferation. *ChemMedChem* **2017**, *12* (4), 288–291. https://doi.org/10.1002/cmdc.201600580.

(47) Castagnolo, D. Chemistry and Biological Properties of Amidinoureas: Strategies for the Synthesis of Original Bioactive Hit Compounds. *New Strateg. Chem. Synth. Catal.* **2012**, 97–126. https://doi.org/10.1002/9783527645824.ch5.

(48) Ahmed, M. S.; Annamalai, T.; Li, X.; Seddek, A.; Teng, P.; Tse-Dinh, Y. C.; Moon, J. H. Synthesis of Antimicrobial Poly(Guanylurea)S. *Bioconjug. Chem.* **2018**, *29* (4), 1006–1009. https://doi.org/10.1021/acs.bioconjchem.8b00057.

(49) Wang, M.; Guo, L.; Sun, H. Manufacture of Biomaterials; Narayan, R. B. T.-E. of B. E., Ed.; Elsevier: Oxford, 2019; pp 116–134. https://doi.org/https://doi.org/10.1016/B978-0-12-801238-3.11027-X.

(50) Miel, H.; Rault, S. Conversion of N,N'-Bis(Tert-Butoxycarbonyl)Guanidines to N-(N'-Tert-Butoxycarbonylamidino)Ureas. *Tetrahedron Lett.* **1998**, *39* (12), 1565–1568. https://doi.org/10.1016/S0040-4039(98)00025-2.

CHAPTER 2

PROTON MOTIVE FORCE-DISRUPTING ANTIMYCOBACTERIAL GUANYLUREA POLYMER

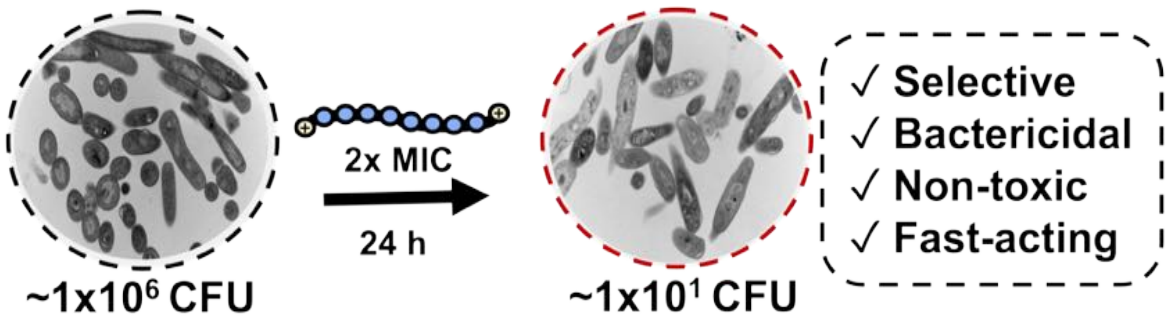

2.1 Abstract

Tuberculosis (TB) is a severe threat to global public health. Nonreplicating TB is extremely difficult to eradicate using current TB drugs which primarily act on replicating cells. Novel anti-TB drugs acting on unconventional targets are urgently needed to efficiently combat TB and shorten TB treatment. The mycobacterial membrane is a putative drug target as many transmembrane proteins and vital processes reside in the membrane. Additionally, macromolecules have shown to be advantageous over small molecules due to strong initial adsorption to the bacterial membrane. Although membrane disrupting antimicrobial peptides and their synthetic mimics exhibit the potential to kill nonreplicating TB, the lack of microbe selectivity, especially towards mycobacteria, has been a concern. Here, we report that the recently developed poly(guanylurea-piperazine)-8K (PGU-P-8K) shows fast (i.e., less than a day) at its minimum bactericidal concentration (MBC). This effect was further explored and attributed it to the interference of the Proton Motive Force (PMF) through disruption of the membrane potential via selective interaction PGU-P-8K to the mycobacterial membrane. PGU-P-8K displayed targeting the mycobacterial cell envelope by disrupting intracellular processes while retaining the cell membrane integrity, confirmed by imagining of post-treatment cells and overexpression of genes related to cell envelope stress. Additionally, PGU-P-8K potentiates bedaquiline, an oxidative phosphorylation-targeting anti-TB drug. Targeting membrane energetics is a promising approach to combat drug-resistant or latent mycobacterial infections as both replicating and dormant mycobacteria rely on a polarized membrane for their survival. The in-depth studies on the mode of action of PGU-P-8K on mycobacteria affect selectivity and

bactericidal activity on mycobacteria contributes to the development of a novel class of membrane-targeting drugs or drug adjuvants for improving TB treatment.

2.2 Introduction

Tuberculosis (TB) is a deadly infectious disease caused by *Mycobacterium tuberculosis* (*Mtb*).[1] The current TB treatment regimen is lengthy (i.e., 4-9 months) and rigorous (i.e., the daily dose of a combination of four drugs) due to difficulties associated with multidrug resistance (MDR) and nonreplicating *Mtb*.[2,3] Because most anti-TB drugs were developed to act on replicating cells, slow or nongrowing cells (i.e., persisters) are especially hard to target using traditional strategies. Therefore, current efforts have focused on developing new drugs and drug combinations that act on unconventional targets to efficiently kill the subpopulation of *Mtb* to shorten the treatment period.[4,5]

Targeting the bacterial membrane has gained recent attention as a promising strategy to overcome MDR and eradicate dormant mycobacteria, since an energized membrane is essential for the survival of both replicating and nonreplicating TB.[6] Additionally, maintaining membrane energetics is vital for mycobacteria as numerous energy metabolic processes reside in the membrane; hence disturbing the membrane would seriously impede the bacteria from acquiring resistance or lead to death.[7] The precise mechanism essential for persistence in dormant *Mtb* is not well-understood. Nonetheless, some of the recently introduced anti-tb drugs that target the membrane energetics have shown to be advantageous. [8] For example, pyrazinamide (PZA), a first-line TB drug, played a crucial role in shortening treatment from 9-12 to 6 months, as it affects membrane transport functions by depolarizing the membrane potential, thus disrupting energy metabolism.[9–11]

Alternatively, broad-spectrum antimicrobial peptides (AMPs) and their synthetic mimics are a promising class of macromolecular antibiotics owing it to their unique bactericidal mechanism.[12,13] By carefully balancing the hydrophobicity and charge density, AMPs selectively induce disruption of the bacterial membranes over mammalian cells.[14] Alternatively, AMPs could adsorb onto the bacterial membrane and cause a non-lytic membrane depolarization. [15]Although a promising approach, AMPs' poor stability to enzymes and selectivity to specific microbes has limited AMPs to primarily topical uses in clinical applications.[16,17]

While most AMPs and AMP mimics exhibit relatively high efficiency against Gram-positive and -negative bacteria, a limited number of AMPs and AMP mimics have been reported to show mycobacterial selectivity with high efficacy (i.e., ubiquitin and ubiquitin derivatives).[18–20] Compared to other bacteria, the mycobacterial envelope is rigid, waxy, and less negatively charged, making the membrane interaction of positively charged AMPs and AMP mimics inefficient.[4,21–23] Therefore, the design principle of AMP mimics, which has high emphasis on a careful balancing on the positive charge and hydrophobicity of the pendant side chains, should be revised to improve mycobacterial selectivity.[16,18,24,25]

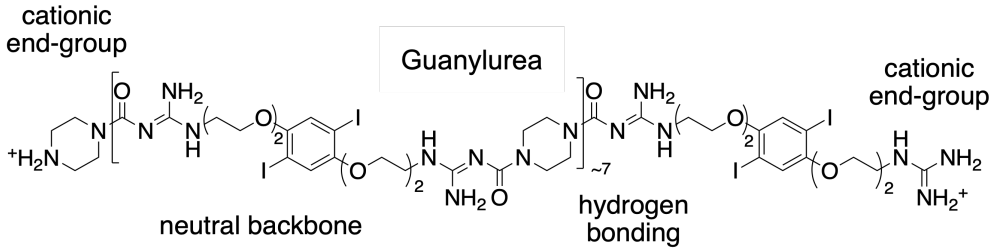

Figure 2.1. Chemical structure of PGU-P-8K.

Previously, our group reported a new class of poly(guanylurea)s (PGUs) (Figure 2.1) exhibiting high antimycobacterial selectivity over other microbes and low toxicity.[19] The

unique poly(guanylurea-piperazine)-8K (PGU-P-8K) backbone showed to mimic AMPs by targeting the mycobacterial membrane. Due to the architectural design, it was initially hypothesized that PGU-P-8K disrupted the membrane integrity. However, the mode of action was further explored to elucidate if the effect of PGU-P-8K on the mycobacterial membrane is direct (i.e., membrane integrity) or indirect (i.e., bioenergetics), as broad-spectrum activity is usually observed upon membrane disruption.

In this article, we report a novel antimycobacterial mechanism of action of PGU-P-8K. We found that the PGU-P-8K backbone is neutral under physiological conditions and PGU-P-8K treatment of *Mycobacterium smegmatis* (*Msm*) does not promote intracellular accumulation of membrane-impermeable dyes or physical membrane damage detectable by transmission electron microscopy (TEM). Instead, PGU-P-8K exhibits fast, and selective bactericidal effects without compromising the viability of hepatic and macrophage cells, depolarization of the membrane potential ($\Delta\psi$), and overexpression of genes associated with membrane-stress sensing. From these observations, we conclude that PGU-P-8K primarily acts on the membrane energetics by dissipating the major component of the proton motive force (PMF). Consistently, PGU-P-8K potentiates anti-TB drugs that act on the membrane energetics. Conclusively, the evidence supports the novel design concept of PGU-P-8K could contribute to developing a new class of fast-acting membrane-targeting macromolecules as anti-TB drugs or drug adjuvants.

2.3 Results and Discussion

PGU-P-8K was synthesized by following the previously reported method.[19] The average molecular weight (8 kDa) of PGU-P-8K was confirmed by both gel permeation chromatography (GPC) and proton nuclear magnetic resonance (H NMR) spectroscopy

(Figure 2.14), indicating that the number of PGU-P repeating unit is ~7. The pKa of PGU-P-8K was determined as ~5 (Figure 2.2), indicating that the PGU-P-8K backbone is neutral in the physiological condition while the two chain end groups (i.e., secondary amine and guanidine, Figure 2.1) are positively charged. [19]

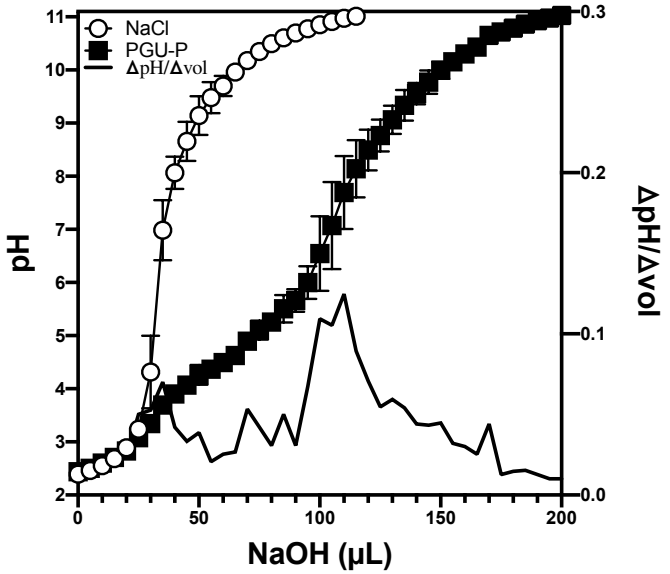

Figure 2.2. Determination of pka via pH titration curve using 2mM PGU-P-8K in 100mM NaCl using 25mM NaOH from pH 2.5 to 11. Data shows the mean of three independent experiments +/- standard deviation.

Toxicity of PGU-P-8K was further explore against macrophages derived from the murine reticulosarcoma cell line J774, and epithelial-like cells derived from human hepatocellular carcinoma cell line HepG2. Since mycobacteria primarily infect macrophages and HepG2 [30,31]is commonly used in drug metabolism and hepatoxicity studies[32], they were selected as a cellular model for toxicity testing. Nonhemolytic PGU-P-8K[19] showed no indication of decreased cell viability of a J774 and Hep G2 up to 200 µg/mL (Figure 2.3).

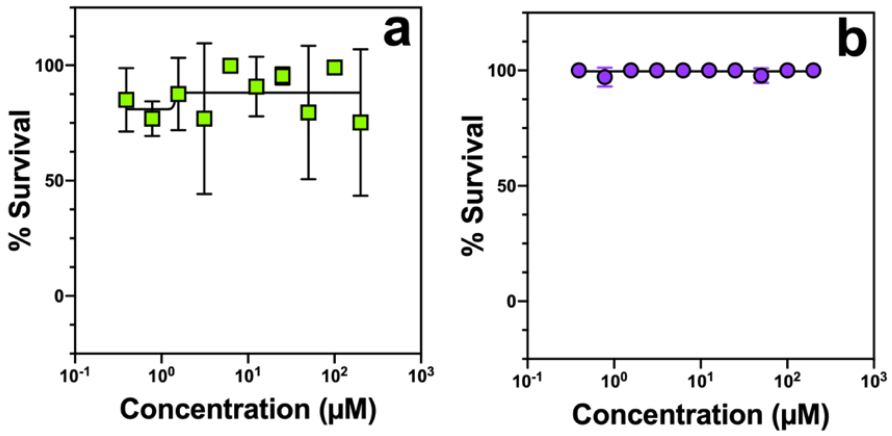

Figure 2.3. Toxicity of PGU-P-8K on cell lines a) J774, murine macrophage, and b HepG2, hepatic cell line) cell lines. It was found to be non-toxic to HepG2 and J774.

Minimum inhibitory concentrations (MICs) of PGU-P-8K confirmed the mycobacterial selectivity over other microbes including Gram-positive (*Staphylococcus aureus*), Gram-negative (*Escherichia coli*, *Burkholderia cepacia*, and *Pseudomonas aeruginosa*), and a fungus (*Candida albicans*) (Table 2.1). Interestingly, the MIC against *Msm* cultured in Luria broth (LB) was increased ~four times compared with that of the same *Msm* cultured in 7H9 medium (Table 2.2). Because the lipid composition could be affected by culturing conditions,[33] lipid extraction was performed after *Msm* cultured in 7H9, or LB and visualized by Thin-Layer Chromatography (TLC), where some subtle differences were observed in the lipid composition, specifically in the glycopeptidolipids (GPLs) region (Figure 2.4).

Table 2.1 Selectivity of PGU-P-8K against to mycobacteria in comparison to standard disinfectant microorganisms' strains.

Microorganisms MIC_{90} (μg/mL)					
Mycobacteria	Gram-positive	Gram-negative			Fungi
Msm [a]	*Sau* [b]	*Eco* [c]	*Bce* [d]	*Pae* [e]	*Cal* [f]
6	50	> 200	> 200	> 200	> 200

Strains tested. [a] *Msm* mc^2 155. [b] *S. aureus ATCC 6538.* [c] *E. coli ATCC 8739.* [d] *B. cepacia ATCC 2516.* [e] *P. aureginosa ATCC 15442.* [f] *C. albicans ATCC 10231.*

Table 2.2 Selectivity of PGU-P-8K against various mycobacteria and conditions.

Mycobacteria MIC_{90} (µg/mL)				
Msm [a]	*Msm* [b]	*BCG* [c]	*Mab* S [d]	*Mab* R [e]
6	25-50	25	65	188

Strains tested. [a] *Msm* mc^2 155 cultured in 7H9 medium. [b] *Msm* mc^2 155 cultured in LB. [c] *M. bovis* BCG cultured in 7H9. [d] *Mab* 3690 S cultured in MHB medium. [e] *Mab* 3690 R cultured in MHB medium.

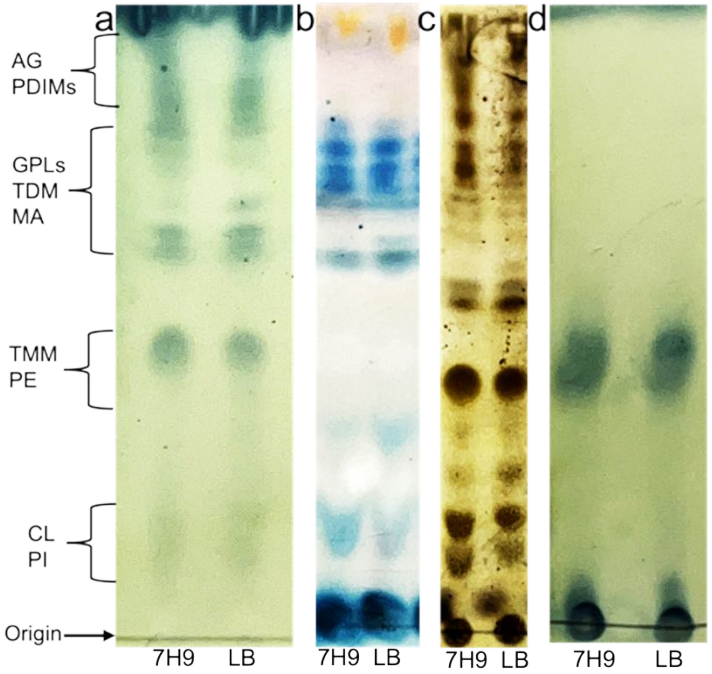

Figure 2.4. Extracted polar lipids developed in chloroform:methanol:water (30:8:1) a) 10% phosphomolybdic acid in ethanol, b) visualizing GPLs by 0.2% anthrone in sulfuric acid:ethanol (1:1,v/v), c) 1.3% molybdenum in 4 M sulfuric acid, d) Extracted nonpolar lipids visualized by TLC (3x 15% diethyl ether in hexane) dipped in 10% phosphomolybdic acid in ethanol. Acylglycerols (AG), phthiocerol dimycocerosates (PDIMs), trehalose dimyoclate (TDM), trehalosemonomycolates (TMMs), mycolic acids (MA), Glycopeptidolipids (GPLs), phosphatidylethanolamine (PE), cardiolipin (CL), and phosphatidylinositol (PI).

To further explore if the ~four-fold MIC change could be related to GPLs composition, MICs of two different morphotypes of *Mycobacterium abscessus* (*Mab*) treated with PGU-P-8K were measured (Table 2.2). *Mab* can form both morphologically

smooth (S) and rough (R) colonies when the surface-associated GPLs are present and absent, respectively, in the cell envelope. The di- or triglycosylated GPLs are considered to screen the hydrophobic mycobacterial mycolic acids, thus the membranes of *Mab* (S) are relatively less hydrophobic than those of *Mab* (R). Initially, a ~three-fold increase in the MIC against the R morphotype suggested the higher degree of hydrophobicity in *Mab* (R) could have played a role in the interaction of PGU-P-8K.[34] Although additional investigations are necessary, the hydrophobicity of the mycobacterial membrane might affect the antimycobacterial activity of PGU-P-8K (Table 2.2) due to an altered interaction of PGU-P-8K with the corresponding envelope.

The Time-Kill assay was conducted via colony forming unit (CFU) analysis at various concentrations of PGU-P-8K to determine the minimal bactericidal concentration (MBC), which is defined as the lowest concentration to reduce bacterial cell viability by more than 99.9% at a concentration no more than 4x MIC.[35] As shown in Figure 2.5, the fast killing of *Msm* was observed within several hours of PGU-P-8K treatments at 2x MIC or higher, indicating that PGU-P-8K is bactericidal. Additionally, the bactericidal activity is fast-acting in comparison to anti-TB drugs including bedaquiline (BDQ),[36] rifampicin (RIF),[20] or verapamil (VER).[37] The fast-acting bactericidal activity of PGU-P-8K could be due to possible multidentate interaction of polyguanylurea (PGU) to the membrane, as macromolecules have shown to have better adsorption to the bacterial membrane in comparison to small molecules.[38,39]

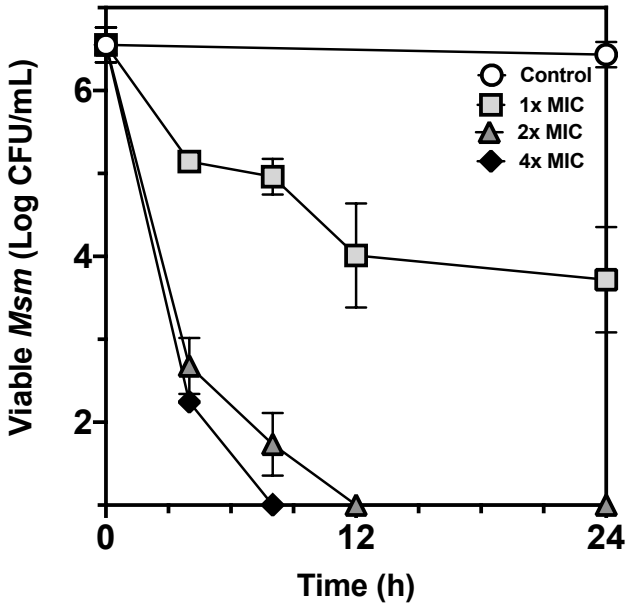

Figure 2.5. Fast bactericidal activity of PGU-P-8K. Within several hours of PGU-P-8K treatment at 2x MIC, the number of viable *Msm* cells rapidly decreased. Results were taken from three independent experiments with at least two technical replicates and averaged +/- standard deviation.

Membrane permeability assay was performed using Sytox green dye to examine whether the bactericidal effect is directly related to the disruption of membrane integrity. Fluorescence intensity of Sytox green increases when the membrane-impermeable dye intercalates into the intracellular nucleic acids upon diffusion through the damaged membranes.[40,41] No fluorescence change was observed from *Msm* treated with PGU-P-8K at 2x MIC for 1 h (Figure 2.6). An additional assay commonly used for membrane damage was also conducted. Non-fluorescent hydrophobic N-phenyl-2-naphthylamine (NPN) becomes fluorescent upon interacting with damaged hydrophobic lipids in the membrane.[42] Even after treating *Msm* with PGU-P-8K at 4x MIC for 1 h, no fluorescence intensity increase was observed (Figure 2.6). Both results indicated bactericidal effects of PGU-P-8K may not be related to direct membrane damage.

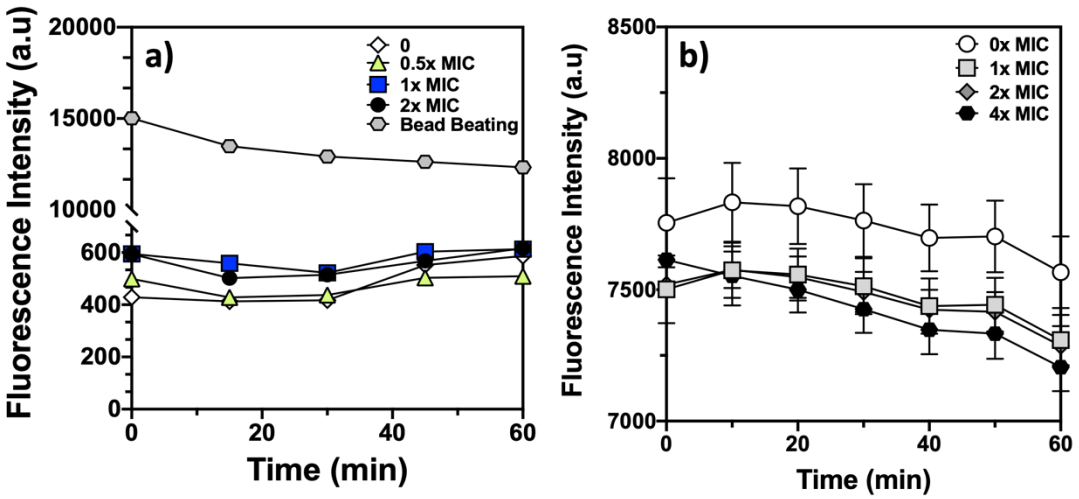

Figure 2.6. Testing of the outer membrane permeability. The fluorescence of a) 5 μM Sytox Green dye was measured at 485nm/590nm (ex,em), and b) 10 μM N-Phenyl-2-naphthylamine at 2% acetone was read 350nm/400nm (ex,em) and monitored for 1 h. Results were taken from three independent experiments and averaged +/- standard deviation.

Transmission electron microscopic (TEM) images of *Msm* treated with PGU-P-8K at 2x MIC for up to 24 h were collected and analyzed to examine the effects of PGU-P-8K on the bacterial cell wall. After PGU-P-8K incubation for 1, 4, and 24 hours, respectively, at 2x MIC, cells were fixed and stained for TEM imagining. As shown in Figure 2.7, typical morphologies, membranes, and cellular contents of intact *Msm* were observed from both treated and nontreated cells along with natural morphological changes (see more images in Figure 2.17). To warrant the objectivity of the image analysis, we took twenty-five images per each treatment group, and then analyzed each image by counting the frequency (%) of membrane ruffling (MR), membrane delamination (MD), cytosolic leakage (CL), and dead cell (DC) per total cells in each image. While no significant difference in the frequency of the cytosolic leakage was observed from both treated and non-treated cells up to 24 h incubation, signs of membrane stress including ruffling and delamination were observed starting from 1 h PGU-P-8K treatment (Figure 2.7b). An intact outer membrane was often

observed from the dead cells, ruling out the damages on the membrane integrity as a bactericidal mode of action. Interestingly, increasing numbers of certain cytosolic aggregations (white arrows) were seen in 24 h PGU-P-8K treated cells. We hypothesized that those aggregation structures could be induced by internalized PGU-P-8K interacting with the cytosolic contents.[43]

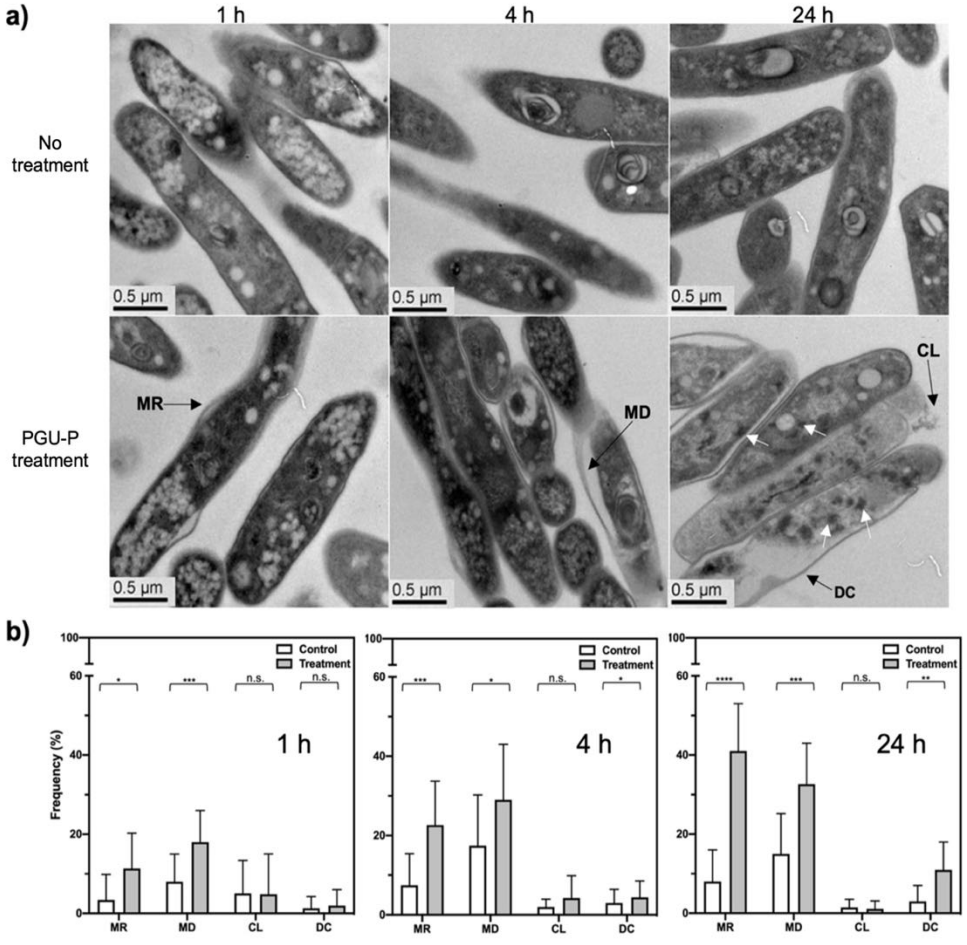

Figure 2.7. a) Representative TEM micrographs of *Msm* cells after treatment with PGU-P-8K at 2x MIC for 1, 4, and 24 hours, respectively. MR: membrane ruffling, MD: membrane delamination, CL: cytosolic leakage, and DC: dead cell. b) By counting the frequency of the specific morphological change in every image, statistical analysis of morphological changes induced by PGU-P-8K was conducted. *P < 0.01, **P < 0.001, ***P < 0.0001, ****P < 0.00001. n.s.: not significant. Additional TEM images are shown in Figure 2.17.

Although the antimicrobial effects of combining multiple drugs are hard to predict and interpret, any combination effects (e.g., synergistic, additive, or antagonistic) from combined drugs could provide mechanistic insight. To evaluate drug potentiation effects of PGU-P-8K, checkerboard assay was conducted for selected anti-TB drugs, and the fractional inhibitory concentration indexes (FICIs, see Table 2.3) of the combinations were calculated.[44] Two sets of drugs were selected based on targeting 1) the membrane energetics [i.e., BDQ: adenosine triphosphate (ATP) synthase,[36] clofazimine (CLZ): NADH dehydrogenase-2,[45] VER: membrane energetics[37]] and 2) intracellular processes [i.e., RIF: RNA polymerase[46] and ciprofloxacin (CIP): DNA gyrase and topoisomerase IV].[47] As shown in Figure 2.8, PGU-P-8K exhibits the synergistic effects (i.e., FICI $\leq$ 0.5) with BDQ and additive effects (i.e., 0.5 < FICI $\leq$ 1.0) with VER and CLZ. The synergistic effect of BDQ could be due to the possible disruption of a component of the proton motive force (PMF) by PGU-P-8K since ATP-synthase relies on the PMF to produce ATP. Meanwhile, drugs acting on the intracellular targets show the indifferent effects (i.e., 1 < FICI < 2). These PGU-P-8K-mediated potentiation and indifferent effects on the tested drugs imply that PGU-P-8K possibly targets the membranes' energetics.

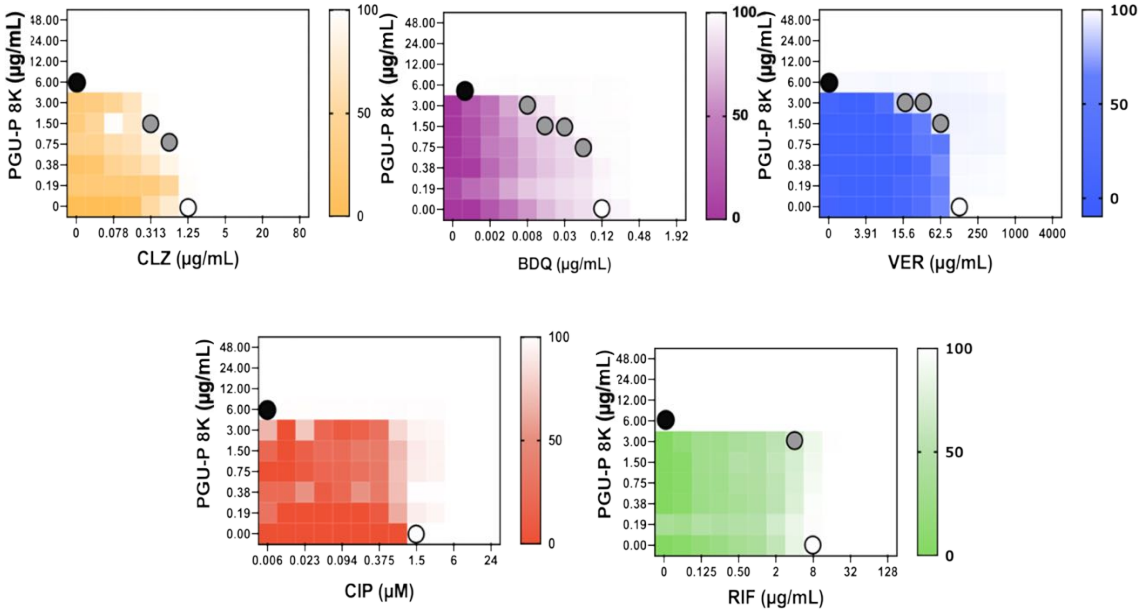

Figure 2.8. Assessment of synergistic interactions between PGU-P-8K, verapamil, and some anti-TB drugs. PGU-P-8K was tested in combination with bedaquiline (BDQ), verapamil (VER), clofazimine (CFZ), ciprofloxacin (CIP) and rifampin (RIF) in checkerboard assay against *M. smegmatis*. The Minimum Inhibitory Concentration (MIC) value of PGU-P-8K (6 µg/mL) was denoted by a black circle, and white for the compounds tested against PGU-P-8K: BDQ is 0.12 µg/mL, VER 250 µg/mL, CLZ 2.5 µg/mL, CIP 1.5 µM and RIF 8 µg/mL. The Fractional Inhibitory Concentration Index (FICI) values were calculated to be 0.38-0.5, 0.623-0.75, 0.50-0.75, 2, and 1-2 for BDQ, VER, CLZ, CIP and RIF, respectively. Synergy was observed in the combination with BDQ, but other PMF disruptors, CLZ and VER, showed some susceptibility in combination with PGU-P-8K. Data was collected in three independent experiments, but one representative experiment for each is shown.

Selectivity is critical when developing novel therapeutics to minimize off-target risk towards mammalian cells or symbiotic bacteria.[48,49] Dissipating the PMF is an appealing mechanism to combat TB, as the collapse of the PMF itself is not bactericidal in most species, but the survival of both replicating and nonreplicating *Mtb* requires a polarized membrane.[49] PZA showed to be most active against nongrowing TB. Since in acidic environments, nicotinamidase can convert PZA to the negatively charged pyrazinoate (POA_C), due to its proton acceptor properties, it can affect the PMF via membrane

depolarization and transport functions in *Mtb*. [50–52] The PMF is composed of two main parameters: $\Delta\psi$ and ΔpH[53], where membrane potential ($\Delta\psi$) plays the greater role in mycobacteria.[54,55] To measure if disruption of the $\Delta\psi$ is caused by PGU-P-8K, an assay using a potential-sensitive fluorescent dye [i.e., 3,3'-dipropylthiadicarbocyanine iodide, $DiSC_3(5)$] was conducted.[56] As shown in Figure 2.9, the self-quenched dye in a hyperpolarized membrane was released to the solution (i.e., fluorescence increase) upon addition of PGU-P-8K at 2x MIC, indicating that PGU-P-8K disrupted $\Delta\psi$, similarly to the positive control, VER (Figure S8). Meanwhile, carbonyl cyanide m-chlorophenyl hydrazone (CCCP), a commonly used protonophore that collapses both components of the PMF[45] did not exhibit concentration-dependent potential changes (Figure 2.10). This is largely due to the interference on the fluorescence signals of $DiSC_3(5)$ dye quenched by the ionophore (Figure 2.10).[56]

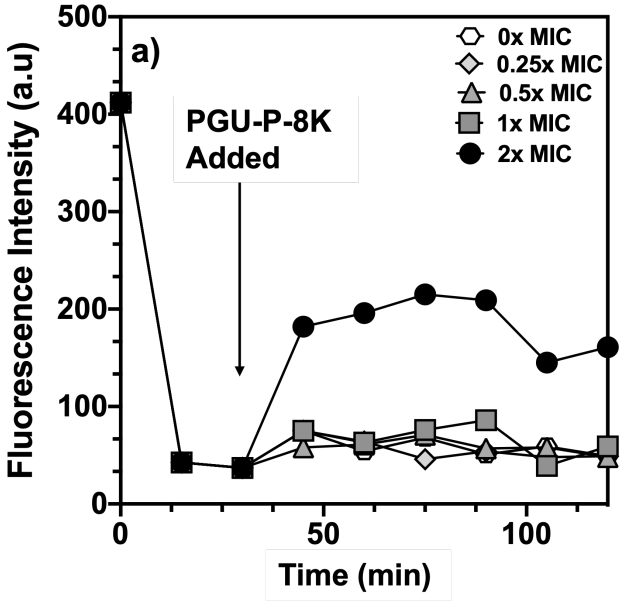

Figure 2.9. PGU-P-8K effect on the membrane potential of *Msm*. The effect of membrane depolarization of PGU-P-8K at various concentrations was measured using $DiSC_3(5)$, where PGU-P-8K at 2x MIC induced an increase in fluorescence signals, indicating disruption of the membrane potentials. Experiment was performed in triplicates (data from one representative experiment is shown for the clarity).

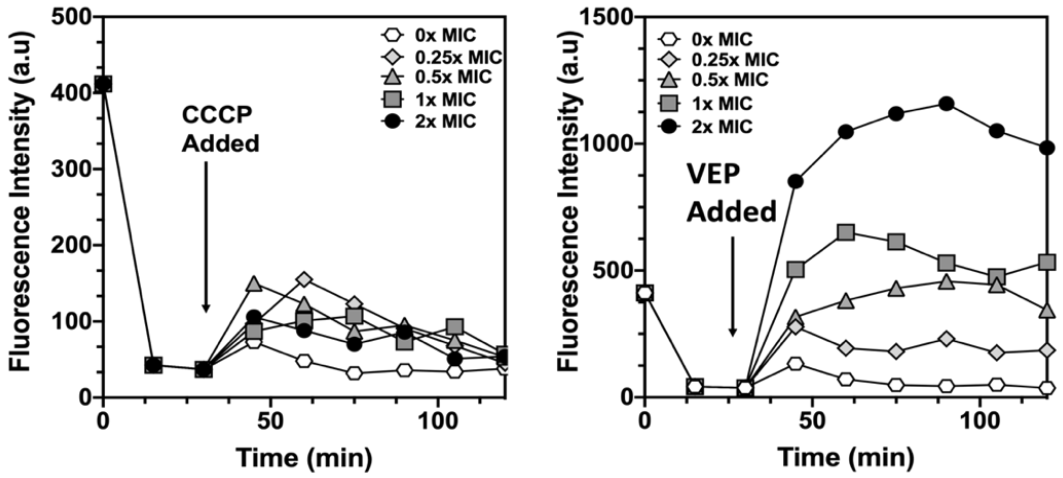

Figure 2.10. Membrane depolarization effect of CCCP and VER against *M. smegmatis* using 5μM $DiSC_3(5)$.

After the collapse of the PMF, the electron transport chain initiates a cycle to restore homeostasis which usually leads to ATP depletion.[38,45] To test if PGU-P-8K affected ATP levels, the intracellular ATP levels was measured of PGU-P-8K-treated *Msm* using BacTiter-Glo™ and normalized the luminescence signal by viable cells via CFU analysis. BDQ, ATP-synthase inhibitor, at 20x MIC was used as a positive control for ATP depletion and isoniazid (INH), cell wall synthesis inhibitor, at 2x MIC to show ATP burst. As expected, BDQ showed decreased ATP production, whereas INH increased intracellular concentrations of ATP (Figure 11). [45,57] At 1x MIC, PGU-P-8K did not show significant changes in ATP levels after 2 h and 8 h of treatment in comparison to the untreated control. *Msm* was tested at 1x MIC PGU-P-8K for accuracy as a longer or stronger treatment would have decreased viable cells. Therefore, significant uncoupling activity was not observed which can be attributed to the ability of *Msm* to upregulate F_1F_0-ATP synthase in response to antibiotic stress.[29,58] Overall, the interaction of PGU-P-8K on the mycobacterial membrane showed membrane depolarization, but no ATP depletion.

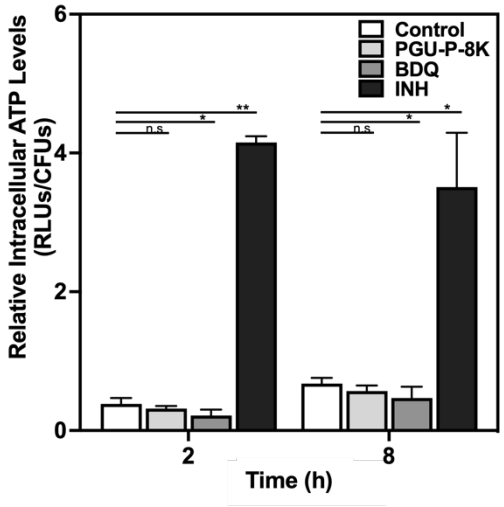

Figure 2.11. Intracellular quantification of ATP levels was performed using relative luminescence units (RLUs) normalized by colony forming units (CFUs) at time 2 h and 8 h after treatment of Msm cells. Experiment was performed in triplicates, and averaged +/- standard deviation using 20x MIC BDQ as a positive control. PGU-P-8K did not show to affect ATP levels after treatment.

The disruption of the PMF from PGU-P-8K via membrane depolarization was further supplemented by exploring the inhibition of efflux pumps. Efflux pumps draw energy from hydrolysis of ATP, ions, or protons. Therefore, disruption of the PMF could lead to inhibition of efflux pumps. Ethidium bromide (EtBr), a fluorescent dye, is an efflux pumps' substrate and damages on the membrane, either directly or indirectly, lead to the accumulation of EtBr. [26–28,59]As shown in Figure 2.12, a concentration-dependent fluorescence increase was observed from both PGU-P-8K- and BDQ-treated cells. The dissipation of the PMF caused by BDQ has been attributed to the indirect inhibition of ATP-dependent efflux pumps due ATP depletion, resulting in the accumulation of EtBr.[60] Similarly, the accumulation of EtBr by PGU-P-8K could be due to the disruption of energy metabolism (i.e., protons or ATP) causing impairment of efflux pumps. While PGU-P-8K did not show ATP depletion, but it did show dissipation of the $\Delta\psi$.

Therefore, membrane depolarization by PGU-P-8K disturbed the PMF and caused accumulation of EtBr.

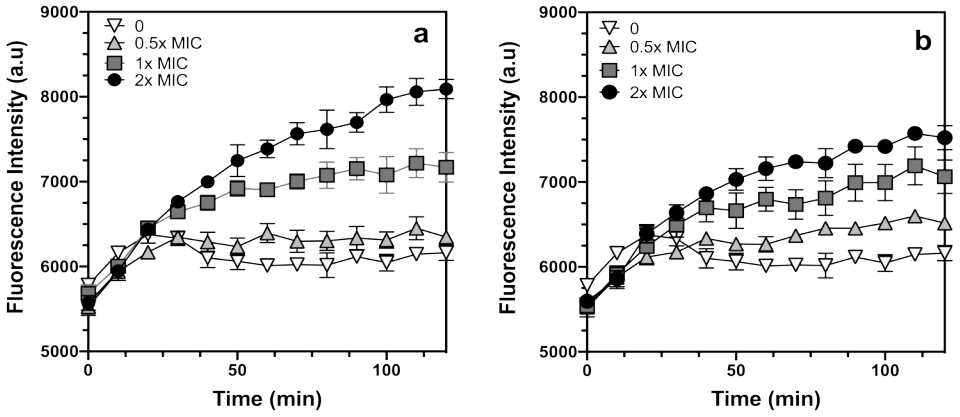

Figure 2.12. Influence on Efflux Pumps Measured through the EtBr Accumulation. Intracellular accumulation assay of ethidium bromide when treating *M. smegmatis* against a) PGU-P-8K and b) BDQ at 0.5xMIC, 1x MIC and 2x MIC. Intracellular concentration of ethidium bromide was increased in a concentration-dependent matter for both PGU-P-8K and BDQ. Experiment is shown in mean of triplicates +/- standard deviation.

The disruption of the membrane potential induces a significant stress on the membrane; therefore, changes in gene expression associated with membrane stress-sensing might occur. A real-time quantitative reverse transcription-polymerase chain reaction (qRT-PCR) assay was conducted to study the regulation of MSMEG_5072 and MSMEG_2694 genes, orthologs of *sigE* and *clgR* in *Mtb*, respectively. These genes are involved in the cell envelope stress-sensing Phage shock protein (Psp) system in *Mtb*, where *sigE* senses envelope stress and *clgR* responds by preventing proton leakage to maintain the PMF.[61] These orthologs have shown upregulation after treatment of compounds dissipating the membrane potential (i.e., CCCP and VER) in *Mtb*.[37,61] As shown in Figure 2.13, PGU-P-8K treatment at 2x MIC for an hour induces a 10- and 50-

fold times increased expression levels of MSMEG_5072 and MSMEG_2694 genes, respectively, compared to control untreated *Msm* and *sigA* as a housekeeping gene. This outcome further cemented the substantial membrane stress caused by the bactericidal PGU-P-8K due to the disruption of the membrane energetics.

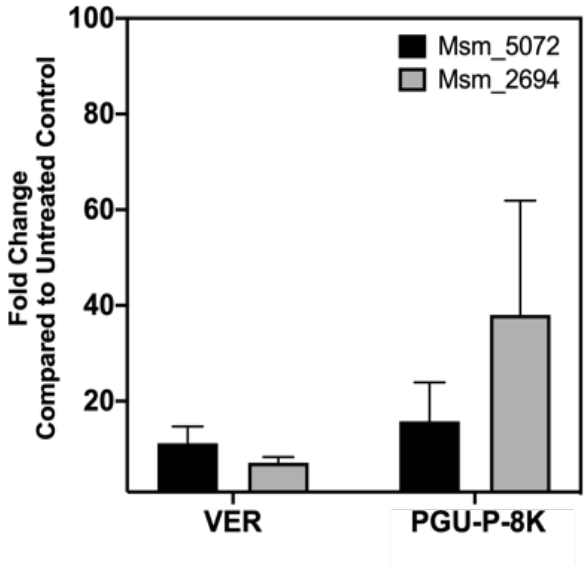

Figure 2.13. Transcriptional induction of membrane stress reporters in *Msm* by PGU-P-8K in comparison to 2x MIC VER. Fold change was calculated in comparison to untreated control with 0.2% DMSO and *sigA* as housekeeping gene. PGU-P-8K induces higher levels of overexpression of the genes related to membrane stress-sensing genes compared with VER, which was reported to disrupt the PMF.

2.4 Conclusion

In conclusion, we have provided evidence of that selective mycobactericidal activities of PGU-P-8K were due to the dissipation of the membrane potential, a major component of the PMF, via selective interaction with the mycobacterial membrane. Additionally, PGU-P-8K showed that the dissipation of the PMF caused inhibition of efflux pumps and upregulation of genes related to membrane stress. In comparison to traditional TB drugs, PGU-P-8K exhibited a fast-acting mycobactericidal effects presumably due to multidentate interactions of the amphiphilic guanylurea group with

mycobacterial cell membrane. Considering the design simplicity of PGU-P-8K, unique targeting ability, and synergistic effects with existing TB drugs, PGU-P-8K could contribute to the development of a novel class of anti-TB macromolecules that efficiently combat deadly TB. Future work can deepen the understanding on the mechanisms of PGU-P-8K including the suspected internalization, interaction with cytosolic components, and mutation rate.

2.5 Experimental and Supporting Information

2.5.1 Physical Characterization

^{1}H Nuclear magnetic resonance (NMR) spectra were obtained using a 400 MHz Avance Bruker NMR spectrometer. Chemical shifts were reported in parts per million (ppm) on the δ scale. Deuterated solvents chloroform-d ($CDCl_3$) or dimethyl sufoxide-d_6 (DMSO-d_6) were used as reference solvents; $CDCl_3$ (δ = 7.26 ppm) for the Boc-protected product and DMSO-d_6 (δ = 2.50 ppm) for the deprotected product.

The number averaged (M_n), the weight averaged (M_w) and polydispersity index (PDI) of the Boc-protected oligomer was confirmed via gel permeation chromatography (GPC) against polystyrene standards using a Shimadzu high performance liquid chromatography (HPLC) system at a flow rate of 1.0 mL/min with 2 tandem PLgel 5 μM MIXED-D columns operating at 40 °C and SPD-20A ultraviolet visible (UV-Vis) as the detector. End-group analysis was performed using reference peaks from guanylurea (i.e., 8.3 and 12.2 ppm) and calculating the ratio of the integration values to the boc-guanidine peaks (i.e., 8.6 and 11.5 ppm).

The pKa of PGU-P-8K was determined via pH titration method. A concentrated solution of PGU-P-8K in DMSO was diluted to 2 mM in 1 mL of an acidified (pH ~2.5) solution of 100 mM NaCl. The pH was measured using a Mettler Toledo in Lab Ultra-Micro pH Probe. The acidified solution was titrated at 5 μL increments of 25 mM NaOH. The pH readings were recorded from pH ~2.5-11. After plotting ΔpH/Δvolume of NaOH, the two points where the largest change in pH occurred were found. The median volume between the two maxima was identified as the point where pH = pKa. Solution of 100 mM NaCl served as control. Experiment was performed in triplicates.

2.5.2 Synthesis of Boc-protected PGU-P-8K

Synthesis was performed as previously reported with minor modifications. Boc-protected guanidine containing diiodo (0.02 mmol) and piperazine (0.02 mmol) monomers were added in a 4 mL amber vial at a 1:1 mole equivalent. A catalytic amount of potassium carbonate (K_2CO_3) and 400 μL of tetrahydrofuran (THF) was subsequently added to the monomers. The vial was closed tightly, and the reaction was left to stir overnight at 70 °C. The resulting viscous solution was filtered through glass wool to remove K_2CO_3 and the filtrate was purified by precipitation twice in diethyl ether and once in methanol (MeOH). Oligomer size was confirmed via GPC and endgroup analysis, and chemical structure via NMR.

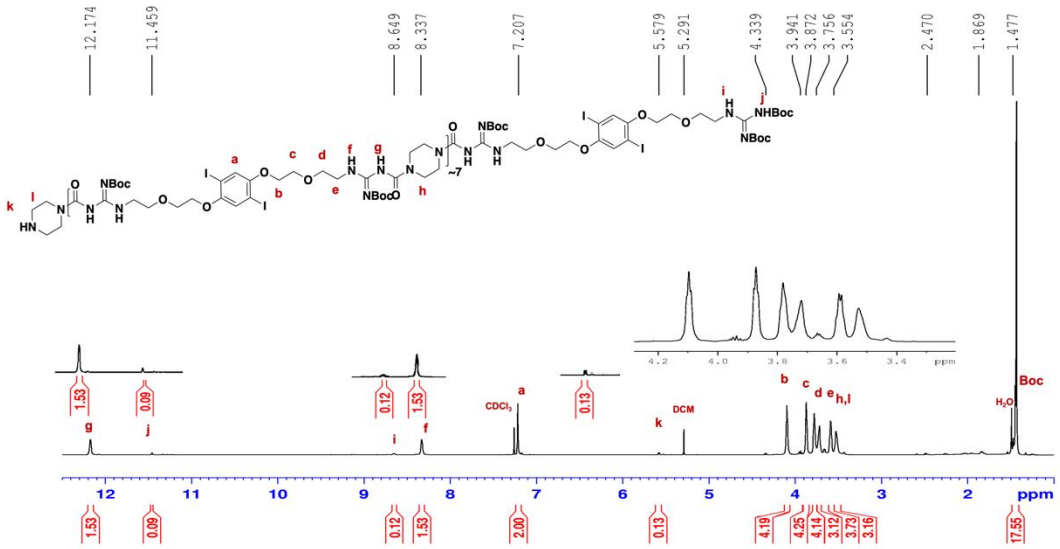

Figure 2.14. NMR of boc-protected PGU-P-8K. White powder. ^{1}H NMR (400 MHz, CDCl3, δ): 12.2 (s, 1H), 8.34 (t, 1H, J = 4.8 Hz), 7.22 (s, 1H), 4.10 (t, 2H, J = 4.6 Hz), 3.88 (t, 2H, J = 4.6 Hz), 3.78 (t, 2H, J = 5.1 Hz), 3.73 (br s, 2H), 3.60 (q, 2H, J = 5.3 Hz, J = 5.1 Hz), 3.53 (br s, 2H), 1.44 (s, 9H).

2.5.3 Deprotection of PGU-P-8K

The white powder of boc-protected product (10mg) was dissolved in 2 mL dichloromethane (DCM). Then 1 mL of trifluoroacetic acid (TFA) was added and left to stir overnight resulting in the deprotected product and dried *in vacuo*. The crude product was dissolved in minimum amount of dimethylformamide (DMF) and precipitated in diethyl ether twice and lastly in ethyl acetate. The product was collected by decanting, and successively dried by high vacuum. The white powder was collected and dissolved in DMSO for future testing. Chemical structure was confirmed via NMR.

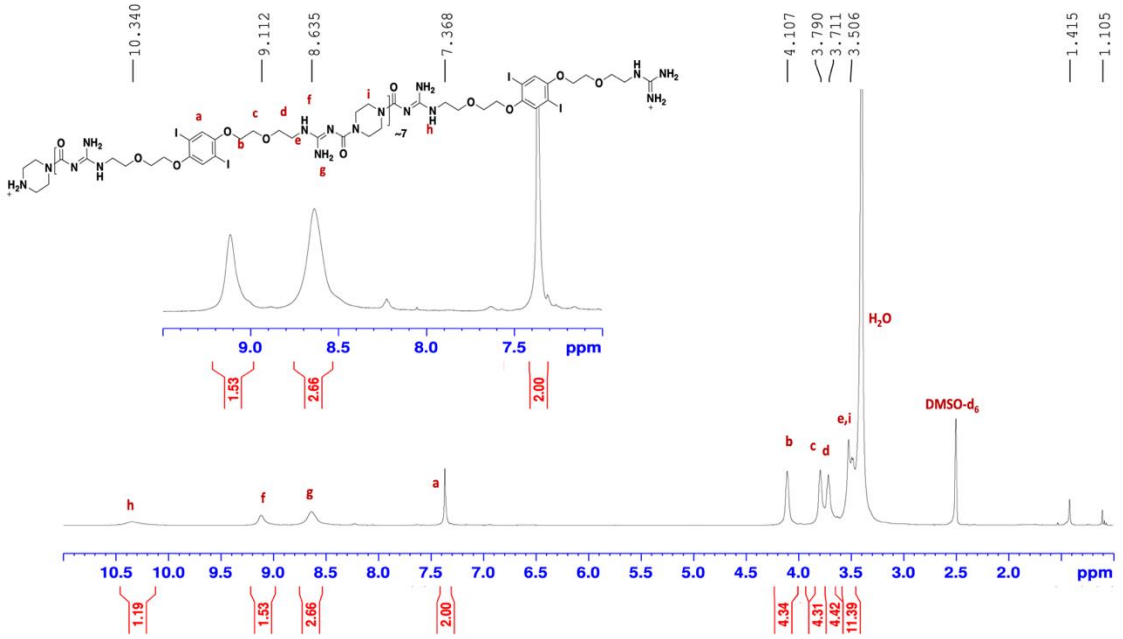

Figure 2.15. NMR of deprotected PGU-P-8K in acidic conditions. White fibrous solid (75% yield). 1H NMR (400 MHz, DMSO-d6, δ): 10.3 (s, 1H), 9.1 (s, 1H), 8.61 (s, 2H), 7.4 (s, 2H), 4.1 (s, 4H), 3.8 (s, 4H), 3.7 (s, 4H), 3.5 (m, 11H).

2.5.4 Selectivity of PGU-P-8K and Time-Kill Assays.

MIC was determined by broth microdilution method according to Clinical and Laboratory Standards Institute (CLSI) guidelines. *M. smegmatis* mc^{2}155 cells (ATCC 700084) were initially grown for 24 h in BD Difco 7H9 medium (0.2% glycerol and 0.05% Tween 80) and supplemented with 10% ADN (0.05% albumin, 0.02% dextrose, 0.0085% NaCl). Then cells were inoculated and grown to late log-phase in 7H9 medium with 0.2 % glycerol (Fisher Scientific) and 0.05% Tween 80 (VWR).

Other microorganisms were grown from a single colony in 5 mL of media, where Yeast extract-Peptone-Dextrose (YPD) medium (Sigma Aldrich) was used to grow *Candida albicans* (ATCC 10231). *Escherichia coli* (ATTC 8739), and *Staphylococcus*

aureus (ATCC 6538) were grown in Luria Broth (LB) medium (US Biological), and *Burkholderia cepacia* (ATCC 2516), and *Pseudomonas aeruginosa* (ATCC 15442) were grown in Nutrient Broth (NB) medium (Difco).

Cell suspensions were allowed to grow to late-log phase at 37 ℃ with shaking at 210 rpm overnight. *M. smegmatis* in LB was supplemented with 0.2% glycerol and 0.05% Tween 80 and grown overnight to late-log phase. *M. bovis* BCG (ATCC 35734), and *M. abscessus* (S and R) (ATCC 19977) with luminescent reporter were incubated in T25 flasks (TPP) at 37 ℃, in 5% CO_2 static for 2-3 days and 5-7 days, respectively. The optical density (OD_{600}) was adjusted for final concentration of 10^5 CFU $well^{-1}$ for bacterial cells, and 10^3 CFU $well^{-1}$ for *C. albicans*. Polymer solution and controls were prepared in the respective media and serially diluted two-fold in a clear round bottom 96-well microtiter plate (Cell treat, 229590), followed by the addition of 50 μL of the cell suspension. Ciprofloxacin was used as positive control for *E. coli*, *M. smegmatis*, and *S. aureus*, and amphotericin B was used as a positive control for *C. albicans*. Positive control for *M. bovis* BCG was kanamycin and for *M. abscessus* was amikacin. Negative control included 50 μL of cell suspension and 50 μL of 2% DMSO media. Plates were incubated statically at 37 ℃ for 48 h for *M. smegmatis*, 20 h for Gram-positive and -negative bacteria, and 30 ℃ for 20 h for yeast, before the adding 10 μL of 0.02 % resazurin dye. After addition of the dye and further incubation time (19 h for *M. smegmatis*, 4 h for other microorganisms), fluorescence was measure 540/590 nm (excitation/emission) on a BioTek Synergy H1 plate reader after further incubation period. For *M. abcessus* (S and R) they were incubated

for 3 days, and luminescence was measured. Assays included two technical replicates and were repeated at least three independent experiments.

For Time-Kill assay, *M. smegmatis* mc^2 155 was cultured as described for the MIC assay. Cells were adjusted to OD_{600} 0.01. PGU-P-8K at 12, 24 and 48 μM were prepared in 7H9 supplemented with 0.2% glycerol and 0.05% Tween 80. A two-fold dilution of the polymer solutions was performed by the addition of 50 μL of subculture suspension for a final volume of 100 μL, and final polymer concentrations of 24 μM, 12 μM and 6 μM in a clear 96-well microtiter plate. Negative control was prepared by adding 50 μL of 2% DMSO in 7H9 medium, and 50 μL of bacterial cells. Aliquots of each sample were serially diluted 10-fold in 1x Phosphate-buffered saline buffer (1x PBS) and plated in LB Agar plates at 4 h, 8 h, 12 h and 24 h. After incubating the plates at 37℃ for six days, the colonies were counted. Experiment included duplicates and performed at least three independent times.

2.5.5 Lipid Extraction and Thin-layer Chromatography (TLC) Assay

Non-covalently linked lipid extractions were performed on *Msm* grown in different culture conditions for comparison and analyzed using ImageJ to warrant objectivity. Late-log phase of *Msm* was inoculated into liquid medium (LB or 7H9) supplemented with ADN (albumin, dextrose and NaCl), 0.05% Tween 80 and 0.2% glycerol and grown overnight. 500 L was inoculated from the supplemented medium into 50 mL of liquid media with 0.05% Tween 80 and 0.2% glycerol (no supplement) and grown overnight in Erlenmeyer flasks. The cell suspension was centrifuged at 10 000 g for 2 min and resuspend in 15 mL

of organic solution composed of chloroform:methanol (1:2, v/v). The flask was left incubating overnight at 37 ℃ while shaking at 210 rpm to extract non-covalent-linked lipids from the mycobacterial cell surface. The organic solvent with extracted lipids was filtered using a funneled filter paper and glass funnel and collected them in an amber glass bottle. The liquid phase was dried *in vacuo* and stored at 4 ℃. The extracted lipids were reconstituted in 150 μL of chloroform, spotted in alumina-backed TLC, developed in either chloroform:methanol:water (30:8:1) to visualize polar lipids or ran three times in 15% diethyl ether in hexane showing non-polar lipids. The TLCs were then dipped in either 10% phosphomolybdic acid in ethanol, 0.2% anthrone in sulfuric acid:ethanol (1:1,v/v), or 1.3% molybdenum in 4 M sulfuric acid, and heated. Finally, calculation of R_f values were performed for identification of lipids using previous reports as reference.[62,63]

2.5.6 Susceptibility with Some Anti-TB Drugs

The bacterial cell suspension for the synergistic studies were prepared as described in the MIC assay. Drug samples were prepared in 7H9 medium with 2% DMSO and serially diluted two-fold horizontally in a clear 96-well microtiter plate. PGU-P-8K was serially diluted two-fold and added vertically to the wells. Lastly, 100 μL of bacterial cell suspension was added in the wells for a total volume of 200 μL and a final concentration of 1% DMSO in each well. The plates were incubated statically at 37 ºC. After 48h incubation, 20 μL of 0.02% resazurin was added to each well. Fluorescence intensity (excitation 540 nm, emission 590 nm) was measured after 19 h incubation on a BioTek Synergy H1 plate reader. Experiment was performed at least three independent times, but one representative experiment was shown.

Fractional Inhibitory Concentration Index value was calculated for each experiment using the following equation: [44,65]

$$\sum \boldsymbol{FIC} = \boldsymbol{FIC_A} + \boldsymbol{FIC_B} = (\left(\frac{\boldsymbol{MIC_{A+B}}}{\boldsymbol{MIC_A}}\right) + (\frac{\boldsymbol{MIC_{A+B}}}{\boldsymbol{MIC_B}})$$

Table 2.3. FICI values and interaction of PGU-P-8K with some representative anti-TB drugs.

Drug	Target	FICI	Interaction
Bedaquiline (BDQ)	F_1/F_0-ATP synthase	0.38-0.5	Synergy
Verapamil (VER)	Membrane energetics	0.63-0.75	Additive
Clofazimine (CLZ)	NADH dehydrogenase-2	0.5-0.75	Additive
Ciprofloxacin (CIP)	DNA gyrase and topoisomerase IV	2	Additive
Rifampin (RIF)	RNA polymerase	1-2	Additive

2.5.7 Influence on Efflux Pumps Measured by Ethidium Bromide Accumulation

M. smegmatis cells were incubated to log-phase in 7H9 at 37 ºC. The bacterial cell suspension was centrifuged at 10000 g for 5 min at 25 °C, washed twice, and resuspended in 1x PBS with 0.05% Tween 80 (PBST). The OD_{600} was adjusted to 0.2. PGU-P-8K, and bedaquiline (BDQ) were prepared in 1x PBST and 50µL pipetted into the wells of a black-sided 96-well microtiter plate (Thermo Scientific Nunc, 165305). The bacterial suspension was pipetted for a ratio one-to-one of cell to polymer for a final volume of 100 µL in each well and a final concentration of 1% DMSO. Ethidium bromide (EtBr) dye at 2.5 µM was added as the fluorescent probe. EtBr can accumulate inside the cell and intercalate with nucleic acids leading to an increase of fluorescence signal. This assay can

give insight on the intracellular accumulation of the dye, since EtBr is a small molecule that can enter the cell and is a substrate of efflux pumps. The accumulation can be attributed to outer membrane damage or due to inhibition of efflux pumps. [27-29] The experiment was repeated at least three independent times and standard deviation depicted by error bars.

2.5.8 Impact on the Membrane Potential Monitored by $DiSC_3(5)$ Dye

Bacterial cells were grown to late log-phase in 7H9. Cells were centrifuged at 3000 g for 5 min at 25 ℃, washed twice and resuspended in 10 mL of 5 mM HEPES buffer, pH 7.2 supplemented with 1 mM glucose. OD_{600} of the cells was then adjusted to 0.4. The cell suspension was treated with 1 μM of the potentiometric probe 3,3'-Dipropylthiadicarbocyanine iodide ($DiSC_3(5)$) was added. It was incubated at 37 ℃, and the quenching of $DiSC_3(5)$ dye in the presence of *M. smegmatis* cells was monitored for 30 min. In a black-sided 96-well microtiter plate, polymer solution was added to the plate and serially diluted two-fold in 50 mM HEPES buffer supplemented with 1 mM glucose and 2% DMSO for a final volume of 50 μL per well and 1% DMSO. After 30 min of quenching $DiSC_3(5)$, 50 μL of the bacterial suspension with dye was added to the polymer-containing wells. Wells without polymer were used as negative controls, verapamil and CCCP were used as positive control. Fluorescence was recorded 590/635 nm (excitation/emission) for 1 h every 10 min on a BioTek Synergy H1 plate reader. Assay was performed at least three independent experiments, but one representative data was shown.

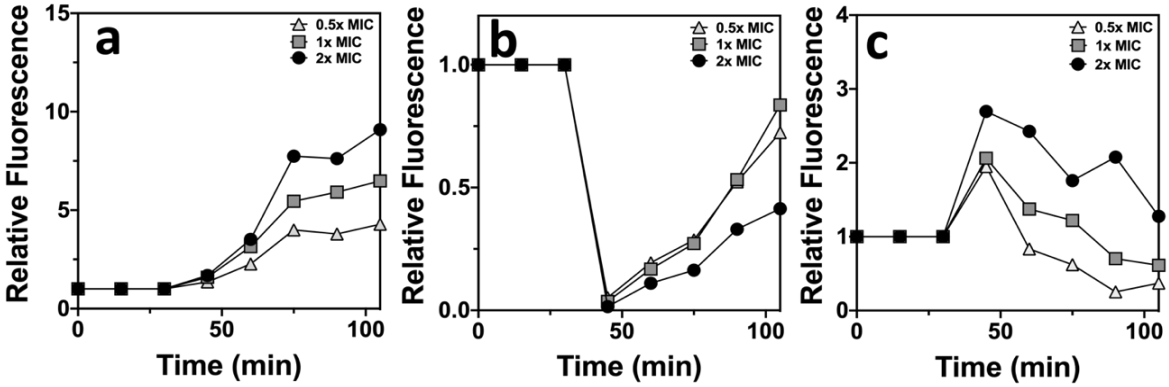

Figure 2.16. Dye interaction of the tested compounds using 5µM $DiSC_35$ Dye and buffer (no cells) in the presence of a) VER, b) CCCP, and c) PGU-P-8K.

2.5.9 Membrane Disruption Assay

M.smegmatis cells were grown as previously mentioned. Cells were centrifuged at 4000 g for 2 min at 25 ºC, washed and resuspended in 1x PBS. The resulting cells were adjusted to OD_{600} 0.4. PGU-P-8K was prepared at 1x MIC, 2x MIC and 4x MIC in 1x PBS buffer with 2% DMSO and 50 µL was added to an optical bottom black-sided 96-well microtiter plate (ThermoFisher, 165305). The bacterial cell suspension with 5 µM Sytox green dye, a membrane impermeable dye, was added to the wells for a final volume of 100 µL in each well. Wells not containing polymer were used as the negative control, and cells lysed in a bead beater as positive control. The fluorescence at 485/590 nm (excitation/emission) was monitor every 5 min for 2 h at 37 ºC on a BioTek Synergy plate reader. Experiments were performed in triplicates.

Similarly, outer membrane permeability assay using 10 µM N-Phenyl-2-naphthylamine in 4% acetone was used as a non-fluorescent dye that upon hydrophobic interaction, it emits fluorescence signal.[4] Cells were grown to mid-log phase (OD_{600} =0.5),

centrifuged at 4000 g for 2 min at 25 ºC, washed and resuspended in 5 mM HEPES buffer, pH 7.2. Compounds were made in HEPES buffer and 50 µL was added to an optical bottom black-sided 96-well microtiter plate. Then 50 µL of 40 µM NPN solution and 100 µL of cell suspension were added to the plate. Fluorescence was measured at 350/400 nm (excitation/emission) for 1 h. Experiments were performed in triplicates.

2.5.10 Effect on Intracellular ATP Levels

Bacterial cells were grown to mid-log phase (OD_{600}= 0.5) and treated with BDQ (2.4 µg/mL), PGU-P-8K (6 µg/mL) or 0.2% DMSO. Aliquots of treated samples were separated for CFU analysis and cell lysing after 2 h and 8 h of treatment. Treated cultures for 2 h were incubated at 37 ℃, while shaking at 210 rpm. The aliquot separated for CFU analysis was serially diluted 10-fold in PBS and plated in LB agar plates to count the colonies after static incubation for six-days at 37 ℃. The aliquot separated for cell lysing was transferred to a O-ring-containing screwcap 2 mL microtubes (Fisher Scientific) with 0.1 mm zirconia/silica beads (Biospec). Cells were lysed in a bead beater for two 1 min intervals with ice-cooling breaks. The cell lysates were added to a white-sided optical bottom 96-well plate (Thermo Scientific Nunc, 165306) and then 50 µL of BacTiter-Glo™ Cell Viability Assay (Promega) was added for a final volume of 100 µL in the wells. Luminescence was then shortly after recorded in a BioTek Synergy H1 plate reader. The relative luminescence units (RLUs) data was divided by the CFUs to normalize the ATP levels per treatment and presented as RLUs/CFUs.

2.5.11 Transmission Electron Microscopy Sample Preparation

M. smegmatis mc^2155 was culture as previously described. Cells at OD_{600} =1.6 were treated with 2x MIC of PGU-P-8K for 1 h, 4 h and 24 h in 7H9 medium. After treatment period, 500 µL of the solution was centrifuge at 3000 g for 30 s at 25 ℃. The pellet was resuspended in 1 mL glutaraldehyde/cacodylate fixative solution and stored at -20 ℃ before imaging. Images were analyzed for significant morphological changes. The frequency of membrane ruffling, membrane delamination, cytosolic leakage, and cells that appeared hollowed (i.e., cell death) were counted and divided by the total cell number per frame. The percent of the observed cell envelope stress indicators was used for statistical analysis.

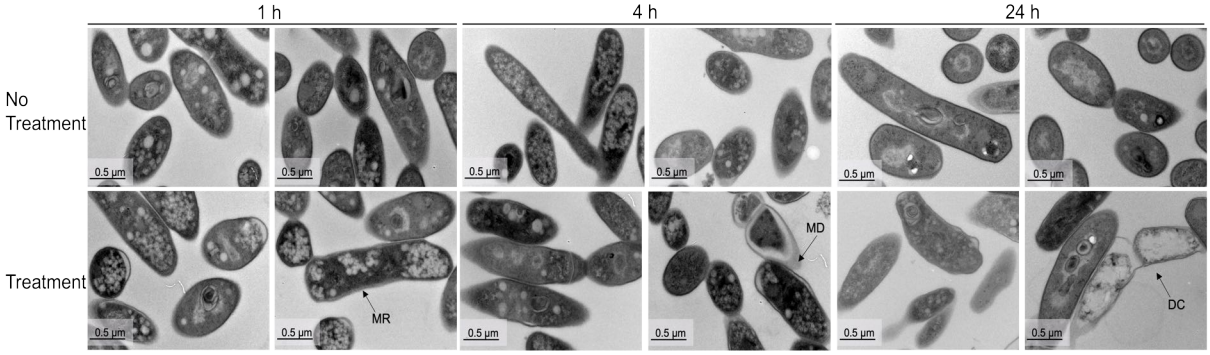

Figure 2.17. Additional inset TEM micrographs with duplicates (vertically) of untreated *Msm* cells at 1 h, 4 h, and 24 h and treatment of PGU-P-8K at 2x MIC for 1 h, 4 h, and 24 h. Each image is representative of the 25 images taken for each nontreated and treated period. Scale bars, 0.5 µm.

2.5.12 Real-Time Quantitative Reverse Transcription-Polymerase Chain Reaction Assay on Cell Envelope-stress Sensing Genes.

M. smegmatis cells were grown to mid-log cultures in 7H9 at 37 ºC and treated with PGU-P-8K and VEP for 1 h at 2x MIC. The bacterial cell suspension centrifuged at 40000 g for 5 min at 25°C and resuspended in 1 mL guanidine thiocyanate (GTC) buffer. The cells were spun down at 12000 x g for 5 min and resuspended in 750 µL of TRIzol reagent (Invitrogen), and 0.5 mL of 0.1mm zirconia/silica beads. Cells were lysed in a bead beater for two 1 min intervals with incubation on ice between intervals. Afterwards, 200 µL of chloroform was added to the tube, mixed, and spun at 12000 x g for 15 min. The aqueous layer was carefully removed to 500 µL of RNase-free ethanol and mixed. From the solution, 700 µL were loaded onto Rnease Kit (Qiagen) miniprep columns and spun at 10000 x g for 1 min. The remainder of the solution was then loaded and spun. The column was washed with 700 µL of RW1 buffer and discarded. The column was then washed twice with 500 µL RPE buffer and spun as previously described. The column was transferred to a new tube to elute the sample using 30 µL of RNase-free water and spun. To ensure there is DNA-free, the sample was treated using TURBO DNA-free kit (Ambion) where a 1 µL of DNase and 3.5 µL of 10x DNase Buffer were added to the 30 µL of RNA and incubated for 1 h at 37 ºC. Then 5 µL of DNase Inactivation reagent was added, incubated for 2 min at room temperature and spun down at 10000 x g for 2 min. The supernatant was removed to a clean tube and stored at -80 ºC. The concentration of RNA was determined through a ThermoFisher multichannel NanoDrop and adjusted to 50 ng/mL for cDNA reaction. The cDNA reaction was performed using iScript cDNA synthesis kit (BioRad), where 14 µL of RNase-free water, 4 µL iScript buffer, 1 µL iScript

Reverse Transcriptase, and 1 μL of 50 ng/mL RNA were added to react in the thermocycler. Finally, the qRT-PCR reaction was performed by adding 5 μL of iTaq Sybr green (BioRad), 3 μL RNase-free H_2O, 0.5 μL forward primer, 0.5 μL reverse primer, 1 μL of cDNA, and added to the thermocycler. SigA was used as the housekeeping gene. Fold change calculations were made in comparison to untreated control. Assay was performed in triplicates with two independent experiments.

2.5.13 PCR primers

Table 2.4. Sequences of PCR primers used to test the cell envelope stress in *Msm*.

Genes	*Mtb* homolog	Forward Primers	Reverse Primers
MSMEG_5072	sigE	5'- ACC TTT TCC TCG ACA TGG TG -'3	5'- TCG TAG GAC AGA CCC TCG AT -'3
MSMEG_2694	ClgR	5'- GAG GTG ATT GGC GAC GTG-'3	5'- CGA AAG TGG TAC GTC GAG TG-'3

2.5.14 Toxicity

J774 or Hep G2 cells were seeded in a black-sided 384-well plate (~10,000 cells/well) in 24 μL of Dulbecco's Modified Eagle Medium (DMEM) and allowed to attach for 4 h at 37 ºC under a humidified atmosphere of 5% CO_2 prior to sample treatment. In separate 384-well plate, PGU-P-8K was tested by serially diluting two-fold with a final concentration of 4% DMSO using the liquid handling robot from Integra Biosciences. After addition of the samples, cells were incubated statically for 20 h prior to addition of 0.01% resazurin dye and incubated for an extra 4 h at 37 ºC. 2% Triton-X was used as positive control while media with 4% DMSO as negative control. Fluorescence was measured as previously described. Cell viability was determined

relative to control wells. Assay was performed in duplicates with three independent experiments.

2.5.15 Optical Density Measurements Post-Treatment

M. smegmatis mc^{2}155 cells were initially grown for 24 h in BD Difco 7H9 medium (0.2% glycerol and 0.05% Tween 80) and supplemented with 10% ADN (0.05% albumin, 0.02% dextrose, 0.0085% NaCl). Then cells were inoculated and grown to late log-phase in 7H9 medium with 0.2 % glycerol (Fisher Scientific) and 0.05% Tween 80 (VWR). To show a decrease in turbidity post-treatment of PGU-P-8K, *Msm* cells *at* mid-log phase were incubated in the presence of 2x MIC and OD_{600nm} measurements were performed and normalized to the initial OD_{600nm}. In comparison to the 0.2% DMSO control, PGU-P-8K-treated cells showed a decreased turbidity in comparison to the initial inoculum concentration, displaying rare properties. This effect is seemingly due to increase of hollow cells seen in TEM images as death cells (Figure 2.7 and 2.17) will still have turbidity but changes in cell density will affect turbidity.

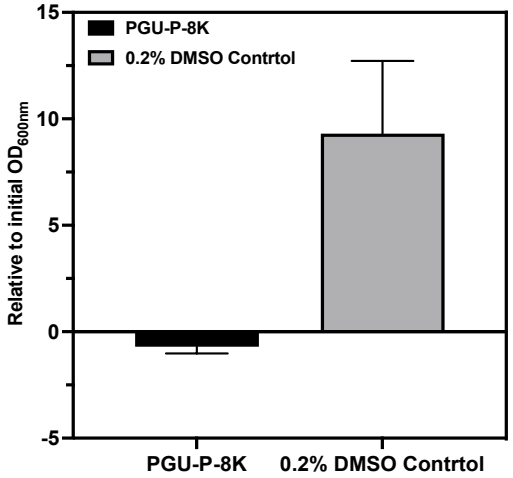

Figure 2.18. PGU-P-8K effect on the turbidity of mid-log phase *Msm* where PGU-P-8K showed decreased turbidity.

2.6 References

(1) WHO. *Tuberculosis*. https://www.who.int/health-topics/tuberculosis#tab=tab_2. (accessed 2022-06-01)

(2) CDC. *Treatment of Tb Disease*. https://www.cdc.gov/tb/topic/treatment/tbdisease.htm. (accessed 2022-06-01)

(3) Ginsberg, A. M. Tuberculosis Drug Development: Progress, Challenges, and the Road Ahead. *Tuberculosis* **2010**, *90* (3), 162–167. https://doi.org/10.1016/j.tube.2010.03.003.

(4) Lederer, E. The Mycobacterial Cell Wall. *Pure and Applied Chemistry* **1971**, *25* (1), 135–166. https://doi.org/10.1351/pac197125010135.

(5) Brennan, P. J.; Goren, M. B. Structural Studies on the Type-Specific Antigen and Lipids of the Mycobacterium Avium. Mycobacterium Intracellulare. Mycobacterium Scrofulaceum Serocomplex. Mycobacterium Intracellulare Serotype 9. *Journal of Biological Chemistry* **1979**, *254* (10), 4205–4211. https://doi.org/10.1016/s0021-9258(18)50716-x.

(6) Boshoff, H. I. M.; Barry, C. E. Tuberculosis - Metabolism and Respiration in the Absence of Growth. *Nature Reviews Microbiology* **2005**, *3* (1), 70–80. https://doi.org/10.1038/nrmicro1065.

(7) Chen, H.; Nyantakyi, S. A.; Li, M.; Gopal, P.; Aziz, D. B.; Yang, T.; Moreira, W.; Gengenbacher, M.; Dick, T.; Go, M. L. The Mycobacterial Membrane: A Novel Target Space for Anti-Tubercular Drugs. *Frontiers in Microbiology* **2018**, *9* (JUL), 1–11. https://doi.org/10.3389/fmicb.2018.01627.

(8) Rao, S. P. S.; Alonso, S.; Rand, L.; Dick, T.; Pethe, K. The Protonmotive Force Is Required for Maintaining ATP Homeostasis and Viability of Hypoxic, Nonreplicating Mycobacterium Tuberculosis. *Proc Natl Acad Sci U S A* **2008**, *105* (33), 11945–11950. https://doi.org/10.1073/pnas.0711697105.

(9) Zhang, Y.; Wade, M. M.; Scorpio, A.; Zhang, H.; Sun, Z. Mode of Action of Pyrazinamide: Disruption of Mycobacterium Tuberculosis Membrane Transport and Energetics by Pyrazinoic Acid. *Journal of Antimicrobial Chemotherapy* **2003**, *52* (5), 790–795. https://doi.org/10.1093/jac/dkg446.

(10) British Thoracic and Tuberculosis Association. Short-Course Chemotherapy in Pulmonary Tuberculosis: A Controlled Trial. *Lancet* **1976**, *308* (7995), 1102–1104.

(11) Bitish Thoracic Society. A Controlled Trial of Six Months'chemotherapy in Pulmonary Tuberculosis, Final Report: Results Duringthe 36 Months after the End of Chemotherapy and Beyond. *Br. J. Dis.Chest* **1984**, *78*, 330–336.

(12) Wimley, W. C. Describing the Mechanism of Antimicrobial Peptide Action with the Interfacial Activity Model. *ACS Chemical Biology* **2010**, *5* (10), 905–917. https://doi.org/10.1021/cb1001558.

(13) Ergene, C.; Yasuhara, K.; Palermo, E. F. Biomimetic Antimicrobial Polymers: Recent Advances in Molecular Design. *Polymer Chemistry*. Royal Society of Chemistry May 14, 2018, pp 2407–2427. https://doi.org/10.1039/c8py00012c.

(14) Ganewatta, M. S.; Tang, C. Controlling Macromolecular Structures towards Effective Antimicrobial Polymers. *Polymer (Guildf)* **2015**, *63*, A1–A29. https://doi.org/10.1016/j.polymer.2015.03.007.

(15) Nguyen, L. T.; Haney, E. F.; Vogel, H. J. The Expanding Scope of Antimicrobial Peptide Structures and Their Modes of Action. *Trends in Biotechnology* **2011**, *29* (9), 464–472. https://doi.org/10.1016/j.tibtech.2011.05.001.

(16) Hancock, R. E. W.; Sahl, H. G. Antimicrobial and Host-Defense Peptides as New Anti-Infective Therapeutic Strategies. *Nature Biotechnology* **2006**, *24* (12), 1551–1557. https://doi.org/10.1038/nbt1267.

(17) Magennis, E. P.; Francini, N.; Mastrotto, F.; Catania, R.; Redhead, M.; Fernandez-Trillo, F.; Bradshaw, D.; Churchley, D.; Winzer, K.; Alexander, C.; Mantovani, G. Polymers for Binding of the Gram-Positive Oral Pathogen Streptococcus Mutans. *PLoS ONE* **2017**, *12* (7). https://doi.org/10.1371/journal.pone.0180087.

(18) Purdy, G. E.; Niederweis, M.; Russell, D. G. Decreased Outer Membrane Permeability Protects Mycobacteria from Killing by Ubiquitin-Derived Peptides. *Molecular Microbiology* **2009**, *73* (5), 844–857. https://doi.org/10.1111/j.1365-2958.2009.06801.x.

(19) Ahmed, M. S.; Annamalai, T.; Li, X.; Seddek, A.; Teng, P.; Tse-Dinh, Y. C.; Moon, J. H. Synthesis of Antimicrobial Poly(Guanylurea)s. *Bioconjugate Chemistry* **2018**, *29* (4), 1006–1009. https://doi.org/10.1021/acs.bioconjchem.8b00057.

(20) Phillips, D. J.; Harrison, J.; Richards, S. J.; Mitchell, D. E.; Tichauer, E.; Hubbard, A. T. M.; Guy, C.; Hands-Portman, I.; Fullam, E.; Gibson, M. I. Evaluation of the Antimicrobial Activity of Cationic Polymers against Mycobacteria: Toward Antitubercular Macromolecules. *Biomacromolecules* **2017**, *18* (5), 1592–1599. https://doi.org/10.1021/acs.biomac.7b00210.

(21) Wolucka, B. A.; McNeil, M. R.; De Hoffmann, E.; Chojnacki, T.; Brennan, P. J. Recognition of the Lipid Intermediate for Arabinogalactan/Arabinomannan Biosynthesis and Its Relation to the Mode of Action of Ethambutol on Mycobacteria. *Journal of Biological Chemistry* **1994**, *269* (37), 23328–23335. https://doi.org/10.1016/s0021-9258(17)31657-5.

(22) Zuber, B.; Chami, M.; Houssin, C.; Dubochet, J.; Griffiths, G.; Daffé, M. Direct Visualization of the Outer Membrane of Mycobacteria and Corynebacteria in Their Native State. *Journal of Bacteriology* **2008**, *190* (16), 5672–5680. https://doi.org/10.1128/JB.01919-07.

(23) Brennan, P. J. Structure, Function, and Biogenesis of the Cell Wall of Mycobacterium Tuberculosis. *Tuberculosis* **2003**, *83* (1–3), 91–97. https://doi.org/10.1016/S1472-9792(02)00089-6.

(24) van der Does, A. M.; Hiemstra, P. S.; Mookherjee, N. *Antimicrobial Host Defence Peptides: Immunomodulatory Functions and Translational Prospects*; 2019; Vol. 1117. https://doi.org/10.1007/978-981-13-3588-4-10.

(25) Mookherjee, N.; Anderson, M. A.; Haagsman, H. P.; Davidson, D. J. Antimicrobial Host Defence Peptides: Functions and Clinical Potential. *Nature Reviews Drug Discovery* **2020**, *19* (5), 311–332. https://doi.org/10.1038/s41573-019-0058-8.

(26) Rodrigues, L.; Ramos, J.; Couto, I.; Amaral, L.; Viveiros, M. Ethidium Bromide Transport across Mycobacterium Smegmatis Cell-Wall: Correlation with Antibiotic Resistance. *BMC Microbiology* **2011**, *11*. https://doi.org/10.1186/1471-2180-11-35.

(27) Du, D.; Wang-Kan, X.; Neuberger, A.; van Veen, H. W.; Pos, K. M.; Piddock, L. J. V.; Luisi, B. F. Multidrug Efflux Pumps: Structure, Function and Regulation. *Nature Reviews Microbiology*. Nature Publishing Group September 1, 2018, pp 523–539. https://doi.org/10.1038/s41579-018-0048-6.

(28) Song, L.; Wu, X. Development of Efflux Pump Inhibitors in Antituberculosis Therapy. *International Journal of Antimicrobial Agents* **2016**, *47* (6), 421–429. https://doi.org/10.1016/j.ijantimicag.2016.04.007.

(29) Black, P. A.; Warren, R. M.; Louw, G. E.; van Helden, P. D.; Victor, T. C.; Kana, B. D. Energy Metabolism and Drug Efflux in Mycobacterium Tuberculosis. *Antimicrobial Agents and Chemotherapy* **2014**, *58* (5), 2491–2503. https://doi.org/10.1128/AAC.02293-13.

(30) Ernst, J. D. *MINIREVIEW Macrophage Receptors for Mycobacterium Tuberculosis*; 1998; Vol. 66.

(31) Glickman, M. S.; Jacobs, J. W. R. Microbial Pathogenesis Review of Mycobacterium Tuberculosis:Dawn of a Discipline. *Cell Press* **2001**, *104*, 477–485.

(32) Protocols in In Vitro Hepatocyte Research. In *Protocols in In Vitro Hepatocyte Research*; Donato, M. T., Tolosa, L., Gómez-Lechón, M. J., Eds.; Springer Protocols, 2015; Vol. 1250.

(33) Wu, M. L.; Gengenbacher, M.; Dick, T. Mild Nutrient Starvation Triggers the Development of a Small-Cell Survival Morphotype in Mycobacteria. *Frontiers in Microbiology* **2016**, *7* (JUN), 1–11. https://doi.org/10.3389/fmicb.2016.00947.

(34) Clary, G.; Sasindran, S. J.; Nesbitt, N.; Mason, L.; Cole, S.; Azad, A.; McCoy, K.; Schlesinger, L. S.; Hall-Stoodley, L. Mycobacterium Abscessus Smooth and Rough Morphotypes Form Antimicrobial-Tolerant Biofilm Phenotypes but Are Killed by Acetic Acid. *Antimicrobial Agents and Chemotherapy* **2018**, *62* (3). https://doi.org/10.1128/AAC.01782-17.

(35) MacFarlane, T. W.; Samaranayake, L. P.; MacFarlane, T. Wallace. Use of the Microbiology Laboratory. *Clinical oral microbiology /*. Wright,: London ; Boston : 1989, pp 187–203. https://doi.org/10.1016/B978-0-7236-0934-6.50018-5.

(36) Hards, K.; Robson, J. R.; Berney, M.; Shaw, L.; Bald, D.; Koul, A.; Andries, K.; Cook, G. M. Bactericidal Mode of Action of Bedaquiline. *Journal of Antimicrobial Chemotherapy* **2015**, *70* (7), 2028–2037. https://doi.org/10.1093/jac/dkv054.

(37) Chen, C.; Gardete, S.; Jansen, R. S.; Shetty, A.; Dick, T.; Rhee, K. Y.; Dartois, V. *Verapamil Targets Membrane Energetics in Mycobacterium Tuberculosis*; 2018.

(38) Kasianowicz, J.; Benz, R.; McLaughlin, S. The Kinetic Mechanism by Which CCCP (Carbonyl Cyanide m-Chlorophenylhydrazone) Transports Protons across Membranes. *The Journal of Membrane Biology* **1984**, *82* (2), 179–190. https://doi.org/10.1007/BF01868942.

(39) Chen, C. Z.; Beck-Tan, N. C.; Dhurjati, P.; van Dyk, T. K.; LaRossa, R. A.; Cooper, S. L. Quaternary Ammonium Functionalized Poly(Propylene Imine) Dendrimers as Effective Antimicrobials: Structure-Activity Studies. *Biomacromolecules* **2000**, *1* (3), 473–480. https://doi.org/10.1021/bm0055495.

(40) Lebaron, P.; Catala, P.; Parthuisot, N. Effectiveness of SYTOX Green Stain for Bacterial Viability Assessment. *Applied and Environmental Microbiology* **1998**, *64* (7), 2697–2700. https://doi.org/10.1128/aem.64.7.2697-2700.1998.

(41) Pulido, D.; Torrent, M.; Andreu, D.; Nogues, M. V.; Boix, E. Two Human Host Defense Ribonucleases against Mycobacteria, the Eosinophil Cationic Protein (RNase 3) and RNase 7. *Antimicrobial Agents and Chemotherapy* **2013**, *57* (8), 3797–3805. https://doi.org/10.1128/AAC.00428-13.

(42) Padwal, P.; Bandyopadhyaya, R.; Mehra, S. Biocompatible Citric Acid-Coated Iron Oxide Nanoparticles to Enhance the Activity of First-Line Anti-TB Drugs in Mycobacterium Smegmatis. *Journal of Chemical Technology and Biotechnology* **2015**, *90* (10), 1773–1781. https://doi.org/10.1002/jctb.4766.

(43) Scutigliani, E. M.; Scholl, E. R.; Grootemaat, A. E.; Khanal, S.; Kochan, J. A.; Krawczyk, P. M.; Reits, E. A.; Garzan, A.; Ngo, H. X.; Green, K. D.; Garneau-Tsodikova, S.; Ruijter, J. M.; van Veen, H. A.; van der Wel, N. N. Interfering with DNA Decondensation as a Strategy against Mycobacteria. *Frontiers in Microbiology* **2018**, *9* (SEP), 1–12. https://doi.org/10.3389/fmicb.2018.02034.

(44) Leber, A. Synergism Testing: Broth Microdilution Checkerboard and Broth Macrodilution Methods. *Clinical Microbiology Procedures Handbook* **2016**, 5.16.1-5.16.23. https://doi.org/10.1128/9781555818814.ch5.16.

(45) Jeon, A. B.; Ackart, D. F.; Li, W.; Jackson, M.; Melander, R. J.; Melander, C.; Abramovitch, R. B.; Chicco, A. J.; Basaraba, R. J.; Obregón-Henao, A. 2-Aminoimidazoles Collapse Mycobacterial Proton Motive Force and Block the Electron Transport Chain. *Scientific Reports* **2019**, *9* (1), 1–13. https://doi.org/10.1038/s41598-018-38064-7.

(46) Wherli, W. Rifampin: Mechanisms of Action and Resistance. *Reviews of Infectious Diseases* **1983**, *5* (3), 407–411.

(47) LeBel, M. Ciprofloxacin: Chemistry, Mechanism of Action, Resistance, Antimicrobial Spectrum, Pharmacokinetics, Clinical Trials, and Adverse Reactions. *Pharmacotherapy: The Journal of Human Pharmacology and Drug Therapy* **1988**, *8* (1), 3–30. https://doi.org/10.1002/j.1875-9114.1988.tb04058.x.

(48) Vandal, O. H.; Nathan, C. F.; Ehrt, S. Acid Resistance in Mycobacterium Tuberculosis. *Journal of Bacteriology* **2009**, *191* (15), 4714–4721. https://doi.org/10.1128/JB.00305-09.

(49) Hurdle, J. G.; O'Neill, A. J.; Chopra, I.; Lee, R. E. Targeting Bacterial Membrane Function: An Underexploited Mechanism for Treating Persistent Infections. *Nature Reviews Microbiology* **2011**, *9* (1), 62–75. https://doi.org/10.1038/nrmicro2474.

(50) Fontes, F. L.; Peters, B. J.; Crans, D. C.; Crick, D. C. The Acid-Base Equilibrium of Pyrazinoic Acid Drives the PH Dependence of Pyrazinamide-Induced Mycobacterium Tuberculosis Growth Inhibition. *ACS Infectious Diseases* **2020**, *6* (11), 3004–3014. https://doi.org/10.1021/acsinfecdis.0c00507.

(51) Zhang, Y.; Wade, M. M.; Scorpio, A.; Zhang, H.; Sun, Z. Mode of Action of Pyrazinamide: Disruption of Mycobacterium Tuberculosis Membrane Transport and Energetics by Pyrazinoic Acid. *Journal of Antimicrobial Chemotherapy* **2003**, *52* (5), 790–795. https://doi.org/10.1093/jac/dkg446.

(52) Lu, P.; Haagsma, A. C.; Pham, H.; Maaskant, J. J.; Mol, S.; Lill, H.; Bald, D. Pyrazinoic Acid Decreases the Proton Motive Force, Respiratory ATP Synthesis Activity, and Cellular ATP Levels. *Antimicrobial Agents and Chemotherapy* **2011**, *55* (11), 5354–5357. https://doi.org/10.1128/AAC.00507-11.

(53) Cook, G. M.; Hards, K.; Dunn, E.; Heikal, A.; Nakatani, Y.; Greening, C.; Crick, D. C.; Fontes, F. L.; Pethe, K.; Hasenoehrl, E.; Berney, M. Oxidative Phosphorylation as a Target Space for Tuberculosis: Success, Caution, and Future Directions. *Tuberculosis and the Tubercle Bacillus: Second Edition* **2017**, *5* (3), 295–316. https://doi.org/10.1128/9781555819569.ch14.

(54) Rao, M.; Streur, T. L.; Aldwell, F. E.; Cook, G. M. Intracellular PH Regulation by Mycobacterium Smegmatis and Mycobacterium Bovis BCG. *Microbiology (N Y)* **2001**, *147* (4), 1017–1024. https://doi.org/10.1099/00221287-147-4-1017.

(55) Rao, S. P. S.; Alonso, S.; Rand, L.; Dick, T.; Pethe, K. The Protonmotive Force Is Required for Maintaining ATP Homeostasis and Viability of Hypoxic, Nonreplicating Mycobacterium Tuberculosis. *Proc Natl Acad Sci U S A* **2008**, *105* (33), 11945–11950. https://doi.org/10.1073/pnas.0711697105.

(56) te Winkel, J. D.; Gray, D. A.; Seistrup, K. H.; Hamoen, L. W.; Strahl, H. Analysis of Antimicrobial-Triggered Membrane Depolarization Using Voltage Sensitive Dyes. *Frontiers in Cell and Developmental Biology* **2016**, *4* (APR), 1–10. https://doi.org/10.3389/fcell.2016.00029.

(57) Shetty, A.; Dick, T. Mycobacterial Cell Wall Synthesis Inhibitors Cause Lethal ATP Burst. *Frontiers in Microbiology* **2018**, *9* (AUG), 1–9. https://doi.org/10.3389/fmicb.2018.01898.

(58) Jiang, T.; Zhan, Y.; Sun, M.; Liu, S.; Zang, S.; Ma, Y.; Xin, Y. The Novel Responses of Ethambutol against Mycobacterium Smegmatis Mc 2155 Revealed by Proteomics Analysis. *Current Microbiology* **2011**, *62* (2), 341–345. https://doi.org/10.1007/s00284-010-9711-5.

(59) Black, P. A.; Warren, R. M.; Louw, G. E.; Van Helden, P. D.; Victor, T. C.; Kana, B. D. Energy Metabolism and Drug Efflux in Mycobacterium Tuberculosis. *Antimicrobial Agents and Chemotherapy* **2014**, *58* (5), 2491–2503. https://doi.org/10.1128/AAC.02293-13.

(60) Lu, P.; Villellas, C.; Koul, A.; Andries, K.; Lill, H.; Bald, D. The ATP Synthase Inhibitor Bedaquiline Interferes with Small-Molecule Efflux in Mycobacterium Smegmatis. *Journal of Antibiotics* **2014**, *67* (12), 835–837. https://doi.org/10.1038/ja.2014.74.

(61) Datta, P.; Ravi, J.; Guerrini, V.; Chauhan, R.; Neiditch, M. B.; Shell, S. S.; Fortune, S. M.; Hancioglu, B.; Igoshin, O. A.; Gennaro, M. L. The Psp System of Mycobacterium Tuberculosis Integrates Envelope Stress-Sensing and Envelope-Preserving Functions. *Molecular Microbiology* **2015**, *97* (3), 408–422. https://doi.org/10.1111/mmi.13037.

(62) Bansal-Mutalik, R.; Nikaido, H. Mycobacterial Outer Membrane Is a Lipid Bilayer and the Inner Membrane Is Unusually Rich in Diacyl Phosphatidylinositol Dimannosides. *Proc Natl Acad Sci U S A* **2014**, *111* (13), 4958–4963. https://doi.org/10.1073/pnas.1403078111.

(63) Guallar-Garrido, S.; Luquin, M.; Julián, E. Analysis of the Lipid Composition of Mycobacteria by Thin Layer Chromatography. *Journal of Visualized Experiments* **2021**, *2021* (170). https://doi.org/10.3791/62368.

(64) Hards, K.; Robson, J. R.; Berney, M.; Shaw, L.; Bald, D.; Koul, A.; Andries, K.; Cook, G. M. Bactericidal Mode of Action of Bedaquiline. *Journal of Antimicrobial Chemotherapy* **2015**, *70* (7), 2028–2037. https://doi.org/10.1093/jac/dkv054.

CHAPTER 3

STRUCTURE-ACTIVITY RELATIONSHIP STUDIES OF POLY(GUANYLUREA)S ON ANTIMYCOBACTERIAL ACTIVITY

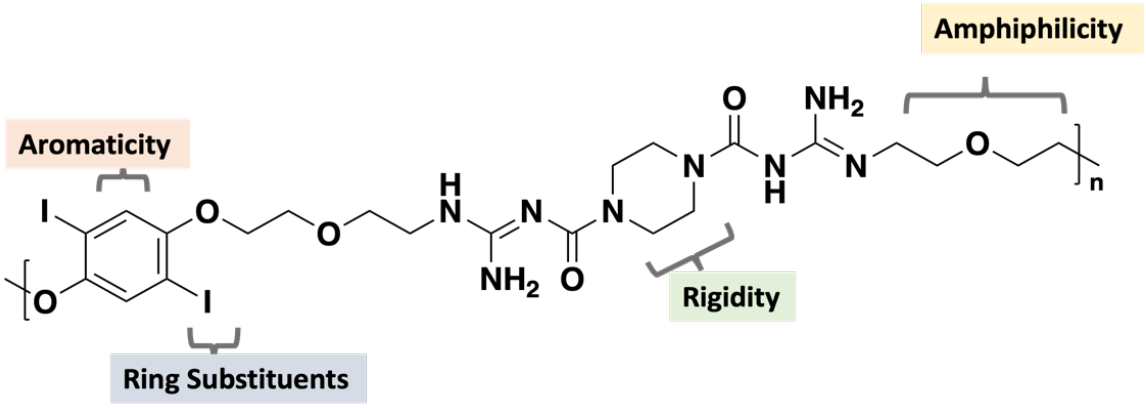

3.1 Abstract

Although great advances have been made in prevention and treatment of tuberculosis (TB), TB infections continue to be a public health treat in developing countries. Latent TB infections caused by dormant TB are hard to treat as most anti-TB drugs disrupt intracellular functions in replicating TB. In addition to both replicating and dormant TB rely on a polarized membrane; therefore, targeting destabilization of vital membrane functions (e.g., membrane potential, energy production) would broaden the antimycobacterial effectiveness of anti-TB drugs. Poly(guanylurea piperazines)s (PGU-P-8K) have shown to disrupt the bioenergetics by targeting the mycobacterial membrane resulting in a fast bactericidal effect on mycobacteria. Here, we explore the effect of key functionalities along the backbone (e.g., aromaticity, rigidity, amphiphilicity) of PGU-P-8K. While most PGUs showed similar activity against non-pathogenic *Msm*, preliminary results showed that retaining high degree of hydrophobicity along the backbone broadened the antimycobacterial spectrum, aromaticity played an important role in broaden antimicrobial activity and increasing PEGylation increased toxicity. An in-depth understanding of the effect of the linear backbone structure of PGU-P-8K on the mycobacterial membrane would contribute to the optimization of anti-TB drug development, as well as expand the biological applications of PGUs.

3.2 Introduction

Tuberculosis (TB) remains being a world-wide public health threat; eradication of TB infections continues to be a top goal of the World Health Organization (WHO).[1]

The treatment of TB consists of a multidrug regimen for a period of 4 to 9 months; if not followed as prescribed, multidrug resistant TB (MDR TB) can emerge.[2-5] Most anti-TB drugs target inhibition of intracellular processes (e.g., DNA, RNA, or cell wall synthesis) in replicating TB, in which case bacteria can genetically develop mechanisms of resistance (i.e., MDR TB).[3,5-7] Additionally, these traditional target sites are not as effective towards phenotypically different bacteria (i.e., dormant TB) [8]. Therefore, novel unconventional therapeutics effective against mycobacterial persisters and drug-resistant TB are warranted for improving TB treatment.

Alternatively, targeting the destabilization of the membrane would cause a plethora of disturbances on vital functions - making it harder for the bacteria to develop resistance - a third of integral cellular processes are housed in the mycobacterial membrane (e.g., transport of nutrients, and energy production).[7,9] In addition, both replicating and dormant TB rely on a polarized membrane for its survival, which would broaden the antimycobacterial effectiveness of membrane targeting drugs.[10]

Previously, we performed mechanism of action studies on a novel class of mycobacterial membrane targeting oligomers, poly(guanylurea piperazines)s (PGU-P-8K).[11] PGU-P-8K showed fast-acting bactericidal activity via dissipation of the membrane potential, increased intracellular ATP levels and efflux pump inhibition, due to suspected multidentate interaction with the membrane. Here, we explore the effects of the structural components in the linear backbone of PGU-P-8K. PGU-P-8K showed that the diiodo substituent in the aromatic ring did not affect its antimycobacterial effect against non-pathogenic mycobacteria, but it decreased effectiveness against pathogenic mycobacteria. Interestingly, increasing PEGylation around the guanylurea functional

group retained antimycobacterial activity, but increased toxicity. As the physicochemical properties of mycobacterial membrane targeting drugs are not well-understood, the structure-activity relationship (SAR) studies of a small library of PGUs would elucidate the key structural components in PGU-P-8K responsible for targeting the mycobacterial membrane, contributing to the development of novel membrane-targeting antimycobacterial agents.[7]

3.3 Results and Discussion

Here, we report the effects of structural changes along the backbone of linear poly(guanylurea)s (PGUs) on antimycobacterial activity. A small library of PGUs was synthesized, characterized, and tested for a comprehensive understanding of the physicochemical properties of mycobacterial membrane targeting compounds (Figure 3.1).

Due to the tunability, vast availability of diamine- and diisocyanate-containing monomers, simple polymerization, and selectivity, PGU oligomers were selected to study the effects on the mycobacterial membrane. The rationale behind the design of the library focused on representing changes in aromaticity, rigidity and amphiphilicity in the backbone of the PGUs (Figure 3.1). *N,N*'-di-*tert*-butyloxycarbonyl (Boc)-guanidine- or guanidinium-containing monomers were polymerized via step-growth polymerization in the presence of

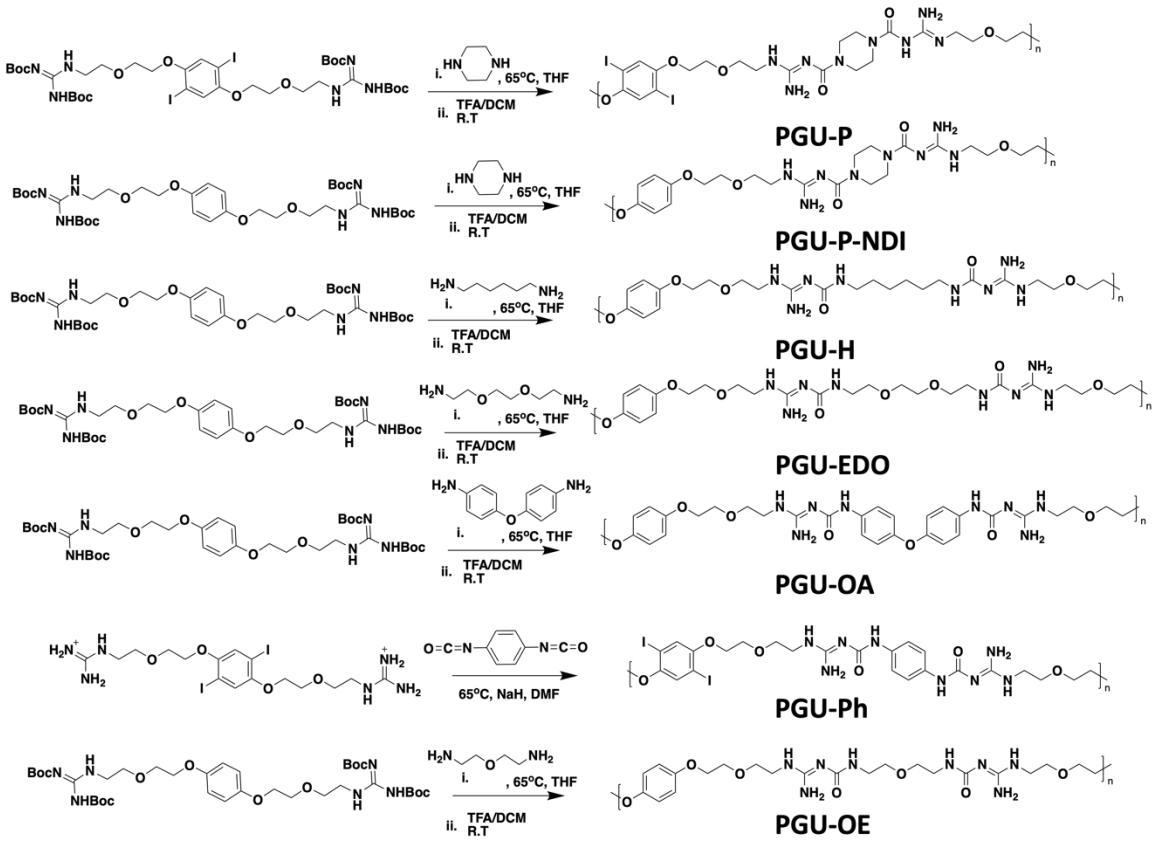

Figure 3.1 General synthetic pathway of poly(guanylurea)s (P, P-NDI, H, EDO, OA, OE and Ph).

a diamine- or diisocyanate-containing monomer at ~70 °C. The oligomer size was controlled via mole-to-mole ratio of the monomers for PGUs to obtain a molecular weight (M_n) close to 8 kDa, except in the case of the aromatic diamine, 4,4'-oxydianiline (OA), which resulted in ~4kDa. Additionally, the oligomers that were synthesized using the diguanidine and diisocyanate monomers were boc-protected for molecular weight analysis (M_n and M_w). The polymerization was confirmed via Gel-Permeation Chromatography (GPC), and the guanylurea-formation via Nuclear Magnetic Resonance (NMR) (Table 3.1). The oligomer size was further analyzed via end-group analysis in NMR. Subsequent deprotection of boc-group in acidic conditions was performed and absence of boc-group established via NMR. The hydrodynamic diameter and zeta potential were measured of

similar M_w to understand the behavior of the PGUs in aqueous environments where aromaticity did not show formation of a stable nanoparticle and removal of diiodo had similar properties as previously published PGU-P [11] (Table 3.2).

Table 3.1 Summary of molecular weights (M_n and M_w), and number of repeating units (n) from end-group analysis.

PGUs	M_n [kDa]	M_w [kDa]	PDI	n
P	13	23	1.8	13
	10	19	1.9	10
	8.0	11	1.4	8
	3.0	5.0	1.7	3
	9.0	19	2.1	19
EDO	5.0	6.0	1.2	7
	9.0	17	1.9	11
H	9.0	17	1.9	12
	6.0	8.0	1.3	8
OA	4.0	6.0	1.5	5
Ph	8.5	13	1.5	

Table 3.2 Summary of physical properties of PGUs with similar repeating units.

PGUs	M_n [kDa]	M_w [kDa]	PDI	Yield (%)	n	HD	ζ
P	9	19	2.1	75	8		
NDI-P	6	9	1.5	24	8	53.0 ± 3.4	-17.50
H	6	8	1.3	23	8		
OA	4	6	1.5	40	5	560.1 ± 95	-33.50
EDO	9	17	1.9	89	11		
OE	4	6	1.5	59	5		

The minimum inhibitory concentration of PGUs was tested against mycobacteria (i.e., *M. smegmatis, Msm*), Gram-positive (i.e., *S. aureus, Sau*) and -negative bacteria (i.e., *E. coli, Eco*) in comparison to PGU-P-8K. The removal of diiodo (NDI) and the presence of the 2,2'-(Ethylenedioxy)diethylamine (EDO), a flexible guanylurea-linker (Table 3.3) showed to enhanced specificity against *Msm*. Interestingly, both aromatic linkers OA, and 1,4-phenylene diisocyanate (Ph) retained similar antimicrobial activity to that of PGU-P-8K; where OA did not contain the diiodo group and had fewer repeating units. This suggested that the additional aromaticity and hydrophobicity from linker played a role in broader spectrum antimicrobial activity, when the hydrophobicity and bulkiness from the diiodo group was missing. To further test this hypothesis, PGU-EDO, and PGU-P-NDI were further tested for antimycobacterial activity against *M. abscessus* (*Mab*) (Table 3.4). *Mab* can form two morphotypes, smooth (S) and rough (R), whether glycopeptidolipids (GPLs) are present or absent, respectively.[14-16] The absence of GPLs in *Mab* R increases the hydrophobicity cell envelope environment, and increasing pathogenicity.[14,15] While the flexibility and increased PEGylation in EDO decreased the effectiveness against Gram-positive bacteria (Table 3.3), it did not affect the antimycobacterial activity, behaving similarly to PGU-P-8K (Table 3.3). Whereas the removal of diiodo-group (NDI) decreased effectiveness against *Mab* S (~3-fold) and *S.aureus*. Similarly, NDI had no effect against replicating *Mtb*, while EDO and P showed some bacterial growth inhibition (Figure 3.3), suggesting the diiodo group played a significant role in membrane destabilization of pathogenic mycobacteria. PGUs with increased hydrophobicity (OA, H,Ph) will be tested against *Mab* upon completion for deeper understanding.

Table 3.3. Antimicrobial activity of poly(guanylurea)s.

Microorganisms MIC^{90} (μM)

Oligomers	Mycobacteria	Gram-positive	Gram-negative
PGUs	*Msm*	*Sau*	*Eco*
P-8K	6	25	>200
P-NDI	6	>200	>200
H	12.5	200	>200
OA	6	25	200
EDO	6-12	>200	>200
Ph	6	50	200

Table 3.4. Antimycobacterial activity of poly(guanylurea)s.

Mycobacteria MIC^{90} (μM)

PGUs	*Msm*	*Mab R*	*Mab S*
P-8K	6	188	65
P-NDI	6	143	198
H	12.5		
OA	6		
EDO	6-12	196	55
Ph	6		

PGU-P and -NDI exhibited negligible toxicity levels at various concentrations when incubated with murine macrophage cell line (i.e., J774) overnight. Though, the higher degree of PEGylation displayed toxicity at 100 μM (Figure 3.2). Supplementary toxicity testing of PGUs using HeLa cells was performed, where increased the PEGylation of 2,2'-oxybis(ethylamine) (OE) and EDO showed to be the most toxic against mammalian cells while removal of diiodo and increased aromaticity did not

show decreased cell viability up to 40 μM (Figure 3.3). Modifications of the backbone in PGUs showed that increased aromaticity can broaden antimicrobial properties while maintaining low toxicity.

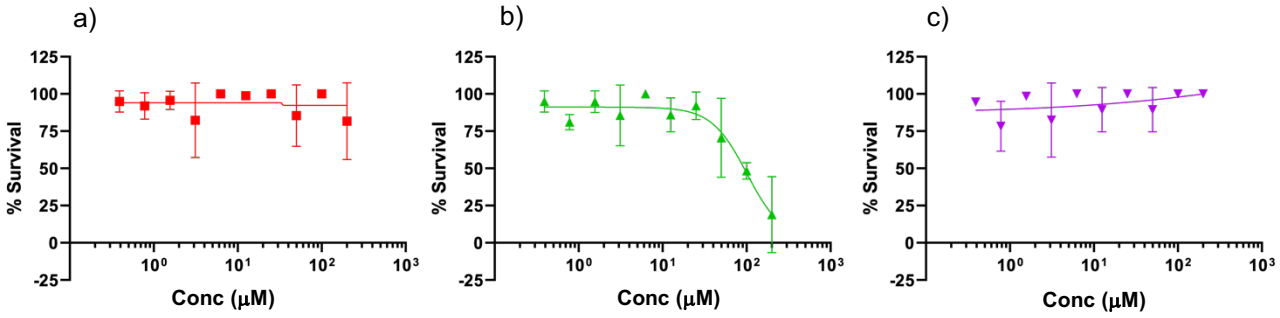

Figure 3.2. Toxicity of a) PGU-P-8K, b) EDO, c) and NDI on J774, murine macrophage cell lines. EDO was found to be the most toxic to J774 at 100 μM.

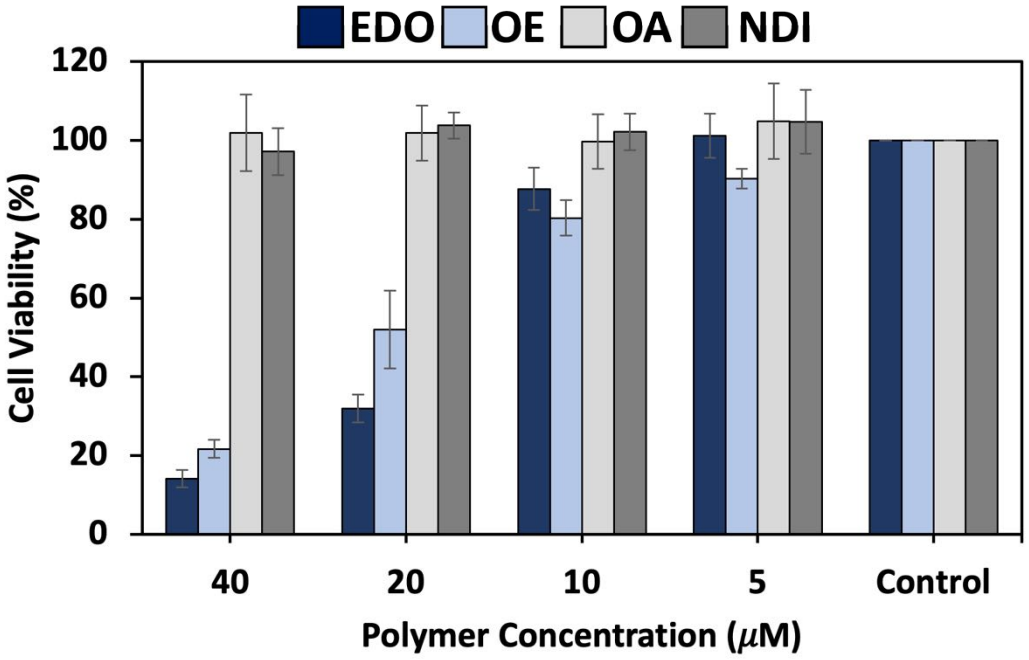

Figure 3.3. Toxicity of EDO, OE, OA, and NDI against HeLa human epithelium cell lines. OE and EDO were found to be the most toxic.

To further investigate the structural changes of PGUs, mode of action assays will be performed with the series of PGUs to study the effect of the backbone modifications on the membrane integrity and membrane functions (i.e., efflux pumps, membrane polarization, and ATP production) of mycobacteria.

Ethidium bromide (EtBr), a fluorescent dye, is an efflux pumps' substrate and damages on the membrane, either directly or indirectly, lead to the accumulation of EtBr. [16-19] As shown in Figure 3.4, a fluorescence increase was observed from PGUs at 1x MIC, where PGU-P-8K showed the lowest accumulation and EDO the highest accumulation of EtBr. The dissipation of the PMF caused by PGU-P-8K has been attributed to the dissipation of the $\Delta\psi$ resulting in the inhibition of efflux pumps, hence the accumulation of EtBr.[60] Otherwise, direct damage to the membrane can cause accumulation of EtBr. While PGU-P-8K did not show direct membrane damage, the increased PEGylation could lead to alternative interaction to the membrane. Although further studies are needed, it is speculated that PGU-EDO increased toxicity, antimycobacterial activity and accumulation of EtBr due to alternate membrane interaction and mode of action.

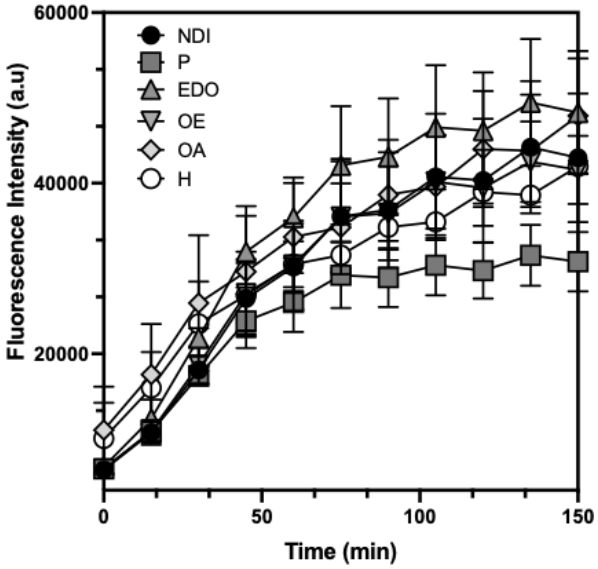

Figure 3.4. Influence on Efflux Pumps Measured through the EtBr Accumulation. Intracellular accumulation assay of ethidium bromide when treating *M. smegmatis* against PGUs at 1x MIC. Intracellular concentration of ethidium bromide EDO but lowest for P. Experiment is shown in mean of triplicates +/- standard deviation.

Membrane permeability assay was performed using Sytox green dye to examine whether the bactericidal effect is directly related to the disruption of membrane integrity. Fluorescence intensity of Sytox green increases when the membrane-impermeable dye intercalates into the intracellular nucleic acids upon diffusion through the damaged membranes.[18] No major fluorescence change was observed from *Msm* treated with PGU-P-NDI at 2x MIC (i.e., 12.5 μM) for 2 h (Figure 3.5); suggesting it acts on the mycobacterial membrane indirectly but that the diiodo group is required for better disruption of bioenergetics since PGU-P-8K showed better MICs against *Mab* S (Table 3.4).

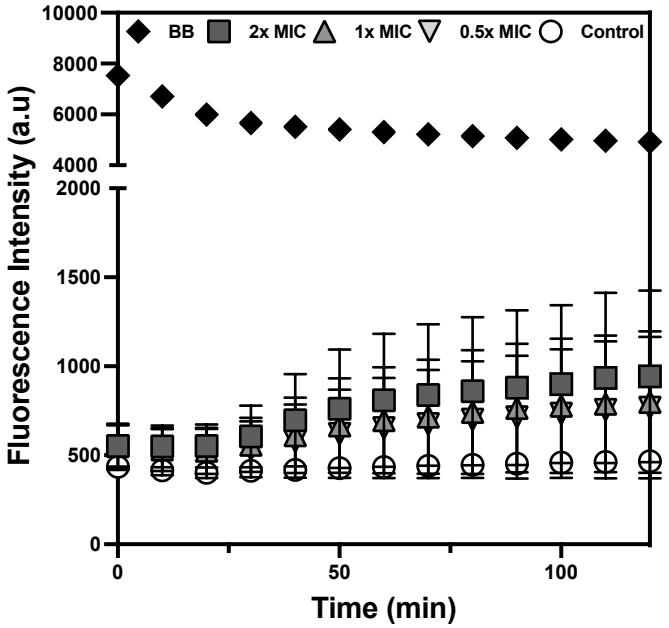

Figure 3.5. Testing of the membrane permeability. The fluorescence of 5 μM Sytox Green dye was measured at 485nm/590nm (ex,em) against *Msm* was tested at various concentrations. Experiment was performed in triplicates, but one representative data is shown for clarity.

3.4 Conclusion

In conclusion, we report the impact of changing core structural modifications in the antimycobacterial activity of PGU-P-8K. A library of PGUs was designed with significant distinctions to investigate the SAR of PGU-P-8K to target the mycobacterial membrane and disrupt bioenergetic processes. Preliminary results of the studies showed removal of diiodo group had no significant effect on non-pathogenic mycobacteria but weakened antimycobacterial activity against pathogenic mycobacteria. Whereas removal of diiodo, but increased PEGylation in EDO retained activity against pathogenic mycobacteria but EDO and OE displayed increased toxicity. Overall, guanylurea in the backbone suggested that is key to inhibit non-pathogenic mycobacterial growth; that the diiodo group played a significant role in membrane

interaction and destabilization of pathogenic mycobacteria and maintaining low cytotoxicity; aromaticity around the guanylurea broaden the antimicrobial spectrum. Upon completion of this work, physical characterization of oligomers will be determined via NMR, GPC, DLS, zeta-potential and octanol-water partition for a thorough physicochemical profile of PGUs. Additionally, membrane assays will perform to study the effect of the backbone modifications on the integrity and functions of the mycobacterial membrane. Culmination will contribute to the optimization of the development of membrane-targeting drug or drug adjuvant for improving TB treatment.

3.5 Experimental Procedures and Supplemental Information

3.5.1 Physical Characterization

^{1}H Nuclear magnetic resonance (NMR) spectra were obtained using a 400 MHz Avance Bruker NMR spectrometer. Chemical shifts were reported in parts per million (ppm) on the δ scale. Deuterated solvents chloroform-d ($CDCl_3$) or dimethyl sufoxide-d_6 (DMSO-d_6) were used as reference solvents; $CDCl_3$ (δ = 7.26 ppm) for the Boc-protected product and DMSO-d_6 (δ = 2.50 ppm) for the deprotected product.

The number averaged (M_n), the weight averaged (M_w) and polydispersity index (PDI) of the Boc-protected oligomer was confirmed via gel permeation chromatography (GPC) against polystyrene standards using a Shimadzu high performance liquid chromatography (HPLC) system at a flow rate of 1.0 mL/min with 2 tandem PLgel 5 μM MIXED-D column operating at 40 °C and SPD-20A ultraviolet visible (UV-Vis) as the detector.

3.5.2 Synthesis of Double-sided *N,N'*-Di-Boc Guanidine Monomers

Synthesis was performed as previously reported with minor modifications.[11] Compound 1 was added to a round bottom flask that contained *N,N'*-Di-Boc-1H-pyrazole-1-carboxamide (2 eq.), and triethylamine (TEA):dichloromethane (DCM) (1:4 v/v) and stirred with heat, overnight. Upon completion of the reaction (i.e., consumption of compound 1 confirmed via TLC), liquid-liquid extraction was performed. The organic layer (DCM) was washed three times and concentrated *in vacuo*. The product was purified via column chromatography using a hexane: ethyl acetate (7:3 v/v) mixture, resulting in white powders.

Scheme 3.2 General synthetic scheme of *N,N'*-Di-Boc guanidine monomers.

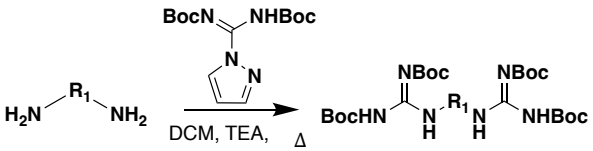

Compound 1

3.5.3 Synthesis of Boc-protected PGUs

Synthesis was performed as previously reported with minor modifications.[11,12] Boc-protected guanidine containing diiodo (0.02 mmol) and piperazine (0.02 mmol) monomers were added in a 4 mL amber vial at a 1:1 mole equivalent. A catalytic amount of potassium carbonate (K_2CO_3) and 400 μL of tetrahydrofuran (THF) was subsequently added to the monomers. The vial was closed tightly, and the reaction was left to stir overnight at 70 °C. The resulting viscous solution was filtered through

glass wool to remove K_2CO_3 and the filtrate was purified by precipitation twice in diethyl ether and once in methanol (MeOH). Oligomer size was confirmed via GPC and end-group analysis, and chemical structure via NMR. NMR data for PGU-Ph will be provided upon completion.

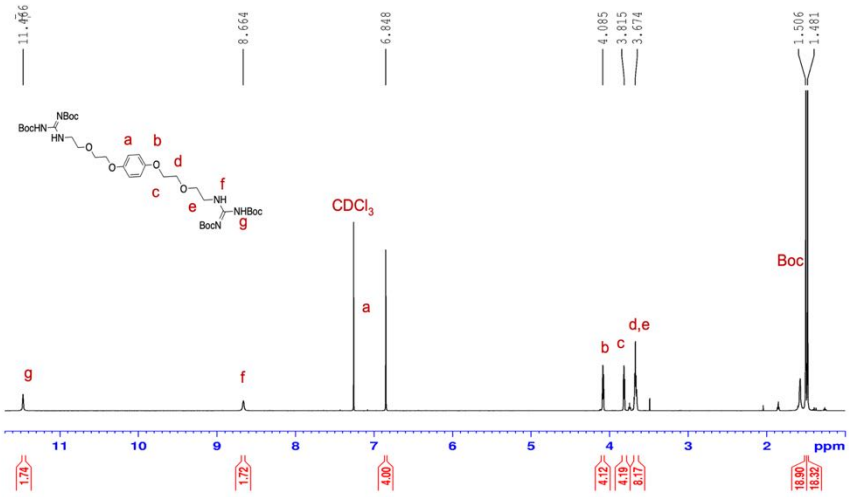

Figure 3.6. *N,N'*-Di-Boc Guanidine Monomer (no diiodo group). White powder was yielded (2.8 g, 98% yield). ^{1}H NMR (600 MHz, $CDCl_3$, δ): 11.47 (s, 2H), 8.66 (s, 2H), 6.85 (s, 4H), 4.09 (t, 4H), 3.82 (t,4.2H), 3.67 (m, 8H), 1.51 (s, 18H), 1.48 (s,18H).

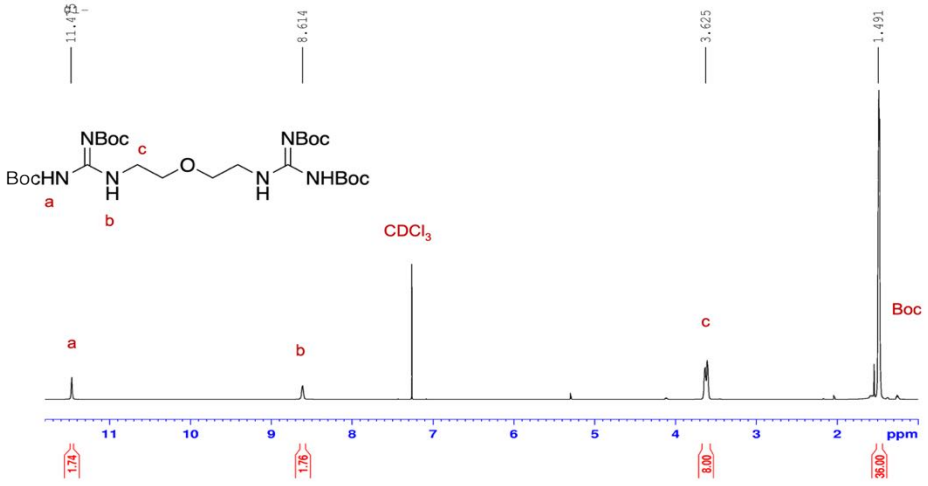

Figure 3.7. *N,N'*-Di-Boc *N,N'*-Di-Boc Guanidine Monomer (no aromatic group). Clear oil was yielded (525 mg, 46% yield). ^{1}H NMR (600 MHz, $CDCl_3$, δ): 11.48 (s, 2H), 8.61 (s, 2H), 3.63 (m, 8H), 1.49 (s, 36H).

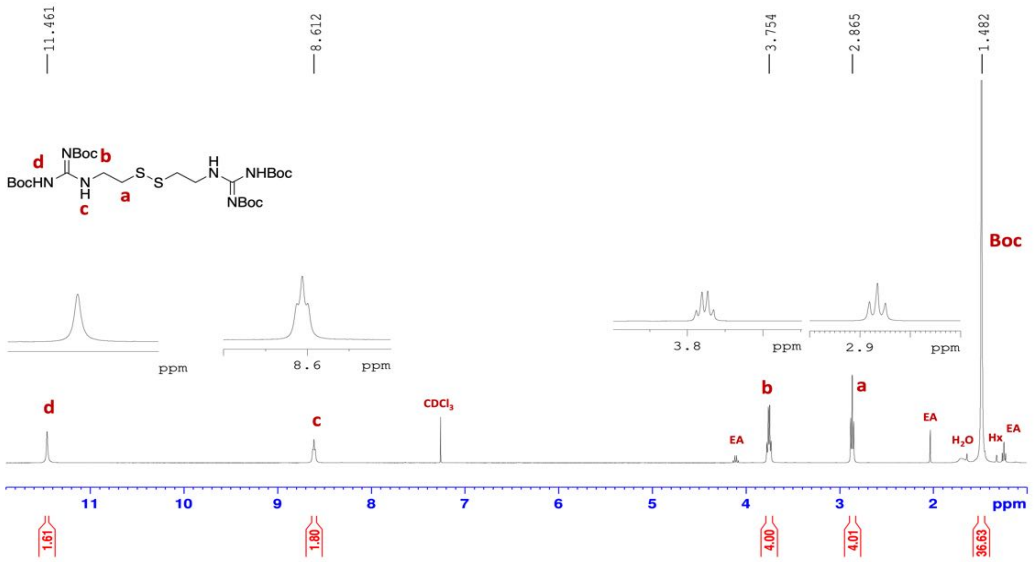

Figure 3.8. *N,N'*-Di-Boc Guanidine Monomer (biodegradable backbone). White powder was yielded (1 g, 83% yield). ^{1}H NMR (400 MHz, $CDCl_3$, δ): 11.48 (s, 2H), 8.61 (t, 2H), 3.75 (q, 4H), 2.87 (t, 4H), 1.48 (t, 36H).

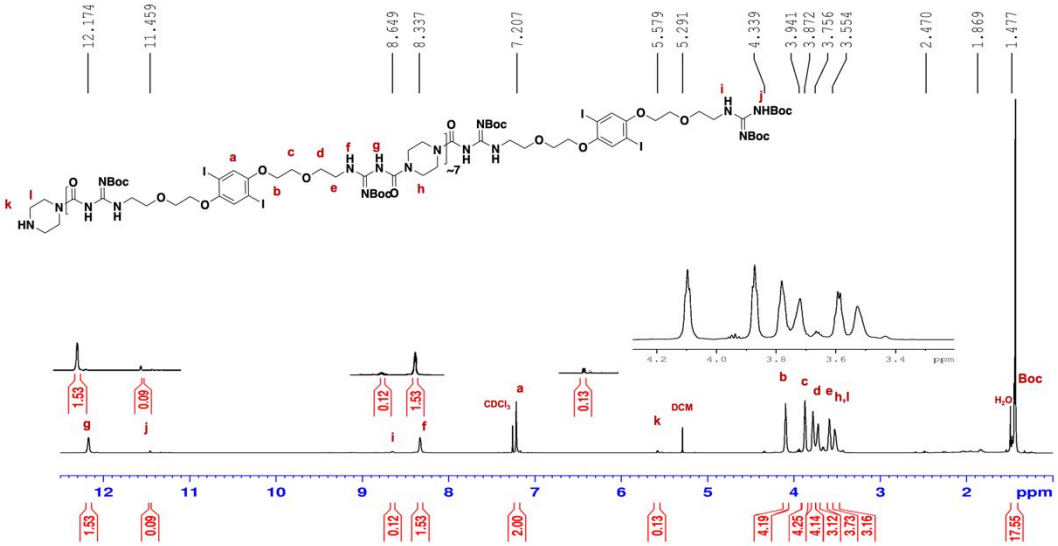

Figure 3.9. ^{1}H NMR of boc-protected PGU-P-8K. White powder. 1H NMR (400 MHz, CDCl3, δ): 12.2 (s, 1H), 8.34 (t, 1H, J = 4.8 Hz), 7.22 (s, 1H), 4.10 (t, 2H, J = 4.6 Hz), 3.88 (t, 2H, J = 4.6 Hz), 3.78 (t, 2H, J = 5.1 Hz), 3.73 (br s, 2H), 3.60 (q, 2H, J = 5.3 Hz, J = 5.1 Hz), 3.53 (br s, 2H), 1.44 (s, 9H).

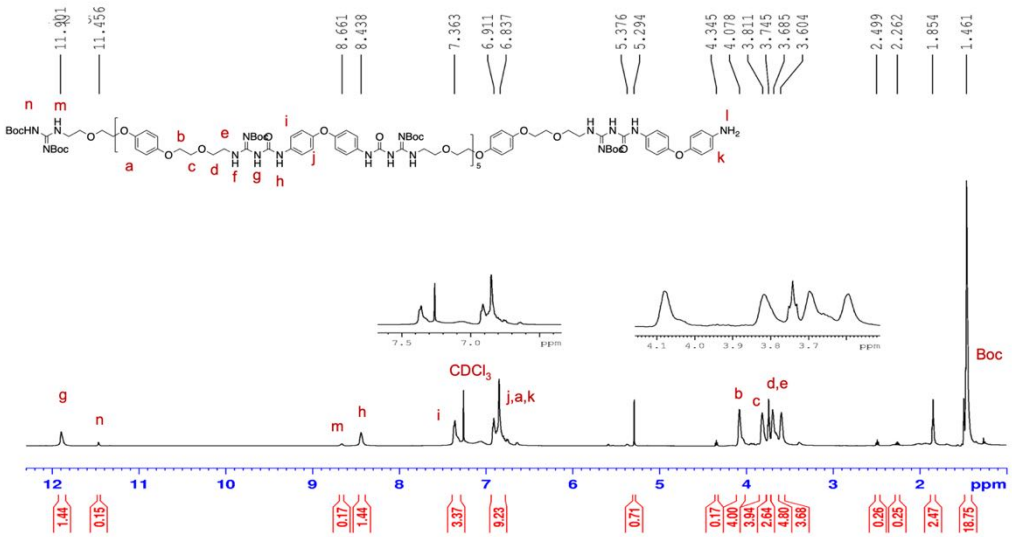

Figure 3.10. ^{1}H NMR of boc-protected PGU-OA. Brown oil was yielded (22.4 mg, 40% yield). ^{1}H NMR (600 MHz, $CDCl_3$, δ): 11.90 (br s, 1H), 8.44 (br s, 1H), 7.36 (br m, 3H), 6.89 (br m, 9H), 5.29 (s, 1H), 4.08 (br s, 4 H), 3.81 (br s, 4H), 3.75 (t, 3H), 3.69 (m, 5H), 3.60 (br s, 4H), 1.85 (s, 2.5H), 1.46 (s, 18H) . GPC: Mn = 4kDa, n=5, PDI = 1.5. End-group analysis: n=5.

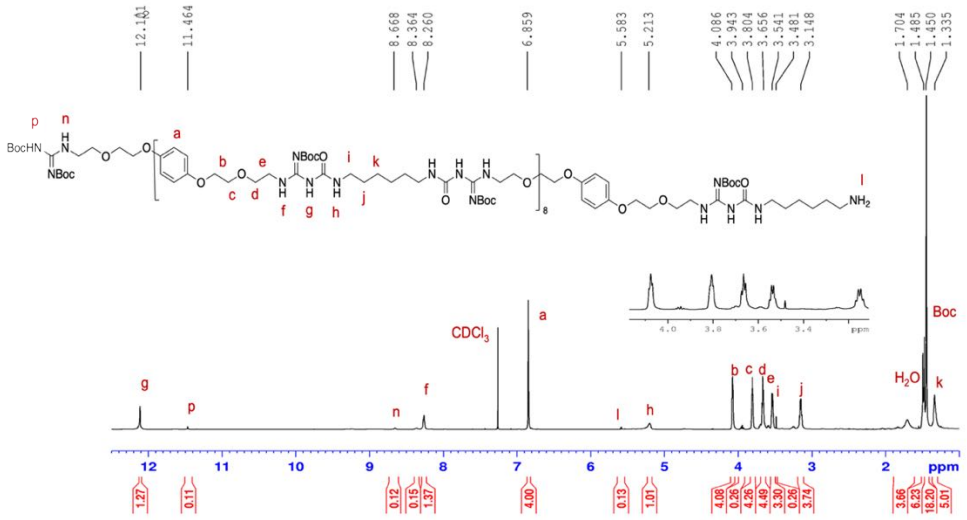

Figure 3.11. ^{1}H NMR of boc-protected PGU-H. White solids were yielded (22.1 mg, 23% yield). ^{1}H NMR (600 MHz, $CDCl_3$, δ): 12.01 (s, 1H), 8.26 (s, 1H), 6.86 (s, 4H), 5.21 (br s, 1H), 4.09 (m, 4H), 3.80 (m, 4H), 3.67 (m, 4H), 3.54 (m, 3H), 3.15 (m, 4H), 1.70 (s, 4H), 1.45 (m, 18H), 1.3 (s, 5H). GPC: Mn = 6kDa, n=8, PDI = 1.3. End-group analysis: n=8.

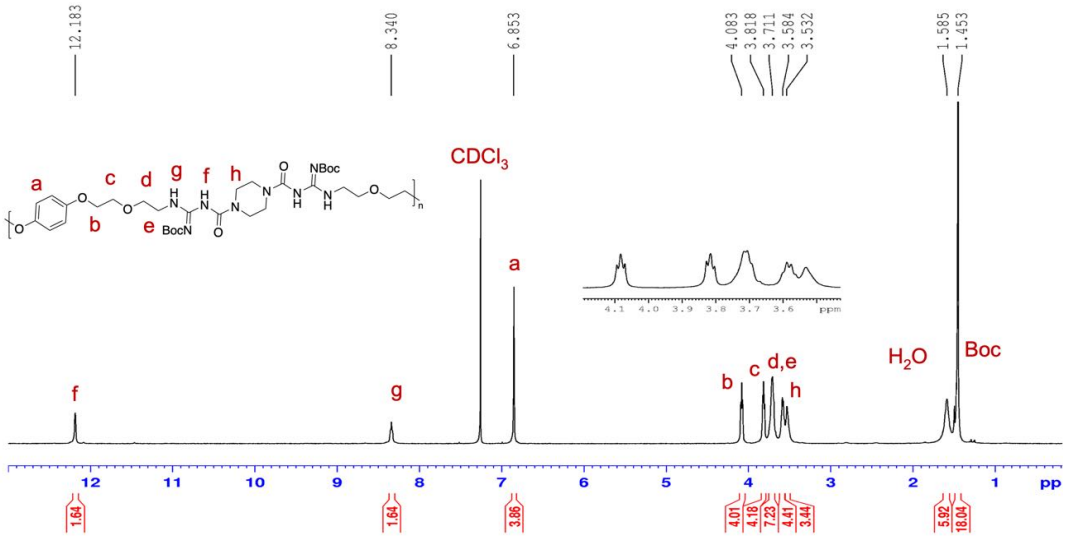

Figure 3.12. [1]H NMR of boc-protected PGU-NDI-P.White solids were yielded (11.0mg, 24% yield). [1]H NMR (600 MHz, $CDCl_3$, δ): 12.18 (s, 2H), 8.34 (s, 2H), 6.85 (s, 4H), 4.08 (t, 4H), 3.82 (t, 4H), 3.71 (br m, 7H), 3.58 (m, 3H),1.45 (m, 18H). GPC: Mn = 6 kDa, n=8, PDI = 1.5.

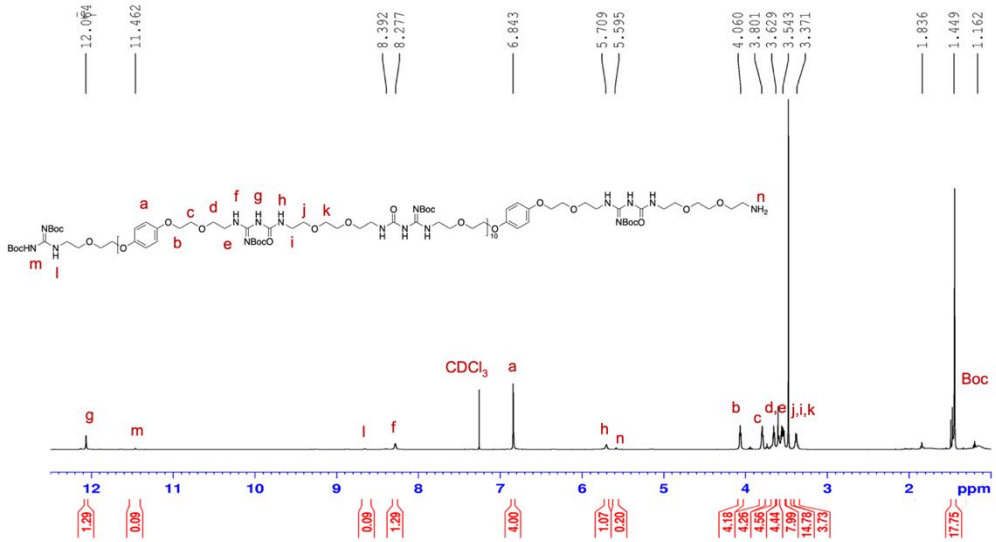

Figure 3.13. [1]H NMR of boc-protected PGU-EDO. White solids were yielded (34.4 mg, 89% yield). [1]H NMR (600 MHz, $CDCl_3$, δ): 12.06 (s, 1H), 8.28 (s, 1H), 6.84 (s, 4 H), 5.71 (br s, 1H), 4.06 (t, 4 H), 3.80 (t, 4H), 3.63 (t, 4H), 3.54 (m, 5H), 3.45 (s, 4H), 3.37 (t, 4H), 1.16 (m, 18H). GPC: Mn = 9 kDa, n=11, PDI = 1.9. End-group analysis: n=10.

3.5.4 Synthesis of Deprotected PGUs

The white powder of boc-protected product (10mg) was dissolved in 2 mL dichloromethane (DCM). Then 1 mL of trifluoroacetic acid (TFA) was added and left to stir overnight resulting in the deprotected product and dried *in vacuo*. The crude product was dissolved in minimum amount of dimethylformamide (DMF) and precipitated in diethyl ether twice and lastly in ethyl acetate. The product was collected by decanting, and successively dried by high vacuum. The white powder was collected and dissolved in DMSO for future testing. Chemical structure was confirmed via NMR.

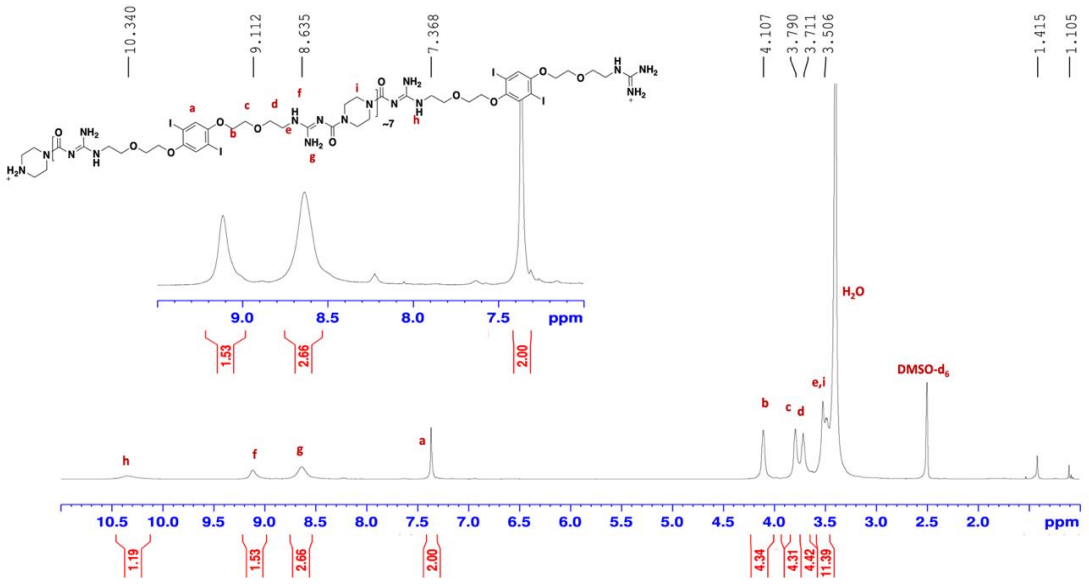

Figure 3.14. ^{1}H NMR of deprotected PGU-P-8K in acidic conditions. White fibrous solid (60% yield). ^{1}H NMR (400 MHz, DMSO-d6, δ): 10.3 (s, 1H), 9.1 (s, 1H), 8.6 (s, 2H), 7.4 (s, 2H), 4.1 (s, 4H), 3.8 (s, 4H), 3.7 (s, 4H), 3.5 (m, 11H).

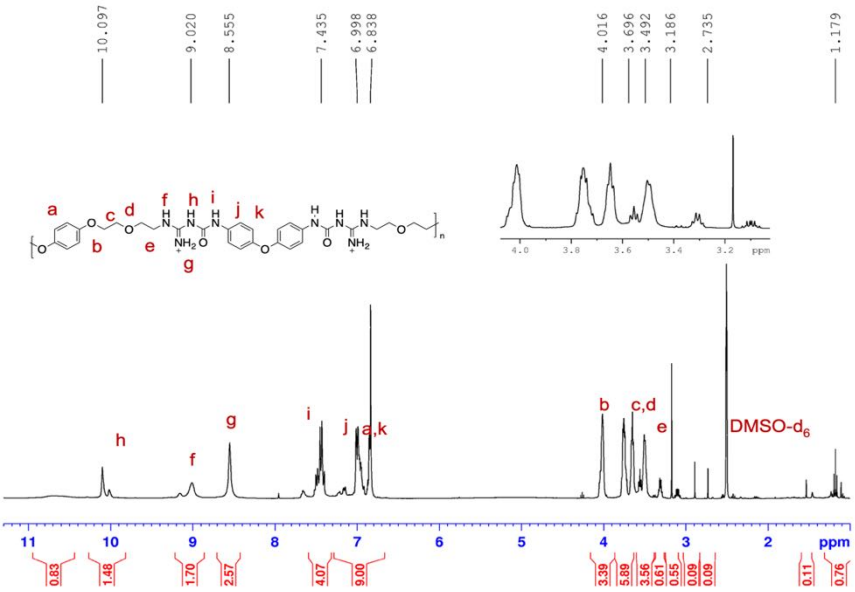

Figure 3.15. [1]H NMR of deprotected PGU- OA.[1]H NMR (600 MHz, DMSO-d_6, δ): 10.10 (m, 1H), 9.02 (m, 2H), 8.56 (br s, 3H), 7.44 (m, 4H), 6.84 (m, 9H), 4.02 (m, 3 H), 3.70 (m, 6H), 3.49 (m, 4H).

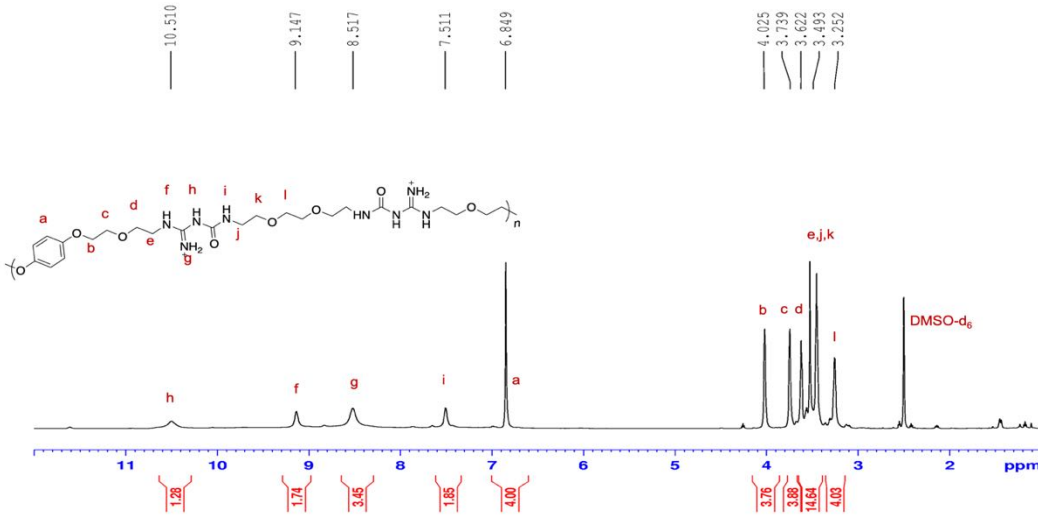

Figure 3.16. [1]H NMR of deprotected PGU- EDO. [1]H NMR (600 MHz, DMSO-d_6, δ): 10.51 (br s, 1H), 9.15 (br s, 2H), 8.52 (br s, 3H), 7.51 (br s, 2H), 6.85 (s, 4H), 4.03 (s, 4 H), 3.74 (s, 4H), 3.62 (s, 15H), 3.25 (s, 4H).

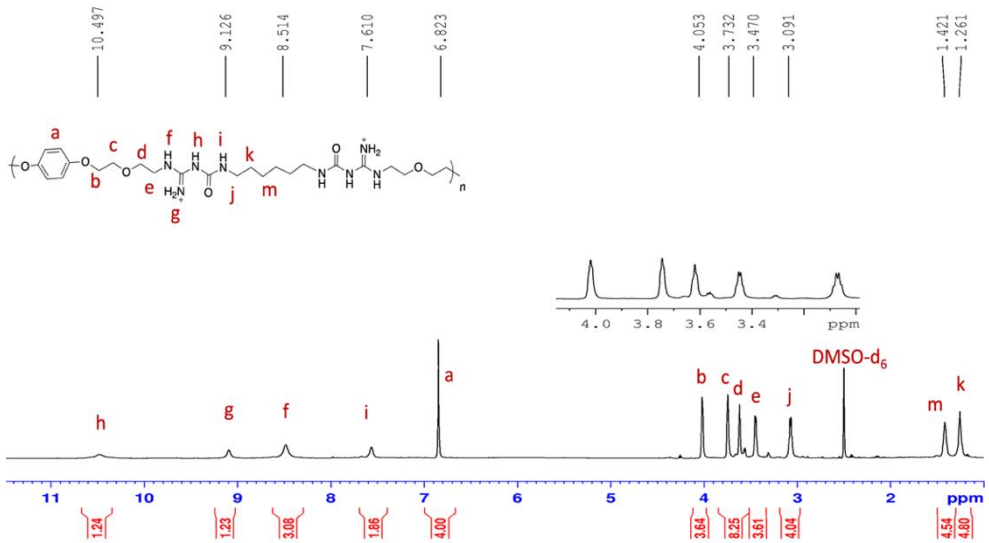

Figure 3.17. ^{1}H NMR of deprotected PGU-H. ^{1}H NMR (600 MHz, DMSO-d$_6$, δ): 10.50 (br s, 1H), 9.13 (br s, 2H), 8.51 (br s, 3H), 7.61 (br s, 2H), 6.82 (s, 4H), 4.05 (s, 4 H), 3.73 (s, 8H), 3.47 (s, 4H), 3.09 (s, 4H), 1.42 (s, 5H)), 1.26 (s, 5H).

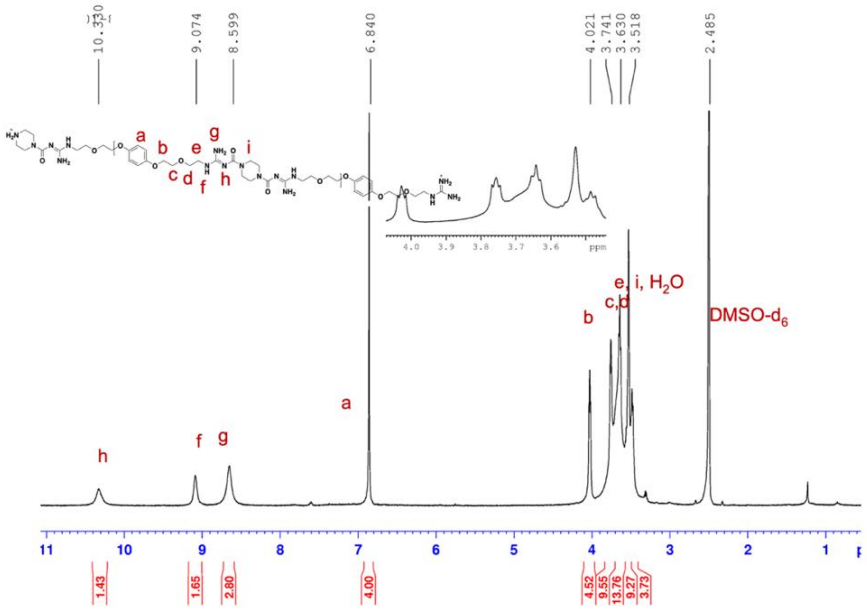

Figure 3.18. ^{1}H NMR of deprotected PGU-P-NDI. White fibrous solid ^{1}H NMR (600 MHz, DMSO-d6, δ): 10.3 (s, 1H), 9.1 (s, 1H), 8.9 (s, 2H), 6.8 (m, 4H), 4.0 (t, 4H), 3.6 (m, 4H), 3.7 (m, 14H), 3.5 (m, 4H).

3.5.5 Toxicity

J774 cells were seeded in a black-sided 384-well plate (~10,000 cells/well) in 24 μL of Dulbecco's Modified Eagle Medium (DMEM) and allowed to attach for 4 h at 37 ºC under a humidified atmosphere of 5% CO_2 prior to sample treatment. In separate 384-well plate, PGU-P-8K was tested by serially diluting two-fold with a final concentration of 4% DMSO using the liquid handling robot from Integra Biosciences. After addition of the samples, cells were incubated statically for 20 h prior to addition of 0.01% resazurin dye and incubated for an extra 4 h at 37 ºC. 2% Triton-X was used as positive control while media with 4% DMSO as negative control. Fluorescence was measured as previously described. Cell viability was determined relative to control wells. Assay was performed in duplicates with three independent experiments.

Additionally, HeLa cells were seeded in a 96-well plate (~10,000/well) in 200 μL of complete medium and allowed to attach for one day at 37 °C under a humidified atmosphere of 5% CO_2 prior to sample treatment as previously published,[22] Final concentrations of 40, 20, 10, and 5 μM were added into the complete media by dilution of the polymer stock solutions. After addition of the samples, cells were incubated for 18 h prior to treatment with 10 μL of methylthiazole tetrazolium (MTT) (5 mg/mL in PBS) and incubated for 4 h at 37 °C. After incubation, 200 μL of medium was gently removed and 100 μL of biological grade DMSO was added to solubilize the purple formazan crystals. Absorbance was measured by microwell plate reader. Cell viability was determined as a function of absorbance of each sample relative to control wells. All measurements represent the average of three independent measurements +/- standard deviation.

3.5.6 Minimum Inhibitory Concentration Assay

MIC was determined by broth microdilution method according to Clinical and Laboratory Standards Institute (CLSI) guidelines. *M. smegmatis* mc^2155 cells were initially grown for 24 h in BD Difco 7H9 medium (0.2 % glycerol and 0.05 % Tween 80) and supplemented with 1% ADN (0.05% albumin, 0.02% dextrose, 0.0085% NaCl). Cell suspensions were grown to late-log phase at 37 ºC with shaking at 210 rpm overnight.

M. abscessus (S and R) with luminescent reporter were incubated in T25 flasks (TPP) at 37 ºC, in 5% CO_2 static for 2-3 days and 5-7 days, respectively. The optical density (OD_{600}) was adjusted for final concentration of 10^5 CFU $well^{-1}$ for bacterial cells. Polymer solution and controls were prepared in the respective media and serially diluted two-fold in a clear round bottom 96-well microtiter plate (Cell treat, 229590), followed by the addition of 50 μL of the cell suspension. Positive control for *M. abscessus* was amikacin. Negative control included 50 μL of cell suspension and 50 μL of 2 % DMSO media. Plates were incubated statically at 37 ºC for 48 h for *M.smegmatis*, 20 h. After addition of the dye and 19 h incubation time, fluorescence was measure at 540 nm excitation wavelength and 590 nm emission wavelength on a BioTek Synergy H1 plate reader after further incubation period. For *M. abcessus* (S and R) they were incubated for 3 days, and luminescence was read. Assays included two technical replicates and were repeated at least three independent experiments.

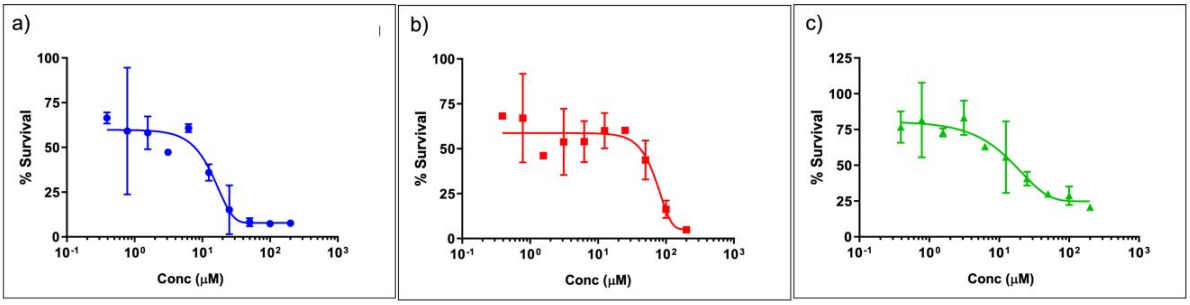

Figure 3.19. Anti-TB activity of a) PGU-P-8K, b) EDO, c) and NDI on on replicating *Mtb*. No MIC_{90} was established for these compounds as percent inhibition did not reach ≥90% .

3.5.7 Ethidium Bromide Accumulation Assay

M. smegmatis cells were incubated to log-phase in 7H9 at 37 ºC. The bacterial cell suspension was centrifuged at 10000 x g for 5 min at 25 °C, washed twice, and resuspended in 1x PBS with 0.05% Tween 80 (PBST). The OD_{600} was adjusted to 0.2. PGUs were prepared in 1x PBST and 50µL pipetted into the wells of a black-sided 96-well microtiter plate (Thermo Scientific Nunc, 165305). The bacterial suspension was pipetted for a ratio one-to-one of cell to polymer for a final volume of 100 µL in each well and a final concentration of 1% DMSO. Ethidium bromide (EtBr) dye at 2.5 µM was added as the fluorescent probe. EtBr can accumulate inside the cell and intercalate with nucleic acids leading to an increase of fluorescence signal. This assay can give insight on the intracellular accumulation of the dye, since EtBr [17] is a small molecule that can enter the cell and is a substrate of efflux pumps. The accumulation can be attributed to outer membrane damage or due to inhibition of efflux pumps. [17-20] The experiment was repeated at least three independent times and standard deviation depicted by error bars.

3.5.8 Membrane Permeability Assay

M.smegmatis cells were grown as previously mentioned. Cells were centrifuged at 4000 x g for 2 min at 25 ºC, washed and resuspended in 1x PBS. The resulting cells were adjusted to OD_{600} 0.4. PGUs were prepared at 1x MIC, 2x MIC and 4x MIC in 1x PBS buffer with 2% DMSO and 50 µL was added to an optical bottom black-sided 96-well microtiter plate (ThermoFisher, 165305). The bacterial cell suspension with 5 µM Sytox green dye, a membrane impermeable dye,[23] was added to the wells for a final volume of 100 µL in each well. Wells not containing polymer were used as the negative control, and cells lysed in a bead beater as positive control. The fluorescence at 485/590 nm (excitation/emission) was monitor every 5 min for 2 h at 37 ºC on a BioTek Synergy plate reader. Experiments were performed in triplicates.

3.5.9 Membrane Depolarization Assay

Bacterial cells were grown to late log-phase in 7H9. Cells were centrifuged at 3000 x g for 5 min at 25 ºC, washed twice and resuspended in 10mL of 5mM HEPES buffer, pH 7.2 supplemented with 1mM glucose. OD_{600} of the cells was then adjusted to 0.4. The cell suspension was treated with 1µM of the potentiometric probe 3,3'-Dipropylthiadicarbocyanine Iodide ($DiSC_3(5)$) was added. It was incubated at 37 °C, and monitored the quenching of $DiSC_3(5)$ dye in the presence of *M. smegmatis* cells for 30 min. In a black-sided 96-well microtiter plate, polymer solution was added to the plate and serially diluted two-fold in 50mM HEPES buffer supplemented with 1mM glucose and 2% DMSO for a final volume of 50µL per well and 1% DMSO. After 30 min of

quenching $DiSC_3(5)$, 50 μL of the bacterial suspension with dye was added to the polymer-containing wells. Wells without polymer were used as negative controls. Verapamil and CCCP were used as positive control. The fluorescence 590/635 nm (excitation/emission) was recorded for 2 h every 10 min on a BioTek Synergy H1 plate reader. Assay was performed at least three independent experiments, but one representative data was shown.

3.5.10 Quantification of Intracellular ATP Levels

Bacterial cells were grown to mid-log phase (OD_{600}=0.5) and treated with PGUs or 0.2% DMSO. Aliquots of treated samples were separated for CFU analysis and for cell lysing at shortly after treatment (time =0 h) and after 2 h of treatment. Treated cultures for 2 h were incubated at 37 °C, with shake (210 rpm). The aliquot separated for CFU analysis was serially diluted 10-fold in PBS and plated in LB agar plates to count the colonies after static incubation for six-days at 37 °C. The aliquot separated for cell lysing was transferred to a O-ring-containing screw-cap 2mL microtubes (Fisher Scientific) with 0.1mm zirconia/silica beads (Biospec). Cells were lysed in a bead beater for two 1 min intervals with ice-cooling in between. The cell lysates were added to a white-sided optical bottom 96-well plate (Thermo Scientific Nunc, 165306) and then 50 μL of BacTiter-Glo™ Cell Viability Assay (Promega) was added for a final volume of 100 μL in the wells. Luminescence was then shortly after recorded in a BioTek Synergy H1 plate reader. The relative luminescence units (RLUs) data was divided by the CFUs to normalize the ATP levels per treatment and presented as RLUs/CFUs.

3.6 References

(1) WHO. *Tuberculosis*. https://www.who.int/health-topics/tuberculosis#tab=tab_2.

(2) Tuberculosis Drugs and Mechanisms of Action. *National Institute of Allergy and Infectious Diseases* **2016**.

(3) CDC. *Treatment of Tb Disease*. https://www.cdc.gov/tb/topic/treatment/tbdisease.htm.

(4) *Global Tuberculosis Data*. https://www.who.int/teams/global-tuberculosis-programme/data.

(5) Ginsberg, A. M. Tuberculosis Drug Development: Progress, Challenges, and the Road Ahead. *Tuberculosis* **2010**, *90* (3), 162–167. https://doi.org/10.1016/j.tube.2010.03.003.

(6) Dookie, N.; Rambaran, S.; Padayatchi, N.; Mahomed, S.; Naidoo, K. Evolution of Drug Resistance in Mycobacterium Tuberculosis: A Review on the Molecular Determinants of Resistance and Implications for Personalized Care. *Journal of Antimicrobial Chemotherapy* **2018**, *73* (5), 1138–1151. https://doi.org/10.1093/jac/dkx506.

(7) Hurdle, J. G.; O'Neill, A. J.; Chopra, I.; Lee, R. E. Targeting Bacterial Membrane Function: An Underexploited Mechanism for Treating Persistent Infections. *Nature Reviews Microbiology* **2011**, *9* (1), 62–75. https://doi.org/10.1038/nrmicro2474.

(8) Gengenbacher, M.; Kaufmann, S. H. E. Mycobacterium Tuberculosis: Success through Dormancy. *FEMS Microbiology Reviews*. May 2012, pp 514–532. https://doi.org/10.1111/j.1574-6976.2012.00331.x.

(9) Rao, S. P. S.; Alonso, S.; Rand, L.; Dick, T.; Pethe, K. The Protonmotive Force Is Required for Maintaining ATP Homeostasis and Viability of Hypoxic, Nonreplicating Mycobacterium Tuberculosis. *Proc Natl Acad Sci U S A* **2008**, *105* (33), 11945–11950. https://doi.org/10.1073/pnas.0711697105.

(10) Chen, H.; Nyantakyi, S. A.; Li, M.; Gopal, P.; Aziz, D. B.; Yang, T.; Moreira, W.; Gengenbacher, M.; Dick, T.; Go, M. L. The Mycobacterial Membrane: A Novel Target Space for Anti-Tubercular Drugs. *Frontiers in Microbiology* **2018**, *9* (JUL), 1–11. https://doi.org/10.3389/fmicb.2018.01627.

(11) Ahmed, M. S.; Annamalai, T.; Li, X.; Seddek, A.; Teng, P.; Tse-Dinh, Y. C.; Moon, J. H. Synthesis of Antimicrobial Poly(Guanylurea)s. *Bioconjugate Chemistry* **2018**, *29* (4), 1006–1009. https://doi.org/10.1021/acs.bioconjchem.8b00057.

(12) Salah, A.; Abdelbaky, A. S.; Shvets, V. I. A Convenient Method for the Synthesis of N, N′-Diprotected-(2-Hydroxyethyl)-Guanidine Organic Synthesis View Project A Convenient Method for the Synthesis of N, N′-Diprotected-(2-Hydroxyethyl)-Guanidine. **2019**.

(13) Ripoll, F.; Deshayes, C.; Pasek, S.; Laval, F.; Beretti, J. L.; Biet, F.; Risler, J. L.; Daffé, M.; Etienne, G.; Gaillard, J. L.; Reyrat, J. M. Genomics of Glycopeptidolipid Biosynthesis in Mycobacterium Abscessus and M. Chelonae. *BMC Genomics* **2007**, *8* (May 2014). https://doi.org/10.1186/1471-2164-8-114.

(14) Roux, A. L.; Viljoen, A.; Bah, A.; Simeone, R.; Bernut, A.; Laencina, L.; Deramaudt, T.; Rottman, M.; Gaillard, J. L.; Majlessi, L.; Brosch, R.; Girard-Misguich, F.; Vergne, I.; de Chastellier, C.; Kremer, L.; Herrmann, J. L. The Distinct Fate of Smooth and Rough Mycobacterium Abscessus Variants inside Macrophages. *Open Biology* **2016**, *6* (11). https://doi.org/10.1098/rsob.160185.

(15) Clary, G.; Sasindran, S. J.; Nesbitt, N.; Mason, L.; Cole, S.; Azad, A.; McCoy, K.; Schlesinger, L. S.; Hall-Stoodley, L. Mycobacterium Abscessus Smooth and Rough Morphotypes Form Antimicrobial-Tolerant Biofilm Phenotypes but Are Killed by Acetic Acid. *Antimicrobial Agents and Chemotherapy* **2018**, *62* (3). https://doi.org/10.1128/AAC.01782-17.

(16) Jankute, M.; Nataraj, V.; Lee, O. Y. C.; Wu, H. H. T.; Ridell, M.; Garton, N. J.; Barer, M. R.; Minnikin, D. E.; Bhatt, A.; Besra, G. S. The Role of Hydrophobicity in Tuberculosis Evolution and Pathogenicity. *Scientific Reports* **2017**, *7* (1). https://doi.org/10.1038/s41598-017-01501-0.

(17) Rodrigues, L.; Ramos, J.; Couto, I.; Amaral, L.; Viveiros, M. Ethidium Bromide Transport across Mycobacterium Smegmatis Cell-Wall: Correlation with Antibiotic Resistance. *BMC Microbiology* **2011**, *11*. https://doi.org/10.1186/1471-2180-11-35.

(18) Du, D.; Wang-Kan, X.; Neuberger, A.; van Veen, H. W.; Pos, K. M.; Piddock, L. J. V.; Luisi, B. F. Multidrug Efflux Pumps: Structure, Function and Regulation. *Nature Reviews Microbiology*. Nature Publishing Group September 1, 2018, pp 523–539. https://doi.org/10.1038/s41579-018-0048-6.

(19) Song, L.; Wu, X. Development of Efflux Pump Inhibitors in Antituberculosis Therapy. *International Journal of Antimicrobial Agents* **2016**, *47* (6), 421–429. https://doi.org/10.1016/j.ijantimicag.2016.04.007.

(20) Black, P. A.; Warren, R. M.; Louw, G. E.; van Helden, P. D.; Victor, T. C.; Kana, B. D. Energy Metabolism and Drug Efflux in Mycobacterium Tuberculosis. *Antimicrobial Agents and Chemotherapy* **2014**, *58* (5), 2491–2503. https://doi.org/10.1128/AAC.02293-13.

(21) Rodrigues, L.; Ramos, J.; Couto, I.; Amaral, L.; Viveiros, M. Ethidium Bromide Transport across Mycobacterium Smegmatis Cell-Wall: Correlation with Antibiotic Resistance. *BMC Microbiology* **2011**, *11*. https://doi.org/10.1186/1471-2180-11-35.

(22) Barrios, A.; Estrada, M.; Moon, J. H. Carbamoylated Guanidine-Containing Polymers for Non-Covalent Functional Protein Delivery in Serum-Containing Media. Angewandte Chemie 2022, 33199. https://doi.org/10.1002/ange.202116722.

(23) Lebaron, P.; Catala, P.; Parthuisot, N. Effectiveness of SYTOX Green Stain for Bacterial Viability Assessment. *Applied and Environmental Microbiology* **1998**, *64* (7), 2697–2700. https://doi.org/10.1128/aem.64.7.2697-2700.1998.

CHAPTER 4
CONCLUSIONS AND FUTURE OUTLOOK

The significant progress of antimicrobial peptides (AMPs) and AMP mimics as novel therapeutics for broad-spectrum activity efficacy has transformed drug development. The unconventional membrane-targeting strategy of AMPs is a promising approach to the worrisome slowdown in the pipeline for new antibiotics. While the mode of action is highly dependent on the structure (i.e., pendants, secondary structures, functional groups), AMPs and AMP mimics have shown that cationic and hydrophobic moieties are essential against bacteria, especially guanidinium-containing polymers due to electrostatic and multidentate interactions with the membrane.

The cell wall of mycobacteria is more complex resulting in the current lengthy and multidrug TB treatment. Although tuberculosis is a world-wide health threat, little is known about the physicochemical properties for targeting the membrane, as only a few AMPs and AMP mimics have shown selectivity against mycobacteria. The thorough studies of PGUs against mycobacteria provided insightful knowledge for future drug development.

Though the results discussed in Chapter 2 and 3 showed that the simple polymerization technique yielded the desired products, the synthetic pathway can be fine-tuned via solid-phase synthesis which would increase efficiency, scalability, and solution dispersity. This technique would yield defined molecular weight products rather than disperse solution of oligomers for better structure-activity relationship (SAR) studies on the effect of molecular weight, repeating units, and end-groups (i.e., ammonium, guanidinium). Additionally, this synthetic pathway would facilitate labeling PGU-P-8K with a fluorescent label (e.g., FITC) for further inspections of PGU-P-8K interactions to the mycobacterial membrane.

Furthermore, Chapter 2 presented the unique properties of PGU-P-8K by detailing the fast bactericidal effect via disruption of membrane bioenergetics, and an increased number of hollow dead cells. This study can be expanded by identifying if *M. smegmatis* can develop resistance to PGU-P-8K, the time required for the development of the mutation(s) and genotyping it which would augment the importance of PGU-P-8K for mycobacterial research and its future applications. Additionally, PGU-P-8K can be further studied for disruption of other bioenergetic processes (i.e., ΔpH, oxygen consumption, electron transport chain) in mycobacteria.

While Chapter 3 is still in process of collecting data, and insightful information will be collected for designing membrane-targeting drug or drug adjuvant against mycobacteria, further studies on PGUs against *M. abscessus* or dormant TB would highlight the importance of the unconventional approach to TB treatment. Additionally, aromaticity on the backbone of PGUs broaden the antimicrobial spectrum;hence widen the biological applications of PGUs.

Due to the low toxicity to eukaryotic cells, PGUs were tested for intracellular delivery of proteins. Preliminary results showed that the additionally aromaticity in PGU-Ph had the best protein loading efficiency of red algae phycoerythrin (R-PE), a fluorescent protein (Figure 4.1). These encouraging results show the translational applications of the PGU-system for a variety of biological applications.

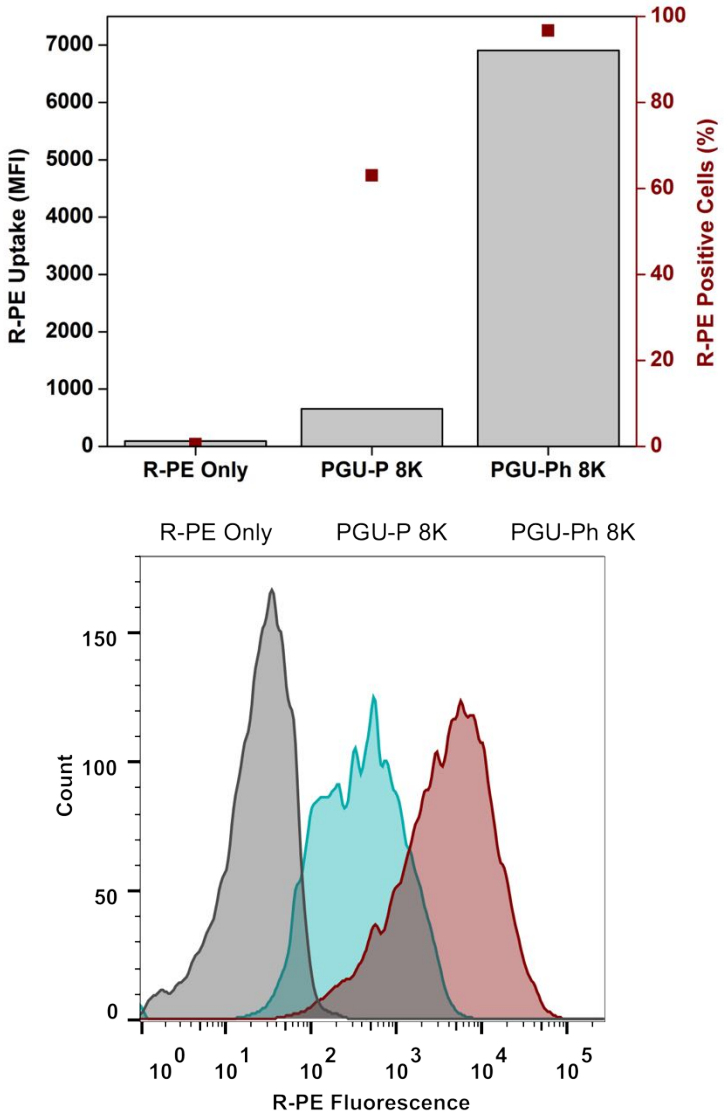

Figure 4.1. PGU-Ph delivery of red algae phycoerythrin (R-PE) fluorescent protein in comparison to PGU-P-8K, where the aromaticity around the guanylurea in PGU-Ph showed better protein loading efficiency.

Overall, PGUs exhibited selectivity, fast bactericidal activity, synergism with an oxidative phosphorylation-targeting anti-TB drug and disruption of the membrane bioenergetics in mycobacteria. The PGU linear system permitted SAR studies of the key components required for targeting the mycobacterial membrane. When altering the backbone of PGU, it displayed changes in selectivity against different microbes, mycobacterial membranes, and translational biological applications.

VITA

MICHELLE M. MIRANDA-VÉLEZ

EDUCATION

2017-Present	Florida International University, Miami, Florida Doctor of Philosophy in Chemistry (expected, 2022) Dissertation title: "Synthesis, structure-activity relationship, and mechanism studies of poly (guanylurea)s against mycobacteria"
2022	South Florida American Chemical Society Travel Award
2017-2020	Florida International University, Miami, Florida Master of Science in Chemistry Thesis topic: "Structure-activity relationship studies of antimicrobial poly(guanylurea)s"
2011-2015	University of Tampa, Tampa, Florida Bachelor of Science in Forensic Science Minor in Criminal Investigation
2015	Dean's List
2013	The National Society of Leadership and Success
2012	Honors Program
2012	Phi Eta Sigma
2011	Minaret Scholarship

PUBLICATIONS AND PRESENTATIONS

Michelle Miranda-Vélez, Thirunavukkarasu Annamalai, Yuk-Ching Tse-Dinh, and Joong Ho Moon, "Mechanism studies of poly(guanylurea) against *Mycobacterium smegmatis*" Biomolecular Sciences Institute 2022 Research Symposium Poster Sessions, Miami, Florida

Michelle Miranda-Vélez, Priscila Halicki, Priya Ramisetty, Thirunavukkarasu Annamalai, Yuk-Ching Tse-Dinh, Kyle Rohde and Joong Ho Moon, "Mechanism studies of poly(guanylurea) 8K against *Mycobacterium smegmatis*" ACS Spring 2022, March 20-24, San Diego, California

Michelle Miranda-Vélez, Thirunavukkarasu Annamalai, Yuk-Ching Tse-Dinh, and Joong Ho Moon, "Mechanism studies of poly(guanylurea) against *Mycobacterium smegmatis*"

Biomolecular Sciences Institute 2021 Research Symposium ePoster Sessions, Miami, Florida

Michelle Miranda-Vélez, Thirunavukkarasu Annamalai, Yuk-Ching Tse-Dinh, and Joong Ho Moon, "Structure-activity relationship studies of novel poly(guanylurea)s" Biomolecular Sciences Institute 2019 Research Symposium Poster Sessions, Miami, Florida

Ashley Windom, Michelle Miranda, and Kenyon Evans-Nguyen, "Characterization of a microwave plasma torch ionization source coupled to an ion trap for atomic mass spectrometry" 2016 IFRI Forensic Science Symposium, Miami, Florida

K.M. Evans-Nguyen, J. Gerling, H. Brown, M. Miranda, A. Windom and J. Speer, "Towards universal ambient ionization: direct elemental analysis of solid substrates using microwave plasma ionization", Analyst, 2016,141, 3811-3820

Kenyon Evans-Nguyen, Michelle Miranda, Ashley Windom, Hilary Brown, Jennifer Speer, Hanany O. Flores Duron, Jon Gerling, and Colleen Quinn, "Combining molecular and atomic ambient ionization technologies for complete sample characterization" Abstracts of Papers, 250th ACS National Meeting & Exposition, Boston, MA